AD-A040 148 TORONTO UNIV (ONTARIO) INST FOR AEROSPACE STUDIES F/G 20/1
WAVE MOTION IN LOW-PRESSURE-RATIO RECTANGULAR AND PYRAMIDAL SHO--ETC(U)
DEC 75 J J GOTTLIEB AF-AFOSR-2274-72
UNCLASSIFIED UTIAS-199 AFOSR-TR-77-0624 NL

| OF |
AD
A040148

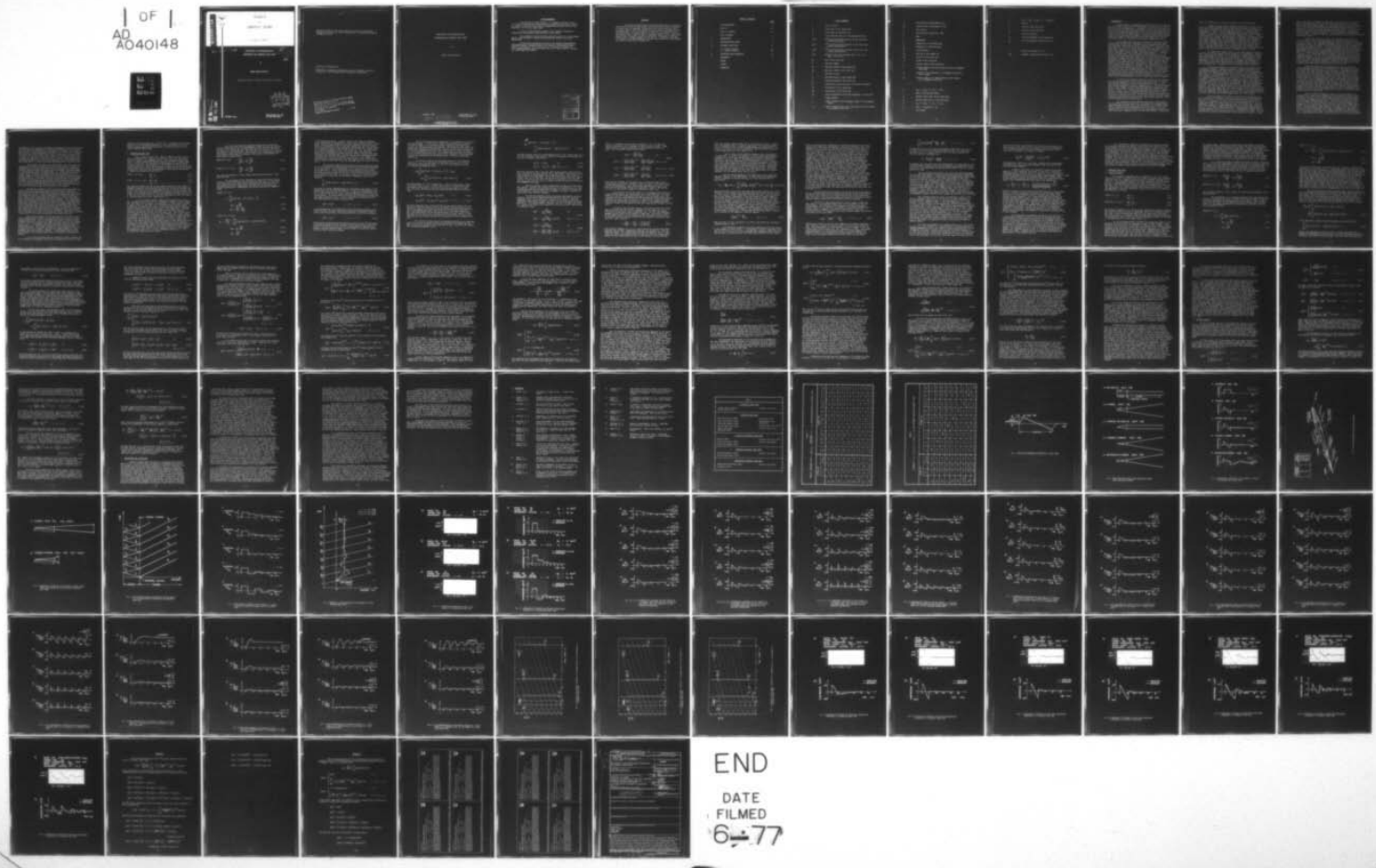

END

DATE
FILMED
6-77

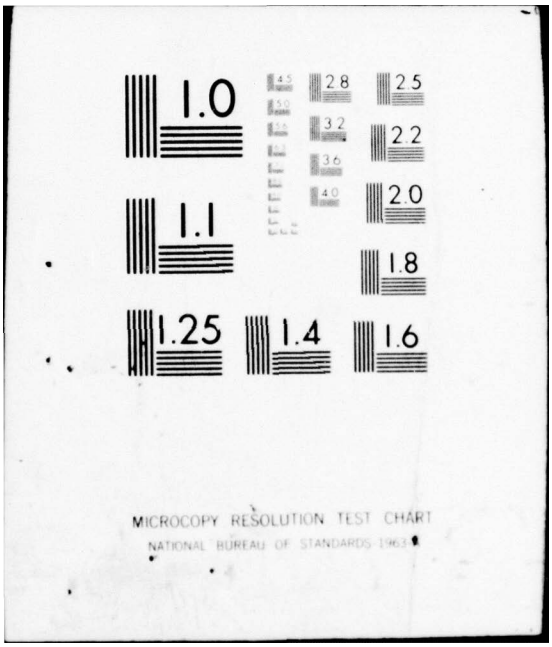
1.0
1.1
1.25
1.4
1.6
1.8
2.0
2.2
2.5
2.8
3.2
3.6
4.0
4.5
5.0
MICROCOPY RESOLUTION TEST CHART
NATIONAL BUREAU OF STANDARDS 1963

INSTITUTE FOR AEROSPACE STUDIES

UNIVERSITY OF TORONTO

WAVE MOTION IN LOW-PRESSURE-RATIO RECTANGULAR AND PYRAMIDAL SHOCK TUBES

by

James Joseph Gottlieb

December 1975

UTIAS Report No. 199
CN ISSN 0082-5255

Qualified requestors may obtain additional copies from the Defense Documentation Center; all others should apply to the National Technical Information Service.

Conditions of Reproduction:

Reproduction, translation, publication, use and disposal in whole or in part by or for the United States Government is permitted.

AIR FORCE OFFICE OF SCIENTIFIC RESEARCH (AFSC)
NOTICE OF TRANSMITTAL TO DDC
This technical report has been reviewed and is approved for public release IAW AFR 190-12 (7b).
Distribution is unlimited.
A. D. BLOSE
Technical Information Officer

WAVE MOTION IN LOW-PRESSURE-RATIO RECTANGULAR AND PYRAMIDAL SHOCK TUBES

by

James Joseph Gottlieb

December, 1975

UTIAS Report No. 199
CN ISSN 0082-5255

Acknowledgements

I should like to thank both Dr. J. H. deLeeuw, Director, and Dr. I. I. Glass for giving me the opportunity of completing the present research. Dr. Glass's continual interest and encouragement and critical review of the manuscript are very much appreciated.

I wish to thank Reinhard Gnoyke for his competent assistance in obtaining the experimental data presented in this report.

The assistance received from Mrs. Mary Fiorellino, Mr. Carlos Basdeo and Mr. John McCormack in typing and printing this report is very much appreciated.

The financial assistance provided by the Canadian Transportation Development Agency, Canadian Ministry of Transport, the National Research Council of Canada, and the Air Force Office of Scientific Research, Air Force Systems Command, and United States Air Force, under Grant No. 72-2274, are acknowledged with thanks.

Abstract

Closed-form solutions based on acoustic theory have recently been obtained to describe the wave motion in both low-pressure-ratio rectangular (constant area) and pyramidal shock tubes which utilize different driver and channel gases. These new solutions are in excellent agreement with experimental data. This work should be of interest to researchers who are using shock tubes or similar devices to produce impulse noise, in particular the simulated sonic boom, in order to facilitate studies of the effects of impulse sound on humans, animals and structures. Furthermore, this work is relevant to the understanding of the wave motion produced by weak planar and spherical explosions of finite size.

Table of Contents

List of Symbols

a	speed of sound
a_1	sound speed of the channel gas
a_2	sound speed of the driver gas
A	cross-sectional area of a rectangular shock tube
$f_i(\eta)$	i^{th} velocity potential function of the driver gas (inward moving waves)
$g_i(\xi)$	i^{th} velocity potential function of the channel gas (outward moving waves)
$h_i(\beta)$	i^{th} velocity potential function of the driver gas (outward moving waves)
$H\{t\}$	Heaviside unit step function; $H\{t\} = 0$ if $t < 0$, $H\{t\} = 1$ if $t > 0$.
m_o	mass of the driver gas
M	molecular weight
M_1	molecular weight of the channel gas
M_2	molecular weight of the driver gas
p	absolute pressure
p_1	absolute pressure of the channel gas
p_2	absolute pressure of the driver gas
Δp	overpressure, excess pressure or pressure difference
Δp_1	overpressure of the channel gas
Δp_2	overpressure of the driver gas
Δp_o	pressure difference across the diaphragm in a shock tube
r	radial distance
r_o	radial location of the diaphragm, length of the pyramidal driver
r_*	initial radial location of a fluid particle in the channel of a pyramidal shock tube

Δr	fluid-particle displacement $(r-r_*)$
Δr_o	contact-surface displacement $(r-r_o)$
R	gas constant
R_o	universal gas constant $(R_o = MR)$
t	time
T	temperature
T_1	temperature of the channel gas
T_2	temperature of the driver gas
Δu	fluid velocity
Δu_1	velocity of the channel gas
Δu_2	velocity of the driver gas
V	volume of the driver gas
V_o	initial volume of the driver gas
x	distance measured from the closed end of the rectangular shock tube
x_o	location of the diaphragm in a rectangular shock tube, driver length
x_*	initial location of a fluid particle in the channel of a rectangular shock tube
β	$(a_2 t - x)/x_o$ or $(a_2 t - r)/r_o$
γ	ratio of the specific heats
γ_1	specific heats ratio of the channel gas
γ_2	specific heats ratio of the driver gas
η	$(a_2 t + x)/x_o$ or $(a_2 t + r)/r_o$
ℓ	$(a_1\rho_1 + a_2\rho_2)/a_1(\rho_2 - \rho_1)$
λ	wave length

ξ	$(a_1 t - x)/x_o$ or $(a_1 t - r + r_o)a_2/a_1 r_o$
ρ	density
ρ_1	density of the channel gas
ρ_2	density of the driver gas
Φ	velocity potential
Φ_1	velocity potential of the channel gas
Φ_2	velocity potential of the driver gas
!	factorial function (0! = 1)
$\binom{m}{n}$	binomial coefficients [m!/n!(m - n)!]

1. INTRODUCTION

Noise pollution is becoming more significant in recent times and is contributing to the stresses affecting man. Ongoing studies into the effects of noise on humans (e.g., see Kyter's book - Ref. 1), animals and even structures are proceeding, fortunately, at a corresponding accelerated pace. One important and active area of current noise research is the study of the effects of impulse noise. A particularly important impulse sound is the sonic boom, whose impact on society is being assessed before supersonic transport (SST) aircraft such as the Anglo-French Concorde and Soviet TU-144 are introduced into extensive commercial service.

At the University of Toronto, Institute for Aerospace Studies (UTIAS), three different but complementary sonic-boom simulators have been developed to help assess current societal problems associated with the sonic boom. The first of two major facilities, a loudspeaker-driver booth (Refs. 2 and 3), can easily accommodate one human subject or a few small caged animals in its solidly built and sealed chamber (volume of $2m^3$) to facilitate studies of human and animal response to a simulated full-scale sonic boom. The second major facility (Refs. 2, 3, 4, 5, and 6), a travelling-wave horn in the form of a horizontal concrete pyramid (25 m long, 3-m-square base), has at its apex a specially designed valve which regulates the air discharge from a large reservoir into the pyramidal horn. This controlled discharge of air generates in the horn interior a simulated full-scale sonic boom for human, animal or structural response investigations. Alternatively a shock-tube driver can be installed at the horn apex to produce a simulated short-duration sonic boom to facilitate certain response tests. The third sonic-boom simulator (Refs. 3 and 7), a portable shock tube (11 kgm., 1 m long) having a constant-area driver and an exponential horn, can be easily transported and operated by one person to conduct wildlife field tests. A simulated short-duration sonic boom can be produced and directed at wildlife in their natural habitat in order to study their startle response.

In order to illustrate the type of wave that must be produced by a sonic-boom simulator, and also for future reference, an idealized overpressure signature of a sonic boom is sketched in Fig. 1. The more important parameters which are commonly used to describe the various parts of the signature include the peak overpressure, rise time, duration (or wave length), and wave form which may vary somewhat from the ideal 'N' shape. It is worth noting that respective values of peak overpressure, duration and rise time are 100 N/m^2, 300 ms and 1 ms for a typical sonic boom from a current SST aircraft and also from large military bomber supersonic aircraft. In the case of shorter military fighter supersonic aircraft only the duration is significantly different, being correspondingly shorter at about 100 ms.

The analytical and experimental work given in this report on the wave motion in low-pressure-ratio rectangular and pyramidal shock tubes utilizing different driver and channel gases is a natural continuation of previous sonic-boom-simulation work at UTIAS. Also, the present work is a direct extension of sonic-boom-simulation research on shock tubes made in England, France and the United States. These state-

ments are elaborated on in the following part of this introduction.

A number of geometrically different shock tubes have been constructed and tested by English, French, American and Canadian researchers to assess their capability of producing a good 'N-wave' to simulate the sonic boom (Fig. 1). Some of the more important shock tubes are illustrated schematically in Fig. 2, and the developmental and research efforts made by various researchers on such shock tubes are summarized in Table 1. Each shock tube shown in Fig. 2 has been named according to the geometrical shape of its driver and channel. The adjectives 'rectangular' and 'pyramidal' arise quite naturally owing to the geometry of the driver and channel of shock tubes commonly used in the laboratory. More generally, however, in this report rectangular will refer to any duct where the cross-sectional area is constant with distance (e.g., cylindrical), and pyramidal will refer to any duct where the cross-sectional area increases directly with the square of the distance from the center of symmetry (e.g., conical).

For shock tubes commonly used for sonic-boom simulation purposes the driver and channel gases are both normally air at atmospheric temperature. The driver air, however, is initially at a slightly higher pressure than the atmospheric pressure air in the channel. Consequently the pressure ratio for the driver and channel gases separated initially by a thin diaphragm is very nearly equal to unity. On breaking the diaphragm in such a low-pressure-ratio shock tube the ensuing wave motion results in a very weak shock wave or simulated sonic boom moving in the channel gas.

Closed-form solutions for the wave motion in low-pressure-ratio rectangular, pyramidal, pyramidal-rectangular, pyramidal-pyramidal and rectangular-pyramidal shock tubes which use identical driver and channel gases have been obtained previously (Refs. 5 and 6). The rectangular shock tube produces a constant-amplitude pulse as illustrated by the overpressure signature sketched in Fig. 3a. In the case of the pyramidal shock tube an N-shaped pulse is produced as shown in Fig. 3b. The other pyramidal-rectangular, pyramidal-pyramidal and rectangular-pyramidal shock tubes each produces a distorted N-wave followed by additional waves or disturbances as illustrated in Fig. 3c, 3d and 3e respectively. Obviously the pyramidal shock tube is best for producing a good N-wave for sonic-boom simulation purposes. Note that the rapid pressure rise across both the front and rear shocks of the N-wave equals $\Delta p_o r_o/2r$ and the duration of the N-wave is $2r_o/a$, where the respective symbols Δp_o, a, r and r_o denote the pressure difference across the diaphragm, sound speed of the driver gas, radial distance measured from the driver apex, and the diaphragm location or driver length.

A large pyramidal shock tube is required if the N-wave produced in the channel is to simulate a full-scale sonic boom from an SST aircraft. Since the duration of the N-wave in the shock tube equals $2r_o/a$ and the duration of a simulated sonic boom has to be approximately 300 ms, the corresponding length of the shock-tube (r_o) needs to be about 50 m. Owing to inadequate breakage of a large diaphragm in a low-pressure-ratio shock tube (Ref. 12), the largest diaphragm having sufficiently good breaking characteristics appears to be about 1 m^2 in area. The maximum divergence angle of a pyramidal shock tube is therefore about one-fiftieth of a radian. Now the interior test section of the pyramidal channel must be at least 3 m on each

side to adequately accommodate a human subject without unduly blocking the path of the simulated sonic boom. For such a test section size and divergence angle the resulting length of the pyramidal shock tube is an incredible 150 m. In practice the shock tube is even longer because a reflection eliminator is required to cover the open end of the channel. For the sake of interest the large Franco-German pyramidal shock tube (Ref. 14), which is 189 m in length, is depicted in Fig. 4. Note that different diaphragm stations have been provided such that the N-wave duration can be varied conveniently from 100 to 300 ms.

Owing to the large size required of a pyramidal shock tube if a full-scale sonic boom is to be simulated, the initial construction can be a costly endeavour. If a pyramidal-pyramidal shock tube instead of a pyramidal shock tube could be used, then the shock-tube length and thus the initial construction cost might be reduced. The idea behind this scheme is brought out by the diagrams given in Fig. 5. In order to maintain the same sized driver, diaphragm and test section of a pyramidal shock tube (Fig. 5a), the divergence angle of the channel is increased, thereby producing a shorter shock tube (Fig. 5b). This resulting pyramidal-pyramidal shock tube, however, produces a distorted N-wave (Fig. 3d), which is normally undesirable for sonic-boom simulation purposes. In fact it is worth mentioning that, based on the experimental results obtained from prototype pyramidal-pyramidal shock tubes (Ref. 12), French and German researchers deemed the distortion in the N-wave as unacceptable, and they consequently constructed the large Franco-German pyramidal shock tube mentioned previously and shown in Fig. 4.

Another possible method of achieving a shorter and thus less costly pyramidal shock tube for the simulation of a full-scale sonic boom is to use a driver gas which has a low sound speed. (Although the channel gas could be the same as the driver gas, it would probably be more convenient to use air in the channel.) Because the predicted duration of the N-wave produced in the shock tube is $2r_o/a$, if a gas having a lower sound speed (a) than air is used in the driver, the correct full-scale duration of a sonic boom can be accomplished with a shorter-than-normal driver (length r_o) and hence a shorter pyramidal shock tube. For example, the use of an economical gas like carbon dioxide (CO_2) instead of air in the driver and air in the channel would result in a fairly significant reduction of 22% in shock-tube length. The use of more exotic and expensive dichlorodifluoromethane ($C\ Cl_2\ F_2$), sulfur hexafluoride (SF_6) or octofluorocyclobutane ($C_4\ F_8$) would result in an even more significant reduction in shock-tube length by 56%, 60% or 67% respectively.

Another possible advantage of using a driver gas having a low sound speed is to improve the capability of an existing low-pressure-ratio pyramidal shock tube. Most of the existing shock tubes have been designed to be short to minimize construction costs, and they consequently produce a short-duration simulated sonic boom. (Such short-duration booms can be used for studies of wave diffraction over and into model buildings, wave propagation over reduced-scale land topologies, and certain animal response tests). Since atmospheric temperature air is normally used in both the driver and channel the standard technique of changing the N-wave duration for new tests is to alter the driver length by changing the diaphragm location. As existing shock tubes are normally short (less than 15 m long) an upper limit exists on the driver length and therefore on the N-wave duration.

Consequently, the only means of further increasing the N-wave duration and thus extending the capability of existing shock tubes is to use a driver gas which has a sufficiently low sound speed. For example, the N-wave duration can be increased markedly by a factor of 1.3, 2.3, 2.5 or 3.0 when the driver gas is CO_2, CCl_2F_2, SF_6 or C_4F_8, respectively, instead of air. It should be noted that the N-wave duration can be increased further by lowering the temperature of the driver gas. However, this method is not only impracticable but the increase in duration is not very significant, being only 20% for a decrease in driver-gas temperature from 300 to 200 K.

The technique of using a driver gas with a low sound speed in a pyramidal shock tube to increase the N-wave duration both to extend the capability of an existing shock tube and to investigate the feasibility of using different driver and channel gases in a larger sonic-boom simulator was originally tested in England (Ref. 9). Carbon dioxide was used in the driver of a small conical shock tube (driver length of 60 cm, channel length of 140 cm) and showed that a good N-wave could be produced in the channel air. The N-wave duration was an expected 1.3 times longer than that for the case when air was used in both the driver and channel. To obtain an even longer duration N-wave with the same shock tube the use of a special gas having the trade name 'Arcton' was proposed, as its low sound speed is only 43% of that for air. Test results for the case of Arcton as the driver gas were unfortunately not reported.

The British researchers (Ref. 9) did not notice any significant distortion in the overpressure signature of the N-wave produced in their conical shock tube when carbon dioxide was used in the driver and the channel gas was air. However experiments at UTIAS showed that if the sound speeds of the driver and channel gases were radically different (e.g., CCl_2F_2, SF_6 or C_4F_8 being the driver gas with air in the channel) then a noticeably distorted N-wave would be produced. This distortion in the N-wave is similar to that in the N-wave produced by a pyramidal-pyramidal shock tube which used identical driver and channel gases (Fig. 3d). If the undesirable distortion in the N-wave is significant then the concept of using different driver and channel gases in a pyramidal shock tube either to increase the duration of an N-wave produced in an existing short shock tube or to enable a short and inexpensive shock tube to produce a simulated full-scale sonic boom is not valid. This will be verified subsequently in this report by analytical and experimental data.

The acoustic analysis for the wave motion in a pyramidal shock tube utilizing different driver and channel gases was found to be quite complex analytically. Prior to obtaining the acoustic solution for the pyramidal shock tube a similar but simpler acoustic solution was obtained for the case of a rectangular shock tube utilizing different driver and channel gases. For interest and completeness both of these acoustic analyses are given. The simpler analysis for the rectangular shock tube is presented first in Chapter 2 and the more complex analysis for the pyramidal shock tube follows in Chapter 3. Experimental data for both the rectangular and pyramidal shock tubes are also given, verifying the analyses.

It is worth mentioning that the respective acoustic analyses for the rectangular and pyramidal shock tubes are applicable directly to weak

planar and spherical explosions of finite size. Consequently the acoustic analyses are of fundamental importance to the understanding of the wave motion of planar and spherical explosions, for which the explosion gas differs from the ambient gas.

2. RECTANGULAR SHOCK TUBE

The rectangular shock tube, which is depicted in Fig. 2a, consists essentially of a constant cross-sectional area driver and channel which are joined at the diaphragm station. The diaphragm initially separates a normally atmospheric pressure channel gas from a slightly higher pressure driver gas. For generality of the analysis let the initially quiescent driver and channel gases be not only different but also have different temperatures. Before the diaphragm is broken the appropriate initial conditions of the driver and channel gases for the analysis can therefore be summarized mathematically as follows.

Channel $(x > x_o)$: $\Delta p_1 = 0$ (2.1)

$\Delta u_1 = 0$ (2.2)

Driver $(0 < x < x_o)$: $\Delta p_2 = \Delta p_o$ (2.3)

$\Delta u_2 = 0$ (2.4)

The respective symbols Δp, Δu, and Δp_o denote overpressure with respect to atmospheric pressure, perturbation flow velocity or particle velocity, and pressure difference across the diaphragm, whereas the respective subscripts 1 and 2 refer the appropriate symbols to the channel and driver gases. The distance x is measured along the shock tube starting from the closed end of of the driver as shown in Fig. 2a, and the diaphragm is located at distance x_o, thereby making the driver length equal to x_o.

For the preceding initial conditions the ensuing wave motion in the rectangular shock tube after the diaphragm is broken is rather complex. This wave motion can be depicted conveniently on a time-distance diagram, as shown in Fig. 6, where the locus of each wave front has been drawn. On breaking the diaphragm in the shock tube the resulting rapidly expanding driver gas produces a weak shock wave (g_1) in the channel gas. Simultaneously a weak rarefraction wave (f_1) moves into the driver gas and eventually reaches and reflects from the closed end. This reflected wave (h_1) propagates through the driver gas and encounters the contact surface or interface of the driver and channel gases. Because the contact-surface displacement is negligible in comparison with the driver length, the contact-surface path is shown in Fig. 6 simply as a vertical dashed line. Owing to the change in specific impedance (product of the density and sound speed) across the contact surface the reflected wave (h_1) is partially transmitted to the channel (g_2) and partially reflected back into the driver (f_2). The subsequent oscillatory wave motion between the contact surface and closed end of the driver creates a sequence of waves in the channel. The integrated result of all of these individual waves (g_i, $i = 1, 2, \ldots, \infty$) yields the total wave in the channel.

For a low-pressure-ratio rectangular shock tube for which the pressure difference across the diaphragm Δp_o is much less than the absolute pressure of the channel gas, the individual and total waves in the driver and channel are relatively weak. The wave motion can therefore be described adequately by using well-known acoustic theory. The one-dimensional planar wave equations which govern the acoustic wave motion in the channel and driver gases are given below.

Channel ($x > x_o$):
$$\frac{\partial^2 \phi_1}{\partial t^2} = a_1^2 \frac{\partial^2 \phi_1}{\partial x^2} \tag{2.5}$$

Driver ($0 < x < x_o$):
$$\frac{\partial^2 \phi_2}{\partial t^2} = a_2^2 \frac{\partial^2 \phi_2}{\partial x^2} \tag{2.6}$$

The respective symbols ϕ, a and t denote total velocity potential, sound speed and time.

For the analysis it is convenient to express the total velocity potential of the channel gas (ϕ_1) and the driver gas (ϕ_2) in a more basic form consisting of the sum of velocity potentials of individual waves in the channel and driver respectively. The new forms of ϕ_1 and ϕ_2, and related expressions for overpressure and particle velocity, are summarized below.

Channel ($x > x_o$):
$$\phi_1 = \sum_{i=1}^{\infty} \left[g_i(\xi)\, H\{\xi - 2(i-1)a_1/a_2 + 1\} \right] \tag{2.7}$$

$$\Delta p_1 = -\rho_1 \frac{\partial \phi_1}{\partial t} \tag{2.8}$$

$$\Delta u_1 = \frac{\partial \phi_1}{\partial x} = \frac{\Delta p_1}{a_1 \rho_1} \tag{2.9}$$

Driver ($0 < x < x_o$):
$$\phi_1 = \frac{-\Delta p_o t}{\rho_2} + \sum_{i=1}^{\infty} \left[f_i(\eta)\, H\{\eta - 2i + 1\} + h_i(\beta)\, H\{\beta - 2i + 1\} \right] \tag{2.10}$$

$$\Delta p_2 = -\rho_2 \frac{\partial \phi_2}{\partial t} \tag{2.11}$$

$$\Delta u_2 = \frac{\partial \phi_2}{\partial x} \tag{2.12}$$

In the above expressions: ρ denotes density; the respective nondimensional variables ξ, η, β equal $(a_1t - x)/x_o$, $(a_2t + x)/x_o$ and $(a_2t - x)/x_o$; $g_i(\xi)$, $f_i(\eta)$ and $h_i(\beta)$ denote the velocity potentials of the i^{th} disturbances as illustrated in Fig. 6; and $H\{T_i\}$ denotes the unit step function which equals zero prior to the arrival of the i^{th} wave ($T_i < 0$) and equals unity after the passage of the i^{th} wave front ($T_i > 0$). The form of the total velocity potentials ϕ_1 (Eq. 2.7) and ϕ_2 (Eq. 2.10) are quite general but not arbitrary, as they have been chosen to satisfy both their respective wave equations (Eqs. 2.5 and 2.6) and their associated initial conditions (Eqs. 2.1 and 2.2 and Eqs. 2.3 and 2.4). As an example of satisfying the initial conditions the term $-\Delta p_o t/\rho_2$ in Eq. 2.10 accounts for the pressure difference across the diaphragm (Δp_o) for time t less than zero.

The presently unknown velocity potentials $g_i(\xi)$, $f_i(\eta)$ and $h_i(\beta)$ can now be determined by evaluating the effects of two different boundaries on the wave motion. The first boundary to be considered is the closed end of the driver. At this stationary boundary the particle velocity of the driver gas must be zero for all time. By setting the particle velocity of the driver gas Δu_2 (Eqs. 2.10 and 2.12) equal to zero at this boundary where distance x equals zero the following intermediate result can be obtained.

$$\sum_{i=1}^{\infty} \left[f_i'(\eta)\, H\{\eta - 2i + 1\} - h_i'(\beta)\, H\{\beta - 2i + 1\} \right] = 0 \qquad (2.13)$$

The prime (') denotes differentiation of the variable with respect to the argument given in the following brackets. Owing to the mathematical structure of this expression (Eq. 2.13) it will in general be identically zero for all time if and only if certain terms having equivalent step functions cancel exactly. As η and β both equal a_2t/x_o at the boundary x equals zero, the lengthy expression of Eq. 2.13 can consequently be expressed in the following equivalent and more convenient form.

$$h_i'(\beta) = f_i'(\eta) \qquad i = 1, 2, \ldots, \infty \qquad (2.14)$$

On integrating each one of these first-order differential equations with respect to time, and after setting the constants of integration equal to zero as they are arbitrary, the following desired result can be obtained.

$$h_i(\beta) = f_i(\eta) \qquad i = 1, 2, \ldots, \infty \qquad (2.15)$$

These results illustrate that the particle velocity of the i^{th} wave having a velocity potential $f_i(\eta)$ is countered exactly at the closed end of the driver by the particle velocity of the corresponding i^{th} reflected wave having a velocity potential $h_i(\beta)$, thereby having a net particle velocity of zero at this stationary boundary.

The second boundary to be considered is the interface of the driver and channel gases. At this contact surface the overpressure and particle velocity are taken to be continuous, and the effects of diffusion, heat transfer and turbulent mixing are neglected. The matching of the driver and channel gas overpressures and particle velocities at the contact surface can be difficult mathematically because the contact surface is not stationary nor is its motion known a priori. To circumvent this difficulty the effects of the contact-surface motion are assumed to be negligible and the matching procedure is performed at the diaphragm station - a fixed or stationary location x_o.

For the first step in the matching procedure at the diaphragm station ($x = x_o$) the overpressures of the channel gas Δp_1 (Eqs. 2.7 and 2.8) and the driver gas Δp_2 (Eqs. 2.10 and 2.11) are equated, yielding the following intermediate result.

$$a_1\rho_1 \sum_{i=1}^{\infty} \left[g_i'(\xi)\ H\{\xi - 2(i-1)a_1/a_2 + 1\} \right] = -\Delta p_o x_o$$

$$+ a_2\rho_2 \sum_{i=1}^{\infty} \left[f_i'(\eta)\ H\{\eta-2i+1\} + h_i'(\beta)\ H\{\beta-2i+1\} \right] \qquad (2.16)$$

For this boundary ($x = x_o$) ξ equals $(a_1t - x_o)/x_o$, β equals $(a_2t - x_o)/x_o$ and η equals $(a_2t + x_o)/x_o$. Certain terms in Eq. 2.16 consequently have equivalent step functions, which can be grouped accordingly, such that Eq. 2.16 can be rewritten in the following equivalent and more convenient form.

$$a_1\rho_1\ g_1'(\xi) = -\Delta p_o x_o + a_2\rho_2\ f_1'(\eta) \qquad i = 1 \qquad (2.17)$$

$$a_1\rho_1\ g_i'(\xi) = a_2\rho_2\ h_{i-1}'(\beta) + a_2\rho_2\ f_i'(\eta) \qquad i = 2, 3, \ldots, \infty \qquad (2.18)$$

The first expression (Eq. 2.17) shows that at the contact surface the overpressure of the first (shock) wave in the channel (g_1) matches exactly the sum of the initial overpressure in the driver (Δp_o) and the overpressure of the first (rarefaction) wave in the driver (f_1). The second expression (Eq. 2.18) shows that, for the i^{th} wave interaction at the contact surface (see Fig. 6), the sum of the overpressures of the incident wave (h_{i-1}) and reflected wave (f_i) matches exactly the overpressure of the transmitted wave (g_i).

The second and final step of the matching procedure at the diaphragm station ($x = x_o$) is to equate the particle velocity of the channel gas Δu_1 (Eqs. 2.7 and 2.9) to that of the driver gas Δu_2 (Eqs. 2.10 and 2.12), giving the following intermediate result.

$$\sum_{i=1}^{\infty} \left[g_i'(\xi)\, H\{\xi - 2(i-1)a_1/a_2 + 1\} \right] =$$

$$\sum_{i=1}^{\infty} \left[h_i'(\beta)\, H\{\beta - 2i + 1\} - f_i'(\eta)\, H\{\eta - 2i + 1\} \right] \qquad (2.19)$$

Like the previous result for the overpressure (Eq. 2.16) certain terms in Eq. 2.19 have equivalent step functions, which can be grouped accordingly, and Eq. 2.19 rewritten as shown below.

$$g_1'(\xi) = -f_1'(\eta) \qquad i=1 \qquad (2.20)$$

$$g_i'(\xi) = h_{i-1}'(\xi) - f_i'(\eta) \qquad i=2, 3, \ldots, \infty \qquad (2.21)$$

The first expression (Eq. 2.20) shows that at the contact surface the particle velocity of the first (shock) wave in the channel (g_1) matches exactly that of the first (rarefaction) wave in the driver (f_1). The second expression (Eq. 2.21) shows that, for the i^{th} wave interaction at the contact surface (see Fig. 6), the sum of the particle velocities of the incident wave (h_{i-1}) and reflected wave (f_i) matches exactly the particle velocity of the transmitted wave (g_i).

There is actually a third boundary which is the end of the shock-tube channel. However, this boundary need not be considered here as it has already been implicitly assumed that the channel is either infinitely long or terminated by a perfect reflection eliminator such that no reflected or other waves arise from this boundary.

Now that the matching procedure has been completed the resulting equations can be used to obtain final expressions for the i^{th} velocity potentials $g_i(\xi)$, $f_i(\eta)$ and $h_i(\beta)$. From Eqs. 2.17 and 2.20, which are simultaneous expressions in $g_1'(\xi)$ and $f_1'(\eta)$, one can obtain $g_1'(\xi)$ and $f_1'(\eta)$ explicitly. In a similar manner, from Eqs. 2.18 and 2.20, $g_i'(\xi)$ and $f_i'(\eta)$ for i greater than unity can be obtained in terms of $h_{i-1}(\beta)$. These results are summarized below.

$$g_1'(\xi) = \frac{-\Delta p_o x_o}{a_1\rho_1 + a_2\rho_2} \qquad i=1$$

$$g_i'(\xi) = \frac{2a_2\rho_2}{a_1\rho_1 + a_2\rho_2}\, h_{i-1}'(\beta) \qquad i=2, 3, \ldots, \infty \qquad (2.22)$$

$$f_1'(\eta) = \frac{\Delta p_o x_o}{a_1\rho_1 + a_2\rho_2} \qquad i=1$$

$$f_i'(\eta) = \frac{a_1\rho_1 + a_2\rho_2}{a_1\rho_1 + a_2\rho_2}\, h_{i-1}'(\beta) \qquad i=2, 3, \ldots, \infty \qquad (2.23)$$

Then, in a straight-forward procedure using Eqs. 2.14, 2.22 and 2.23, explicit expressions can be obtained for $g_i'(\xi)$, $f_i'(\eta)$ and $h_i'(\beta)$. These expressions can be easily integrated to yield the final results for $g_i(\xi)$, $f_i(\eta)$ and $h_i(\beta)$, which are given below.

$$g_1(\xi) = \frac{-\Delta p_o \, x_o \, \xi}{a_1\rho_1 + a_2\rho_2} \qquad i=1$$

$$g_i(\xi) = \left[\frac{a_1\rho_1 - a_2\rho_2}{a_1\rho_1 + a_2\rho_2}\right]^{i-2} \frac{2a_2\rho_2 \, \Delta p_o \, x_o \, \xi}{(a_1\rho_1 + a_2\rho_2)^2} \qquad i=2, 3, \ldots, \infty \tag{2.24}$$

$$f_i(\xi) = \left[\frac{a_1\rho_1 - a_2\rho_2}{a_1\rho_1 + a_2\rho_2}\right]^{i-1} \frac{\Delta p_o \, x_o \, \eta}{a_1\rho_1 + a_2\rho_2} \qquad i=1, 2, \ldots, \infty \tag{2.25}$$

$$h_i(\beta) = \left[\frac{a_1\rho_1 - a_2\rho_2}{a_1\rho_1 + a_2\rho_2}\right]^{i-1} \frac{\Delta p_o \, x_o \, \beta}{a_1\rho_1 + a_2\rho_2} \qquad i=1, 2, \ldots, \infty \tag{2.26}$$

Note that the constants of integration have all been set equal to zero because they are arbitrary, and $g_i'(\xi)$, $f_i'(\eta)$ and $h_i'(\beta)$ can be easily recovered by differentiation. Also, these final expressions for $g_i(\xi)$, $f_i(\eta)$ and $h_i(\beta)$ are valid away from the two boundaries x equal to zero and x_o as x in ξ, η and β need no longer be restricted to zero or x_o.

The solution for the wave motion in a rectangular shock tube utilizing different driver and channel gases has now been obtained. The final results for the i^{th} velocity potentials $g_i(\xi)$, $f_i(\eta)$ and $h_i(\beta)$ (Eqs. 2.24, 2.25 and 2.26) can be substituted into the expressions for the total velocity potentials ϕ_1 and ϕ_2 (Eqs. 2.7 and 2.10). Then the two respective expressions for the overpressure and particle velocity of the channel gas follow from Eqs. 2.8 and 2.9, and those for the driver gas follow from Eqs. 2.11 and 2.12.

It can be seen from the solution of the wave motion in the rectangular shock tube that the specific impedances of the channel gas ($a_1\rho_1$) and the driver gas ($a_2\rho_2$) play an important role. In fact, the important parameter is the ratio of these specific impedances. This ratio is denoted by the symbol $\mathcal{B}$ and it can be expressed in the following alternate forms by using the equation of state ($p=\rho RT$) and the isentropic sound-speed relation ($a^2 = \gamma p/\rho = \gamma R_o T/M$).

$$\mathcal{B} = \frac{a_2\rho_2}{a_1\rho_1} = \frac{\gamma_2 a_1}{\gamma_1 a_2} = \left[\frac{\gamma_2 \, M_2 \, T_1}{\gamma_1 \, M_1 \, T_2}\right]^{\frac{1}{2}} \tag{2.27}$$

The respective symbols γ, p, R, T, R_o and M denote the specific heat ratio, pressure, gas constant, temperature, universal gas constant ($R_o = MR$) and molecular weight. It is worth mentioning that the impedance ratio $\mathcal{B}$ equals unity not only for the simplest case of identical driver and channel gases having the same temperatures but also for the specific case of different

driver and channel gases provided that $\gamma_1 M_1/T_1$ equals $\gamma_2 M_2/T_2$. Furthermore, the impedance ratio ε equals $(\gamma_2 M_2/\gamma_1 M_1)^{\frac{1}{2}}$ for the very important case of different driver and channel gases having equal temperatures, and ε equals $(T_1/T_2)^{\frac{1}{2}}$ for the not so practicable case of identical driver and channel gases having different temperatures.

A set of values of the specific impedance ratio ε ($a_2\rho_2/a_1\rho_1 = (\gamma_2 M_2/\gamma_2 M_2)^{\frac{1}{2}}$ if $T_1=T_2$) was compiled for certain interesting different combinations of driver and channel gases having identical temperatures, and they are given in Table 2. The smallest values of ε occur when a light driver gas such as hydrogen (H_2) or helium (He) is used in conjunction with a heavy channel gas such as dichlorodifluoromethane ($CCl_2 F_2$), sulfer hexafluoride (SF_6) or octafluorocyclobutane ($C_4 F_8$). On the other hand the largest values of ε occur when the driver gas has a high molecular weight and the channel gas has a low molecular weight. For nearly equivalent molecular weights of the driver and channel gases the specific impedance ratio is always nearly equal to unity.

The wave that propagates in the channel gas is one of the most important features of the wave motion. For this reason the signature of pressure signature, as derived from Eqs. 2.7, 2.8, 2.24 and 2.27, is given below:

$$\Delta p_1 = \frac{\Delta p_o}{1+\varepsilon} H\{\xi + 1\} - \sum_{i-2}^{\infty}\left[\frac{2\varepsilon\, \Delta p_o}{(1+\varepsilon)^2} \left(\frac{1-\varepsilon}{1+\varepsilon}\right)^{i-2} H\{\xi - 2(i-1)\frac{a_1}{a_2} + 1\}\right] \quad (2.28)$$

After the arrival of the first shock wave (g_1) at time $(x-x_o)/a_1$ at a fixed distance x in the channel, each successive wave (g_i) arrives at time $(x-x_o)/a_1 + 2(i-1)x_o/a_2$, or after equal time intervals of $2x_o/a_2$. Each successive wave has an initial overpressure of zero and features a sudden change in overpressure at its wave front to a constant value thereafter. The first wave has an amplitude of $\Delta p_o/(1+\varepsilon)$, and each of the following waves has a successively smaller amplitude by virtue of the factor $(1-\varepsilon)/(1+\varepsilon)$ raised to the power i-2. Because each successive wave is superposed on the previous ones the total overpressure signature consists of an infinite sequence of constant overpressure segments, each segment having a duration of $2x_o/a_2$. The sum of terms giving each segment of the signature has the form of a finite geometric progression. Consequently the following geometric sequence can be derived for the amplitude of the i^{th} segment.

$$\left[\frac{1-\varepsilon}{1+\varepsilon}\right]^{i-1} \frac{\Delta p_o}{1+\varepsilon} \qquad i=1, 2, \ldots, \infty \quad (2.29)$$

This expression is more convenient to use when constructing the overpressure signature than Eq. 2.28.

Five different predicted overpressure signatures of the wave moving in the channel are shown in Fig. 7, corresponding to specific impedance ratios (ε) of 0.2, 0.5, 1.0, 2.0 and 5.0. Although these impedance ratios represent general cases of different driver and channel gases having different tempera-

tures, various important combinations of equivalent-temperature driver and channel gases which have such impedance ratios and would thus produce such signatures can be readily deduced from the information given in Table 2. The top two signatures in Fig. 7 for the case of a light driver gas and a heavy channel gas (low ε values of 0.2 and 0.5) exhibit a series of very noticeable descending 'steps' and have relatively high peak overpressures ($0.83\Delta p_o$ and $0.67\Delta p_o$) for a given pressure difference across the diaphragm (Δp_o). In general the duration of each constant overpressure segment ($2x_o/a_2$) would be relatively short because the sound speed of a light or heated driver gas (a_2) in relatively high (see the information in Table 2 on the sound speed of different driver gases). The center signature for the case when ε has the value of unity exhibits a single step having an amplitude of $0.5\Delta p_o$ and a duration of $2x_o/a_2$. This signature corresponds to the well-known case of identical driver and channel gases having the same temperature. However, it can also correspond to the specific case of different driver and channel gases provided $\gamma_2 M_1/T_1$ equals $\gamma_2 M_2/T_2$. The bottom two signatures for the case of a heavy driver gas and a light channel gas (high values of ε of 2 and 5) exhibit a series of steps that alternate markedly in amplitude from positive to negative values as they diminish in absolute magnitude. The relatively low peak overpressure of these two signatures ($0.33\Delta p_o$ and $0.17\Delta p_o$) in comparison to the pressure difference across the diaphragm (Δp_o) illustrates the inefficiency of using a heavy driver gas to produce a relatively strong wave in a light channel gas. Note that these two signatures will have relatively long durations because the sound speed of the heavy driver gases will generally be low.

The particle-velocity signature of the wave moving in the channel gas has the same features as the overpressure profile, because the particle velocity of this planar wave is directly proportional to the overpressure ($\Delta u_1 = \Delta p_1/a_1\rho_1$). The preceding remarks concerning the overpressure profile therefore apply equally well to the particle-velocity signature.

The motion of the channel gas and contact surface, owing to the wave motion in the rectangular shock tube, can be determined in the following manner. The particle-velocity signature like the overpressure profile consists of a sequence of descending or alternating constant overpressure steps or segments. The particle velocity ($\Delta u_1 = \Delta p_1/a_1\rho_1$) associated with the i^{th} segment of its profile follows from Eq. 2.29 for the overpressure and is given below.

$$\frac{1}{1+\varepsilon}\left[\frac{1-\varepsilon}{1+\varepsilon}\right]^{i-1}\frac{\Delta p_o}{a_1\rho_1} \qquad i = 1, 2, \ldots, \infty \qquad (2.30)$$

During each constant particle-velocity segment of the profile, which has a fixed duration of $2x_o/a_2$, the particle path will be a linear function of time. The displacement of a fluid particle by the i^{th} segment of the wave is thus equal to the result of Eq. 2.30 multiplied by $2x_o/a_2$. The accumulated displacement of a fluid particle after n successive segments of duration $2x_o/a_2$, or at successive times $2nx_o/a_2$ measured from the wave front, can be determined by addition, and this result is shown below.

$$\sum_{i=1}^{n}\left[\frac{1}{1+\varepsilon}\left[\frac{1-\varepsilon}{1+\varepsilon}\right]^{i-1}\frac{\Delta p_o}{a_1\rho_1}\quad\frac{2x_o}{a_2}\right]\qquad n=1,2,\ldots,\infty \tag{2.31}$$

Because this sum is in the form of a geometric progression, Eq. 2.31 can be easily expressed in an alternate and shorter form. By noting that a_2^2 equals $\gamma_2 p_2/\rho_2$ or $\gamma_2 p_1/\rho_2$ to first order, the final expression for Eq. 2.31 takes the following form.

$$\left[1-\left(\frac{1-\varepsilon}{1+\varepsilon}\right)^{n}\right]\frac{\Delta p_o\, x_o}{\gamma_2\, p_1}\qquad n=1,2,\ldots,\infty \tag{2.32}$$

In summary, this expression gives the displacement of a fluid particle $x-x_*$ from its initial location x_* at successive times $2nx_o/a_2$ measured from the wave front. The displacement during each time interval $2x_o/a_2$ is a linear function of time.

The wave moving in the channel gas induces the same displacement $x-x_*$ for each fluid particle because its predicted signature and amplitude are invariant with distance. Consequently, the contact-surface displacement $x-x_o$ is also given by Eq. 2.32. The total displacement of any fluid particle and also the contact surface for large times ($n\to\infty$) becomes independent of the specific impedance ratio (ε) and tends to a constant value of $\Delta p_o\, x_o/\gamma_2\, p_1$. This total displacement is normally small when compared with the driver length (x_o). For example, even if the pressure difference across the diaphragm (Δp_o) is quite high at $p_1/20$ (one twentieth of an atmosphere) and γ_2 equals 1.4 for a diatomic driver gas, the total displacement is only $x_o/28$ or 3.6% of the driver length. Note that the original assumption for the analysis that the contact-surface displacement was negligible compared with the driver length was therefore very reasonable.

Three different particle paths corresponding to values of the specific impedance ratio ε of 0.2, 1.0 and 5.0 are shown superposed on the time-distance diagram in Fig. 8. The displacement $x-x_*$ of a fluid particle from its initial location x_* has been exaggerated for clarity. For the case when ε equals 0.2 the displacement increases monotomically to its maximum value of $\Delta p_o\, x_o/\gamma_2\, p_1$. This particle-path behaviour is typical for the case when ε lies in the range from zero to unity, or when a light driver gas is used in conjunction with a heavy channel gas. For a driver and channel gas having a specific impedance ratio of unity the displacement increases linearly to its maximum value $\Delta p_o\, x_o/\gamma_2\, p_1$ in a time interval of $2x_o/a_2$, after which the displacement is constant. For cases when the specific impedance ratio is greater than unity the displacement alternately increases and decreases linearly as the final value $\Delta p_o\, x_o/\gamma_2\, p_1$ is approached, as illustrated in Fig. 8 by the particle path for which ε equals 5.

The final displacement of the contact surface $x-x_o$, which equals $\Delta p_o\, x_o/\gamma_2\, p_1$, can be derived in an alternate manner, thereby providing a valuable independent check on the results of the preceding analysis for the rectangular shock tube. Let the driver gas have an initial pressure of $p_1 + \Delta p_o$ and an initial density given by m_o/Ax_o, where m_o is the total mass of the driver gas, Ax_o is the driver volume and A is the cross-sectional area of the shock tube. Now let the driver gas expand isentropically (as

it would for acoustic wave motion) to a final density of m_o/Ax and a final pressure of p_1 which is the initial pressure of the channel gas. The following isentropic expression relating the initial and final pressures and densities can therefore be applied.

$$\frac{p_1 + \Delta p_o}{p_1} = \left[\frac{m_o/Ax_o}{m_o/Ax}\right]^{\gamma_2} = \left[\frac{x_o + x - x_o}{x_o}\right]^{\gamma_2} \tag{2.33}$$

Consequently, to first order, the final contact-surface displacement $x-x_o$ equals $\Delta p_o\, x_o/\gamma_2\, p_1$, in exact agreement with the result of the previous acoustic analysis.

A further interesting and independent check on the acoustic analysis for the rectangular shock tube is provided by conventional shock-tube theory, which can be found in Ref. 17. For a constant-area shock tube utilizing perfect driver and channel gases having a small or large pressure difference across the diaphragm (Δp_o), the following conventional shock-tube equation can be used to predict the peak overpressure (Δp_1) of the constant-amplitude shock wave in the channel gas.

$$\left[1 + \frac{\Delta p_o}{p_1}\right] = \left[1 + \frac{\Delta p_1}{p_1}\right]\left[1 - \frac{(\gamma_2-1)(a_1/a_2)(\Delta p_1/p_1)}{\sqrt{2\gamma_1(\gamma_1-1)\,\Delta p_1/p_1 + 4\gamma_1^2}}\right]^{\frac{-2\gamma_2}{\gamma_2-1}} \tag{2.34}$$

From this equation it can be easily shown that, when Δp_o is much smaller that p_1, the peak overpressure of the first shock wave (Δp_1) equals $\Delta p_o/(1+\varepsilon)$, in exact agreement with the corresponding result of the previous acoustic analysis. It is worth mentioning that although the conventional shock-tube equation is valid for large as well as small pressure differences across the diaphragm, the equation is limited in that it can predict the amplitude of only the first but most important part of the wave in the channel gas. Admittedly, additional shock-tube theory can be applied to predict the complete wave motion for all time in the constant-area shock tube. However, the procedure is prohibitively difficult. Consequently, the acoustic solution for the complete wave motion in the shock tube, even though it is restricted to acoustic waves, is very valuable.

Some overpressure measurements were made in the channel of a constant-area shock tube, in order to provide an experimental check on the validity of the acoustic analysis for the rectangular shock tube. Three of the measured overpressure signatures are presented in Fig. 9. For the profile shown in Fig. 9a the driver and channel gases were both air having the same temperature. The profile shown in Fig. 9b corresponds to the case of helium in the driver and equivalent-temperature air in the channel. For the opposite case of air in the driver and helium in the channel, the signature appears in Fig. 9c. Other pertinent data are given in the figure. Qualitatively the measurements substantiate the main features of the acoustic solution.

For a quantitative comparison of measured and predicted overpressure signatures the measured results of Fig. 9 have been reproduced in Fig. 10 and compared directly with the predicted signatures. Even for these extremely strong acoustic waves (amplitudes of about 5 kN/m^2 or one-twentieth of an atmosphere) the predicted and measured profiles are in good agreement. From experimental data such as those shown in Fig. 9 it was found that the acoustic analysis was still valid when the pressure difference across the diaphragm (Δp_o) was as high as 25 kN/m^2, giving wave amplitudes of approximately 10 kN/m^2. Note that one of the main differences between measured and predicted signatures is that the rapid changes in overpressure in each experimental profile are not instantaneous (see Fig. 9). The long rise time of about 0.5 ms associated with each of these shocks is due to poor diaphragm breakage resulting from the relatively small pressure difference across the diaphragm.

3. PYRAMIDAL SHOCK TUBE

3.1 General Solution

The pyramidal shock tube, which is depicted in Fig. 2b, consists essentially of both a pyramidal driver and channel having the same divergence angle and joined at a common-area station where a suitable diaphragm can be installed. This diaphragm separates a normally atmospheric pressure channel gas from a slightly higher pressure driver gas. For generality of the analysis, which follows that in Chapter 2, let the initially quiescent driver and channel gases be different and also have different temperatures. Before the diaphragm is broken the appropriate initial conditions can be summarized mathematically as follows.

Channel ($r > r_o$): $\Delta p_1 = 0$ (3.1)

$\Delta u_1 = 0$ (3.2)

Driver ($0 < r < r_o$): $\Delta p_2 = \Delta p_o$ (3.3)

$\Delta u_2 = 0$ (3.4)

The respective symbols Δp, Δu, and Δp_o denote overpressure, particle velocity, and pressure difference across the diaphragm, whereas the respective subscripts 1 and 2 refer the appropriate symbols to the channel and driver gases. The radial distance r is measured along the shock tube starting from the apex of the pyramid as shown in Fig. 2b, and the diaphragm is located at a distance r_o, thereby making the driver length equal to r_o.

For the preceding initial conditions the ensuing wave motion in the pyramidal shock tube after the diaphragm is broken is rather complex. This wave motion can be depicted conveniently on a time-distance diagram, as shown in Fig. 6, where the locus of each wave front has been drawn. On breaking the diaphragm in the shock tube the resulting rapidly expanding driver gas produces a weak shock wave (g_1) in the channel gas. Simultaneously a weak rarefaction wave (f_1) moves into the driver gas and eventually reaches and reflects from the driver apex. This reflected wave (h_1) propagates through the driver gas and interacts with the contact surface or interface of the driver

and channel gases. Because the contact-surface displacement is normally negligible in comparison with the driver length, the contact-surface path is shown in Fig. 6 simply as a vertical dashed line. Owing to the change in specific impedance (product of the density and sound speed) across the contact surface the reflected wave (h_1) is partially transmitted to the channel (g_2) and partially reflected back into the driver (f_2). The subsequent oscillatory wave motion between the contact surface and driver apex creates a sequence of waves in the channel. The integrated result of all of these individual waves (g_i, $i = 1, 2, \ldots, \infty$) yields the total wave in the channel.

For a low-pressure-ratio pyramidal shock tube for which the pressure difference across the diaphragm Δp_o is much less than the absolute pressure of the channel gas, the waves in the driver and channel are relatively weak. The wave motion can consequently be described adequately by using well-known acoustic theory. The one-dimensional spherical wave equations which govern the acoustic wave motion in the channel and driver gases are given below.

Channel ($r > r_o$):
$$\frac{\partial^2(r\phi_1)}{\partial t^2} = a_1^2 \frac{\partial^2(r\phi_1)}{\partial r^2} \tag{3.5}$$

Driver ($0 < r < r_o$):
$$\frac{\partial^2(r\phi_2)}{\partial t^2} = a_2^2 \frac{\partial^2(r\phi_2)}{\partial r^2} \tag{3.6}$$

The respective symbols ϕ, a and t denote the total velocity potential, sound speed and time.

For the analysis it is convenient to express the total velocity potential of the channel gas (ϕ_1) in its more basic form consisting of the sum of velocity potentials of individual waves in the channel. This is similarly so for the total velocity potential of the driver gas (ϕ_2). The new forms, and the related expressions for overpressure and particle velocity, are all summarized below.

Channel ($r > r_o$):
$$\phi_1 = \frac{1}{r} \sum_{i=1}^{\infty} \left[g_i'(\xi)\, H\{\xi - 2i + 2\} \right] \tag{3.7}$$

$$\Delta p_1 = -\rho_1 \frac{\partial \phi_1}{\partial t} \tag{3.8}$$

$$\Delta u_1 = \frac{\partial \phi_1}{\partial r} \tag{3.9}$$

Driver ($0 < r < r_o$):

$$\Phi_2 = - \frac{\Delta p_o \, t}{\rho_2} + \frac{1}{r} \sum_{i=1}^{\infty} \left[f_i'(\eta) \, H\{\eta - 2i + 1\} + h_i'(\beta) \, H\{\beta - 2i + 1\} \right] \tag{3.10}$$

$$\Delta p_2 = - \rho_2 \frac{\partial \Phi_2}{\partial t} \tag{3.11}$$

$$\Delta u_2 = \frac{\partial \Phi_2}{\partial r} \tag{3.12}$$

In the above expressions: ρ denotes density; the respective nondimensional variables ξ, η and β equal $(a_1 t - r + r_o)a_2/a_1 r_o$, $(a_2 t + r)/r_o$ and $(a_2 t - r)/r_o$; $g_i'(\xi)$, $f_i'(\eta)$ and $h_i'(\beta)$ denote the velocity potentials of the i^{th} disturbances (see fig. 6) and the prime (') denotes differentiation of the variable with respect to the argument given in the following brackets; and $H\{T_i\}$ denotes the unit step function which equals zero prior to the arrival of the i^{th} wave ($T_i < 0$) and equals unity after the arrival of its wave front ($T_i > 0$). The form of the total velocity potentials Φ_1 and Φ_2 (Eqs. 3.7 and 3.10) are quite general but not arbitrary, as they have been chosen to satisfy both their respective wave equations (Eqs. 3.5 and 3.6) and their associated initial conditions (Eqs. 3.1 and 3.2 and Eqs. 3.3 and 3.4). As an example of satisfying the initial conditions the term $-\Delta p_o \, t/\rho_2$ in Eq. 3.10 accounts for the pressure difference across the diaphragm (Δp_o) for time t less than zero.

The presently known velocity potentials $g_i'(\xi)$, $f_i'(\eta)$ and $h_i'(\beta)$ can now be determined by evaluating the effects of two different boundaries on the wave motion. The first boundary to be considered is the driver apex. At this stationary boundary the particle velocity of the driver gas must be zero for all time. By setting the particle velocity of the driver gas Δu_2 (Eqs. 3.10 and 3.12) equal to zero at this boundary where distance r is allowed to approach zero the following intermediate result can be obtained.

$$\lim_{r \to 0} \left[\frac{r_o}{r} \sum_{i=1}^{\infty} \left(f_i''(\eta) \, H\{\eta - 2i + 1\} - h_i''(\beta) \, H\{\beta - 2i + 1\} \right) \right.$$

$$\left. - \frac{r_o^2}{r^2} \sum_{i=1}^{\infty} \left(f_i'(\eta) \, H\{\eta - 2i + 1\} + h_i'(\beta) \, H\{\beta - 2i + 1\} \right) \right] = 0 \tag{3.13}$$

In the limit when r equals zero the following result can be obtained.

$$\sum_{i=1}^{\infty} \left[f_i'(\eta) \, H\{\eta - 2i + 1\} + h_i'(\beta) \, H\{\beta - 2i + 1\} \right] = 0 \tag{3.14}$$

Owing to the mathematical structure of Eq. 3.14 this expression will in general be identically zero for all time if and only if certain terms having equivalent step functions cancel exactly. As η and β both equal $a_2 t/r_o$ at

the boundary r equal to zero, the lengthy Eq. 3.14 can consequently be rewritten in the following equivalent and more convenient form.

$$h_i'(\beta) = -f_i'(\eta) \qquad i=1, 2,\ldots,\infty \tag{3.15}$$

This result illustrates that the particle velocity of the i^{th} wave having a velocity potential $f_i'(\eta)$ is countered exactly at the driver apex by the particle velocity of the corresponding reflected wave having a velocity potential $h_i'(\beta)$, thereby leaving no net particle velocity at the stationary boundary.

The second boundary to be considered is the interface of the driver and channel gases. At the contact surface the overpressure and particle velocity are taken to be continuous after the diaphragm is removed, and the effects of diffusion, heat transfer and turbulent mixing are neglected. The matching of the driver and channel gas overpressures and particle velocities at the contact surface can be difficult mathematically because the contact surface is not stationary nor is its motion known apriori. To circumvent this difficulty the effects of the contact-surface motion are assumed to be negligible and the matching procedure is done at the diaphragm station - a fixed or stationary location r_o.

For the first step in the matching procedure at the diaphragm station ($r=r_o$) the overpressure of the channel gas Δp_1 (Eqs. 3.7 and 3.8) and the driver gas Δp_2 (Eqs. 3.10 and 3.11) are equated, thereby yielding the following intermediate result.

$$\rho_1 \sum_{i=1}^{\infty} \left[g_i''(\xi)\, H\{\xi-2i+2\} \right] = -\Delta p_o\, r_o^2/a_2 + \rho_2 \sum_{i=1}^{\infty} \left[f_i''(\eta)\, H\{\eta-2i+1\} + h_i''(\beta)\, H\{\beta-2i+1\} \right] \tag{3.16}$$

For the boundary in question for which r equals r_o, ξ equals $a_2 t/r_o$, η equals $(a_2 t + r_o)/r_o$ and β equals $(a_2 t - r_o)/r_o$. Certain terms in Eq. 3.16 consequently have equivalent step functions, which can be grouped accordingly, and expressed in the following equivalent and more convenient form.

$$\rho_1\, g_1''(\xi) = -\Delta p_o\, r_o^2/a_2 + \rho_2\, f_1''(\eta) \qquad i=1 \tag{3.17}$$

$$\rho_1\, g_i''(\xi) = \rho_2\, h_{i-1}''(\beta) + \rho_2\, f_i''(\eta) \qquad i=2, 3,\ldots,\infty \tag{3.18}$$

The first expression (Eq. 3.17) shows that at the contact surface the overpressure of the first (shock) wave in the channel (g_1) matches exactly the sum of the initial overpressure in the driver (Δp_o) and the overpressure of

the first (rarefaction) wave in the driver (f_1). The second expression (Eq. 3.18) shows that, for the i^{th} wave interaction at the contact surface (see Fig. 6), the sum of the overpressures of the incident wave (h_{i-1}) and reflected wave (f_i) matches exactly the overpressure of the transmitted wave (g_i).

Equation 3.17 and 3.18 can be integrated with respect to time to yield the following useful results.

$$\rho_1 g_1'(\xi) = -\Delta p_o r_o t + \rho_2 f_1'(\eta) \qquad i=1 \tag{3.19}$$

$$\rho_1 g_i'(\xi) = \rho_2 h_{i-1}'(\beta) + \rho_2 f_i'(\eta) \qquad i=2, 3,\ldots,\infty \tag{3.20}$$

The constants of integration are each equal to zero because the velocity potentials $g_i'(\xi)$, $f_i'(\eta)$ and $h_i'(\beta)$ are each equal to zero at their respective wave fronts. Note that Eqs. 3.19 and 3.20 illustrate that the product of density and velocity potential ($\rho\Phi$) is continuous at the contact surface after the diaphragm has been removed, just like the overpressure (Δp) and particle velocity (Δu).

The second and final step of the matching procedure at the diaphragm station ($r=r_o$) is to equate the particle velocity of the channel gas Δu_1 (Eqs. 3.7 and 3.9) with that of the driver gas Δu_2 (Eqs. 3.10 and 3.12), thereby giving the following intermediate result.

$$\sum_{i=1}^{\infty}\left[\left(\frac{a_2}{a_1} g_i''(\xi) + g_i'(\xi)\right) H\{\xi-2i+2\}\right] =$$

$$\sum_{i=1}^{\infty}\left[\left(h_i''(\beta) + h_i'(\beta)\right) H\{\beta-2i+1\} - \left(f_i''(\eta) - f_i'(\eta)\right) H\{\eta-2i+1\}\right] \tag{3.21}$$

Like the previous result for the overpressure (Eq. 3.16) certain terms in Eq. 3.21 have equivalent step functions, which can be grouped accordingly, and expressed in the following equivalent and more useful form.

$$\frac{a_2}{a_1} g_1''(\xi) + g_1'(\xi) = -f_1''(\eta) + f_1'(\eta) \qquad i=1 \tag{3.22}$$

$$\frac{a_2}{a_1} g_i''(\xi) + g_i'(\xi) = h_{i-1}''(\beta) + h_{i-1}'(\beta) - f_i''(\eta) + f_i'(\eta) \qquad i=2, 3,\ldots,\infty \tag{3.23}$$

The first expression (Eq. 3.22) shows that at the contact surface the particle velocity of the first (shock) wave in the channel (g_1) matches that of the first (rarefaction) wave in the driver (f_1). The second expression Eq. 3.23 shows that, for the i^{th} wave interaction at the contact surface (see Fig. 6),

the sum of the particle velocities of the incident wave (h_{i-1}) and reflected wave (f_i) matches exactly the particle velocity of the transmitted wave (g_i).

There is actually a third boundary which is the large end of the pyramidal channel. However, this boundary need not be considered here as it has already been implicitly assumed that the channel is either infinitely long or terminated by a perfect reflection eliminator such that no reflected or other waves arise from this boundary.

Now that the matching procedure has been completed the resulting differential equations for $g_i(\xi)$, $f_i(\eta)$ and $h_i(\beta)$ can be cast into a more amendable form. From Eqs. 3.17, 3.19 and 3.22 one can obtain differential equations for $g_1(\xi)$ and $f_1(\eta)$. In a similar manner, from Eqs. 3.18, 3.20 and 3.23, differential equations can be obtained for $g_i(\xi)$ and $f_i(\eta)$, where i is greater than unity. These results associated with the boundary r equal to r_o and the previous result (Eq. 3.15) for the other boundary r equal to zero are summarized below.

$$g_i''(\xi) + \frac{a_1(\rho_2-\rho_1)}{a_1\rho_1+a_2\rho_2}\, g_i'(\xi) = \begin{cases} \dfrac{\Delta p_o\, r_o^2}{a_1\rho_1+a_2\rho_2}\, \dfrac{a_1}{a_2}\, (\xi-1) & i=1 \\ \dfrac{2a_2\rho_2}{a_1\rho_1+a_2\rho_2}\, \dfrac{a_1}{a_2}\, h_{i-1}''(\beta) & i=2,\ 3,\ldots,\infty \end{cases} \tag{3.24}$$

$$f_i''(\eta) + \frac{a_1(\rho_2-\rho_1)}{a_1\rho_1+a_2\rho_2}\, f_i'(\eta) = \begin{cases} \dfrac{\Delta p_o\, r_o^2}{a_1\rho_1+a_2\rho_2}\, \dfrac{a_1}{a_2}\, (\eta-1+\dfrac{a_2}{a_1}) & i=1 \\ \dfrac{a_1\rho_1-a_2\rho_2}{a_1\rho_1+a_2\rho_2}\, h_{i-1}''(\beta) - \dfrac{a_1(\rho_2-\rho_1)}{a_1\rho_1+a_2\rho_2}\, h_{i-1}'(\beta) & i=2,\ 3,\ldots,\infty \end{cases} \tag{3.25}$$

$$h_i'(\beta) = -f_i'(\eta) \qquad i=1,\ 2,\ldots,\infty \tag{3.26}$$

The above set of differential equations for $g_i(\xi)$, $f_i(\eta)$ and $h_i(\beta)$ can be uncoupled and subsequently solved to give explicit expressions for $g_i(\xi)$, $f_i(\eta)$ and $h_i(\beta)$.

A convenient initial step in solving the differential equations is to find a recurrence relationship for $f_i'(\eta)$. Using Eq. 3.26 we can rewrite Eq. 3.25 in the following form.

$$f_i''(\eta) + \frac{1}{\ell}\, f_i'(\eta) = \begin{cases} \dfrac{\Delta p_o\, r_o^2}{a_2\rho_2(\varepsilon+1)} \left[(1+\varepsilon+\ell)\, \dfrac{n-1}{\ell} + \varepsilon \right] & i=1 \\ \dfrac{\varepsilon-1}{\varepsilon+1}\, f_{i-1}''(\eta-2) + \dfrac{1}{\ell}\, f_{i-1}'(\eta-2) & i=2,\ 3,\ldots,\infty \end{cases} \tag{3.27}$$

The nondimensional parameters ε and ℓ are equal to $a_2\rho_2/a_1\rho_1$ and $(a_1\rho_1+a_2\rho_2)/a_1(\rho_2-\rho_1)$ respectively. It should be noted that $f''_{i-1}(\eta-2)$ and $f'_{i-1}(\eta-2)$ in Eq. 3.27 are expressed correctly, as the variable $\eta-2$ in the brackets (instead of simply η) is required to ensure that the function $f_{i-1}(\eta-2)$ on the right-hand side of the equation is properly phased in time with the function $f_i(\eta)$ on the left-hand side. After multiplying the i^{th} differential equation for $f_i(\eta)$ (Eq. 3.27) by $\exp[(\eta-2i+1)/\ell]$ and partially integrating with respect to time the following recurrence relation for $f'_i(\eta)$ can be obtained.

$$f'_i(\eta) = \begin{cases} \dfrac{\Delta p_o\, r_o^2\, \ell}{a_2\rho_2(\varepsilon+1)} \exp\left(-\dfrac{n-1}{\ell}\right) \displaystyle\int_o^{(\eta-1)/\ell} [(1+\varepsilon+\ell)\, y + \varepsilon] \exp(y)\, dy & i=1 \\ \dfrac{\varepsilon-1}{\varepsilon+1} f'_{i-1}(\eta-2) + \dfrac{2}{\varepsilon+1} \exp\left(-\dfrac{\eta-2i+1}{\ell}\right) \displaystyle\int_o^{(\eta-2i+1)/\ell} f'_{i-1}(\ell y+2i-3) \exp(y)\, dy & \\ & i=2,\ 3,\ldots,\infty \end{cases} \tag{3.28}$$

From these results the i^{th} velocity potential can be determined, and it is given below.

$$f'_i(\eta) = \frac{\Delta p_o\, r_o^2\, \ell}{a_2\rho_2(\varepsilon+1)} \sum_{j=1}^{i} \binom{i-1}{j-1} \left(\frac{\varepsilon-1}{\varepsilon+1}\right)^{i-j} \left(\frac{2}{\varepsilon+1}\right)^{j-1} I_j(\eta-2i+1) \tag{3.29}$$

The notation $\binom{m}{n}$ denotes the well-known binomial coefficients, which can be expressed as $m!/n!(m-n)!$, where the symbol ! denotes the factorial function. For convenience and illustrative purposes the first five velocity potentials $f'_i(\eta)$ are given in expanded form in Appendix A, along with the corresponding first four expanded functions $I'_j(\eta-2i+1)$. The functions $I_j(\eta-2i+1)$ can be expressed in the following recurrence form.

$$I'_j(\omega) = \begin{cases} \exp(-\omega/\ell) \displaystyle\int_o^{\omega/\ell} [(1+\varepsilon+\ell)y + \varepsilon] \exp(y)\, dy & j=1 \\ \exp(-\omega/\ell) \displaystyle\int_o^{\omega/\ell} I'_{j-1}(y) \exp(y)\, dy & j=2,\ 3,\ldots,\infty \end{cases} \tag{3.30}$$

Alternatively the j^{th} function $I'_j(\eta-2i+1)$ can be expressed in the following more elegant form.

$$I'_j(\omega) = \exp(-\omega/\ell) \int_o^{\omega/\ell} \ldots j \ldots \int_o^{\omega/\ell} [(1+\varepsilon+\ell)\, y + \varepsilon] \exp(y)\, dy \tag{3.31}$$

In either case the final results for the j^{th} function $I'_j(\eta-2i+1)$ can be determined, and it is given below.

$$I'_j(\omega) = (1+\varepsilon+\ell)\left(\frac{\omega}{\ell} - j\right) + \varepsilon + \sum_{k=1}^{j} \frac{k(1+\varepsilon+\ell)-\varepsilon}{(j-k)!} \left(\frac{\omega}{\ell}\right)^{j-k} \exp(-\omega/\ell) \tag{3.32}$$

The solution for the wave motion in the pyramidal shock tube utilizing different driver and channel gases has now been obtained, although further work is required to get explicit expressions for the overpressure, particle velocity and particle path of the driver and channel gases. The result for the i^{th} velocity potential $f_i'(\eta)$ as given by Eqs. 3.29 and 3.32 can now be used to obtain the i^{th} velocity potentials for $h_i'(\beta)$ and $g_i'(\xi)$. The appropriate expressions for $h_i'(\beta)$ and $g_i'(\xi)$ which stem from Eqs. 3.15, 3.19 and 3.20, are given below.

$$h_i'(\beta) = - f_i'(\beta) \qquad i = 1, 2, \ldots, \infty \tag{3.33}$$

$$g_i'(\xi) = \begin{cases} - \dfrac{\Delta\rho_o}{a_1 \rho_1} \dfrac{r_o^2}{a_2} \dfrac{a_1}{\xi} + \dfrac{\rho_2}{\rho_1} f_1'(\xi+1) & i = 1 \\ \dfrac{\rho_2}{\rho_1} f_i'(\xi+1) - \dfrac{\rho_2}{\rho_1} f_{i-1}'(\xi-1) & i = 2,3,\ldots, \infty \end{cases} \tag{3.34}$$

These results for $g_i'(\xi)$, $f_i'(\eta)$ and $h_i'(\beta)$ can be substituted into the expressions for the total velocity potentials ϕ_1 and ϕ_2 (Eqs. 3.7 and 3.10). Then the two respective expressions for the overpressure and particle velocity of the channel gas follow from Eqs. 3.8 and 3.9, and those for the driver gas follow from Eqs. 3.11 and 3.12. Although the solution is rather complex and lengthy, the overpressure and particle velocity signatures for both the channel and driver gases can be obtained fairly easily by using a digital computer.

It can be seen from the solution of the wave motion in the pyramidal shock tube that both the ratios of the driver and channel gas sound speeds (a_2/a_1) and densities (ρ_2/ρ_1) play important roles not only separately but also in a combined form (e.g., see Eqs. 3.29, 3.32 and 3.34). The important combination $a_2\rho_2/a_1\rho_1$ has been denoted by the symbol $\mathfrak{s}$. This nondimensional parameter can be expressed in the following alternate forms by using the equation of state ($p = \rho RT$) and the isentropic sound-speed relation ($a^2 = \gamma p/\rho = \gamma R_o T/M$).

$$\mathfrak{s} = \frac{a_2\rho_2}{a_1\rho_1} = \frac{\gamma_2 a_1}{\gamma_1 a_2} = \left[\frac{\gamma_2 M_2 T_1}{\gamma_1 M_1 T_2} \right]^{1/2} \tag{3.35}$$

The respective symbols γ, p, R, T, R_o and M denote the specific heat ratio, pressure, gas constant, temperature, universal gas constant ($R_o = MR$) and molecular weight. It is worth noting that the specific impedance ratio $\mathfrak{s}$ equals unity not only for the simplest case of identical driver and channel gases having the same temperatures but also for the specific case of different driver and channel gases provided that $\gamma_1 M_1/T_1$ equals $\gamma_2 M_2/T_2$. Furthermore, the specific impedance ratio $\mathfrak{s}$ equals $(\gamma_2 M_2/\gamma_1 M_1)^{1/2}$ for the very important case of different driver and channel gases having equal temperatures and $\mathfrak{s}$ equals $(T_1/T_2)^{1/2}$ for the not so practicable case of identical driver and channel gases having different temperatures.

A set of values of the specific impedance ratio $\mathfrak{s}$ was compiled for certain different combinations of driver and channel gases having identical temperatures, and they are given in Table 2. The smallest values of $\mathfrak{s}$ occur

when a light driver gas such as hydrogen (H_2) or helium (He) is used in conjunction with a heavy channel gas such as dichlorodifluoromethane (CCl_2F_2), sulfur-hexafluoride (SF_6) or octofluorocyclobutane (C_4F_8). On the other hand the largest values of $\mathfrak{s}$ occur when the driver gas is heavy or has a large molecular weight and the channel gas has a low molecular weight. For nearly equivalent molecular weights of the driver and channel gases the specific impedance ratio is always nearly equal to unity.

Another important combination of sound speed and density ratios, $(a_1\rho_1 + a_2\rho_2)/a_1(\rho_2 - \rho_1)$ or $(1 + a_2\rho_2/a_1\rho_1)/(\rho_2/\rho_1 - 1)$, has been denoted by the symbol ℓ. This nondimensional parameter can be expressed in the following alternate forms.

$$\ell = \frac{1 + \dfrac{a_2\rho_2}{a_1\rho_1}}{\dfrac{\rho_2}{\rho_1} - 1} = \frac{1 + \mathfrak{s}}{\dfrac{\gamma_1}{\gamma_2}\mathfrak{s}^2 - 1} = \frac{1 + \left[\dfrac{\gamma_2 M_2 T_1}{\gamma_1 M_1 T_2}\right]^{1/2}}{\dfrac{M_2 T_1}{M_1 T_2} - 1} \tag{3.36}$$

The parameter ℓ, which plays the role essentially of a nondimensional time constant for the wave motion (e.g., see Eq. 3.32), can take on values that range from positive to negative infinity. A set of values of the parameter ℓ was compiled for certain interesting combinations of driver and channel gases having identical temperatures, and these results are shown for interest in Table 3.

The wave that propagates in the channel gas is one of the most important features of the wave motion in the pyramidal shock tube. For this reason the overpressure and particle velocity signature of this wave will be explored. The mathematical expression for the overpressure signature, resulting from Eqs. 3.7, 3.8, 3.29, 3.32, 3.34, 3.35 and 3.36, can be expressed as given below.

$$\Delta p_1 = \frac{\Delta p_o}{z+1}\frac{r_o}{r}\sum_{i=1}^{\infty}\left[g_i''(\xi)H[\xi-2i+2]\right] \tag{3.37}$$

$$g_i''(\xi) = \begin{cases} J_o''(\xi) & i = 1 \\ \displaystyle\sum_{j=1}^{i-1}\binom{i-2}{j-1}\left(\frac{\mathfrak{s}-1}{\mathfrak{s}+1}\right)^{i-j-1}\left(\frac{2}{z+1}\right)^{j} J_j''(\xi-2i+2) & i = 2,3,\ldots,\infty \end{cases} \tag{3.38}$$

$$J_j''(\omega) = \begin{cases} -\ell + (1+\ell)\exp(-\omega/\ell) & j = 0 \\ \left[\dfrac{1+\ell}{j!}\left(\dfrac{\omega}{\ell}\right)^{j} + \dfrac{\mathfrak{s}}{(j-1)!}\left(\dfrac{\omega}{\ell}\right)^{j-1}\right]\exp(-\omega/\ell) & j = 1,2,\ldots,\infty \end{cases} \tag{3.39}$$

For convenience and illustration the first five functions of both $g_i''(\xi)$ and $J_j''(\xi-2i+2)$ are given expanded form in Appendix B. Note that the function $g_i(\xi)$

used in Eqs. 3.37 and 3.38 has been redefined slightly, differing from the previous one by a factor of $\Delta p_o r_o^2/a_2\rho_1(z+1)$.

Fifteen nondimensional overpressure signatures for the channel of a pyramidal shock tube, as computed from Eqs. 3.37, 3.38 and 3.39, are displayed in Fig. 11 for fifteen different combinations of driver and channel gases having the same temperature. For each signature the driver and channel gases are depicted in the insert. The fifteen signatures have been arranged in a sequential order based on the specific impedance ratio $\mathfrak{s}$ (shown in the figure). Consequently, the combination of a light driver gas and a heavy channel gas ($z < 1$) appear first in the sequence (Fig. 11a to 11e), and the combination of a heavy driver gas and a light channel gas ($z > 1$) appears last (Fig. 11g to 11o). It can be seen that an overpressure signature corresponding to a $\mathfrak{s}$ value that is small ($z \ll 1$) or large ($\mathfrak{s} \gg 1$) differs markedly from an ideal N-shaped profile for $\mathfrak{s}$ equal to unity (Fig. 11f). However, as both an initially small or large value of $\mathfrak{s}$ approaches and equals unity the differences decrease and disappear. For equivalent-temperature driver and channel gases, therefore, only identical driver and channel gases can produce an N-shaped overpressure signature in the channel of a pyramidal shock tube. This conclusion can be deduced directly from Eqs. 3.37, 3.38 and 3.39, although it is not obvious.

Five nondimensional overpressure signatures for the channel of a pyramidal shock tube, as computed from Eqs. 3.37, 3.38 and 3.39, are shown in Fig. 12 for five different cases of identical driver and channel gases having different temperatures. The five driver gas to channel gas temperature ratios T_2/T_1 are 9, 2, 1, 1/2 and 1/9, as shown in the figure, corresponding to $\mathfrak{s}$ values of 0.33, 0.71, 1.00, 1.41 and 3.00, respectively. The signatures in Fig. 12a and 12b are similar to those for a combination of a light driver gas and a different equivalent-temperature channel gas (see Fig. 11d and 11e), because heating the driver gas or alternatively cooling the channel gas makes the driver gas light in comparison to the channel gas. On the other hand, because cooling the driver gas makes it heavier than the channel gas or alternatively heating the channel gas makes it light than the driver gas, the signatures in Fig. 12d and 12e resemble those for a combination of a heavy driver gas and a different equivalent-temperature channel gas (see Fig. 11i and 11m). For the case of identical driver and channel gases having the same temperature the signature is, of course, N shaped as shown in Fig. 12c.

It is of interest to consider the overpressure signature in the channel of a pyramidal shock tube for the very special case when different driver and channel gases are used but they have equivalent densities. For this special case the parameter ℓ (Eq. 3.36) is infinite, and the parameter $\mathfrak{s}$ (Eq. 3.35) equals a_2/a_1 which is not arbitrary but can be shown to be equal to $(\gamma_2/\gamma_1)^{1/2}$. Furthermore, to achieve such a special case of identical densities for different driver and channel gases the temperature ratio T_2/T_1 must be equal to M_2/M_1. Five overpressure signatures corresponding to values of $\mathfrak{s}$, a_2/a_1 or $(\gamma_2/\gamma_1)^{1/2}$ of 0.89, 0.81, 1.00, 1.13 and 1.23, as computed from Eqs. 3.37, 3.38 and 3.39, are displayed in Fig. 13. Note that specific sets of values for γ_2 and γ_1 could be 1.67 and 1.10, 1.40 and 1.10, 1.10 and 1.40, and 1.10 and 1.67 to give values of $\mathfrak{s}$, a_2/a_1 or $(\gamma_2/\gamma_1)^{1/2}$ equal to 9.89, 0.81, 1.13 and 1.23, respectively. The most interesting feature of these signatures (Fig. 13) is that the variation in overpressure is linear between successive sudden changes in overpressure (shocks). Such a linear variation occurs only when the parameter ℓ is infinite or when the driver and channel densities are equal. For this special case of equivalent-density driver and channel gases a single N-wave results only when the sound

speeds are also equal (see Fig. 13c). Hence, we note once again that a single N-shaped overpressure signature is possible with a pyramidal shock tube only if the driver and channel are identical and have the same temperature.

The overpressure signature predicted by Eqs. 3.37, 3.38 and 3.39, some of which have been shown in Figs. 11, 12 and 13, are invariant with radial distance (wave form does not change shape) but attenuates inversely with distance (acoustic 1/r decay law). The amplitude of the first shock is given by $\Delta p_o r_o/(\varepsilon+1)r$. Consequently, for a given pressure difference across the diaphragm (Δp_o), a combination of a light driver gas and a heavy channel gas having a small specific impedance ratio (ε) produces a relatively strong wave in the channel. However, the duration of this wave is generally very short because the time interval between successive shocks, $2r_o/a_2$, is small owing to the high sound speed (a_2) of a light driver gas. On the other hand, the relatively low-amplitude wave for a combination of a heavy driver gas and a light channel gas can have a very long duration.

Although the overpressure signature described by Eqs. 3.37, 3.38 and 3.39 is tedious to calculate in detail, a simple expression can be found to give the sudden change in overpressure associated with each shock in the signature. Firstly, since ξ equals 2i-2 at the wave front of the i^{th} disturbance where the shock is located, find from Eq. 3.39 that $J_o''(0)$ is equal to unity, $J_1''(0)$ equals ε, and all subsequent $J_j''(0)$ are zero. Secondly, from Eq. 3.38 for $g_i''(\xi)$, obtain $g_1''(0)$ equal to unity and subsequent $g_i''(2i-2)$ equal to $2\varepsilon(\varepsilon-1)^{i-2}/(\varepsilon+1)^{i-1}$. Finally, find from Eq. 3.37 the desired result for the amplitude of the i^{th} shock, which is given below.

$$\begin{cases} \dfrac{\Delta p_o r_o}{(\varepsilon+1)r} & i = 1 \\ \dfrac{\Delta p_o r_o}{(\varepsilon+1)r}\left(\dfrac{2\varepsilon}{\varepsilon+1}\right)\left(\dfrac{\varepsilon-1}{\varepsilon+1}\right)^{i-2} & i = 2, 3, \ldots, \infty \end{cases} \tag{3.40}$$

Relative to the first shock having an amplitude of $\Delta p_o r_o/(\varepsilon+1)r$, the amplitude of the second one is $2\varepsilon/(\varepsilon+1)$. Therefore, depending on the value of the specific impedance ratio ε, the second shock can be smaller ($\varepsilon < 1$), equal ($\varepsilon = 1$), or larger ($\varepsilon > 1$) in amplitude than the first one. However, regardless of the value of ε, the amplitude (absolute) of the third and subsequent shocks always diminish, being smaller than its predecessor by the factor $(\varepsilon-1)/(\varepsilon+1)$. (see the overpressure profiles given in Figs. 11, 12 and 13.)

The mathematical expression for the particle-velocity signature of the wave propagating in the channel gas can be determined directly from Eqs. 3.7, 3.9, 3.29, 3.32, 3.34, 3.35 and 3.36. Alternatively and more simply it can be derived by using the following acoustic expression which relates the particle velocity to the known overpressure (Eqs. 3.37, 3.38 and 3.39) of a spherical wave moving away from the origin.

$$\Delta u = \frac{\Delta p}{a\rho} + \frac{1}{\rho r}\int_{-\infty}^{t} \Delta p(y-r/a)\, dy \tag{3.41}$$

In either case the final results for the particle-velocity signature are given below.

$$\Delta u_1 = \frac{\Delta p_o}{a_1 \rho_1 (g+1)} \frac{r_o}{r} \sum_{i=1}^{\infty} \left[g_i''(\xi) + \frac{a_1}{a_2} \frac{r_o}{r} g_i'(\xi) \right] H\{\xi - 2i + 2\} \tag{3.42}$$

$$g_i'(\xi) = \begin{cases} J_o'(\xi) & i = 1 \\ \sum_{j=1}^{i-1} \binom{j-2}{j-1} \left(\frac{g-1}{g+1}\right)^{i-j-1} \left(\frac{2}{g+1}\right)^j J_j'(\xi - 2i + 2) & i = 2,3,\ldots,\infty \end{cases} \tag{3.43}$$

$$J_j'(\omega) = \begin{cases} \ell(1+\ell) - \ell\omega - \ell(1+\ell)e^{-\omega/\ell} & j = 0 \\ \ell(1+g+\ell) - \left[\frac{\ell(1+\ell)}{j!} \left(\frac{\omega}{\ell}\right)^j + \sum_{k=1}^{j} \frac{\ell(1+g+\ell)}{(j-k)!} \left(\frac{\omega}{\ell}\right)^{j-k} \right] \exp(-\omega/\ell) & j = 1,2,\ldots,\infty \end{cases} \tag{3.44}$$

Note that the i^{th} function $g_i''(\xi)$ and the associated j^{th} function $J_j''(\omega)$ are not given here as they have been defined previously by Eqs. 3.38 and 3.39, respectively.

The particle-velocity profile is not invariant with radial distance like the overpressure profile, because it consists of two parts or two sums of terms which have different dependences on radial distance. The part of the particle-velocity expression containing the sum of the $g_i'(\xi)$ terms has a dependence on radius of $1/r^2$. This part of the particle velocity consequently diminishes relatively rapidly with distance and is therefore significant only at small radii or in the near-field. The other part of the particle-velocity expression has a weaker dependence on radius of $1/r$ and thus becomes dominant at large radii or in the far-field. It can be seen by comparing Eqs. 3.37 and 3.42 for the overpressure and particle velocity respectively that the changing particle-velocity profile tends with increasing distance to take on the shape of the overpressure profile. For the far-field one consequently finds that Δu_1 is simply equal to $\Delta p_1/a_1\rho_1$, a well-known acoustic result. The parameter in Eq. 3.42 that is important as a rough indicator when this far-field result can be applied instead of the more complete Eq. 3.42 is $a_1 r_o/a_2 r$. From detailed calculations of particle-velocity signatures it can be shown that when $a_1 r_o/a_2 r$ is less than about $1/4$, or when radial distances r are greater than $4a_1 r_o/a_2$, the far-field approximation ($\Delta u_1 = \Delta p_1/a_1\rho_1$) is applicable. It is worth noting that, as the wave length λ between successive shocks in the overpressure or particle-velocity signature is simply $2r_o a_1/a_2$, the far-field result applies for radial distances r greater than about 2λ.

Nondimensional particle-velocity signatures at five different radial distances r of r_o, $2r_o$, $4r_o$, $8r_o$ and ∞ in the channel of a pyramidal shock

tube have been computed from Eqs. 3.42, 3.43 and 3.44 for four different combinations of driver and channel gases, and these four sets of results are given in Figs. 14, 15, 16 and 17. The driver and channel gases, which were taken to have the same temperature, are shown at the top of each figure. From the results in each figure, one can see that the change in shape of each signature with increasing distance from the diaphragm station ($r=r_o$) is noticeable only in profiles corresponding to r/r_o values of less than about 2λ or $2r_o a_1/a_2$, or values of $0.7r_o$, $2r_o$, $4r_o$ and $18r_o$ for the He-Air, Air-Air (identical driver and channel gases), SF_6-Air and C_4F_8-He driver-to-channel gas combinations respectively. This waveform distortion persists to large radii for the case of a high a_1/a_2 value which corresponds to a combination of a heavy driver gas and a light channel gas.

It is worth mentioning that a simple expression can be derived to give the sudden change in particle velocity associated with each shock in the signature. The derivation is similar to that for the sudden change in overpressure associated with each shock, which yielded Eq. 3.40. The desired result for the amplitude of the i^{th} shock in the particle-velocity signature is given below.

$$\begin{cases} \dfrac{\Delta p_o r_o}{a_1 \rho_1 (\varepsilon+1) r} & i = 1 \\ \dfrac{\Delta p_o r_o}{a_1 \rho_1 (\varepsilon+1) r} \dfrac{2\varepsilon}{\varepsilon+1} \left(\dfrac{\varepsilon-1}{\varepsilon+1} \right)^{i-2} & i = 2,3,\ldots, \infty \end{cases} \tag{3.45}$$

These results are very similar to those of Eq. 3.40.

The motion of the channel gas and contact surface, owing to the wave motion in the pyramidal shock tube, can be determined by using the previously derived expression for the particle velocity (Eqs. 3.42, 3.43 and 3.44). As Δu_1 is equal to dr/dt exactly or $a_2 d(r/r_o)/d\xi$ to first order (same order of approximation as the acoustic equations approximate the gasdynamic equations), the particle displacement can be obtained by integration. For a fluid particle having an initial location r_* ($r_* \geq r_o$) the first-order particle displacement $r-r_*$ or simply Δr can be shown to be given by the following results.

$$\frac{\Delta r}{r_o} = \frac{\Delta p_o}{3\gamma_2 p_1} \frac{r_o}{r_*} \frac{3\varepsilon}{\varepsilon+1} \sum_{i=1}^{\infty} \left[g_i'(\xi) + \frac{a_1}{a_2} \frac{r_o}{r_*} g_i(\xi) \right] H\{\xi-2i+1\} \tag{3.46}$$

$$g_i(\xi) = \begin{cases} J_o(\xi) & i = 1 \\ \displaystyle\sum_{j=1}^{i-1} \binom{i-2}{j-1} \left(\frac{\varepsilon-1}{\varepsilon+1} \right)^{i-j-1} \left(\frac{2}{\varepsilon+1} \right)^{j} J_j(\xi-2i+2) & i = 2,3,\ldots,\infty \end{cases} \tag{3.47}$$

$$J_j(\omega) = \begin{cases} -\ell^2(1+\ell) + \ell(1+\ell)\omega - \ell\omega^2/2 + \ell^2(1+\ell)e^{-\omega/\ell} & j = 0 \\ \ell^2(1+\ell) + \ell^2(1+\varepsilon+\ell)(\omega-j) + \left[\dfrac{\ell^2(1+\ell)}{j!} \left(\dfrac{\omega}{\ell} \right)^j \right. & \\ \left. + \sum_{k=1}^{j} \dfrac{\ell^2(1+\ell) + k\ell^2(1+\varepsilon+\ell)}{(j-k)!} \left(\dfrac{\omega}{\ell} \right)^{j-k} \right] e^{-\omega/\ell} & j = 1,2,\ldots,\infty \end{cases} \tag{3.48}$$

Note that the i^{th} function $g_i'(\xi)$ and the associated j^{th} function $J_j'(\omega)$ are not given here because they have been defined previously by Eqs. 3.43 and 3.44 respectively.

The displacement of a fluid particle as a function of time, including the total displacement after the wave motion has subsided at large times ($\xi \to \infty$), can be calculated from Eqs. 3.46, 3.47 and 3.48 quite easily by using a digital computer. Such computed results will be given subsequently. First, however, an important, simple expression will be derived for the total displacement of a fluid particle. Let the driver gas have an initial pressure of $p_1+\Delta p_o$, where p_1 is the initial and final pressure of the channel gas and Δp_o is the pressure difference across the diaphragm. For a driver gas having a total mass m_o and an initial total volume V_o, the initial density is simply m_o/V_o. Also, for a pyramidal driver having a spherically shaped diaphragm of radius r_o the driver volume is directly proportional to r_o^3. Now let the driver gas expand isentropically (as it would for acoustic wave motion) to a final pressure p_1. The corresponding final density would be m_o/V, where the final volume V is proportional to r^3. The following isentropic expression relating the initial and final pressures and densities can therefore be applied.

$$\frac{p_1+\Delta p_o}{p_1} = \left[\frac{m_o/V_o}{m_o/V} \right]^{\gamma_2} = \left[\frac{r}{r_o} \right]^{3\gamma_2} \tag{3.49}$$

From this result the total displacement of the contact surface or interface of the driver and channel gases, which is $r-r_o$ or simply Δr_o, is given to first order by the following expression.

$$\frac{\Delta r_o}{r_o} = \frac{\Delta p_o}{3\gamma_2 p_1} \tag{3.50}$$

This result for the contact surface can now be generalized for any fluid particle in the channel. For a contact-surface displacement from radius r_o to $r_o+\Delta r_o$ or simply Δr_o, the volume of fluid displaced is directly proportional to $(r_o+\Delta r_o)^3 - r_o^3$ or $r_o^2\Delta r_o$ to first order. The corresponding displacement of a fluid particle in the channel from radius r_* to $r_*+\Delta r$ or simply Δr produces an equivalent volume displacement (final pressure and density are spatially uniform in the channel) which is directly proportional to $(r_*+\Delta r)^3 - r_*^3$ or $r_*^2\Delta r$ to first order. We therefore obtain the result that $r_o^2\Delta r_o$ equals $r_*^2\Delta r$. By using this result in conjunction with Eq. 3.50, the total displacement of a fluid particle Δr from its initial location r_* in

the channel is given by the following expression.

$$\frac{\Delta r}{r_o} = \frac{\Delta p_o}{3\gamma_2 p_1}\left(\frac{r_o}{r_*}\right)^2 \qquad (3.51)$$

The expressions for the total displacement of the contact surface (Eq. 3.50) and a fluid particle in the channel (Eq. 3.51) are important not only because of their simplicity but also they indicate how to properly normalize the full expression for the particle displacement (see Eq. 3.46).

It would be of interest to derive a simple expression from Eqs. 3.46, 3.47 and 3.48 for the total displacement of a fluid particle and check to see if this result is identical to Eq. 3.51. Such a derived expression proved elusive. Therefore a digital computer was used to calculate (Eqs. 3.46, 3.47 and 3.48) the particle displacement at sufficiently large times to obtain the total displacement. In each case the computed result was in agreement with the prediction of Eq. 3.51. In addition to providing a means of simply normalizing Eq. 3.46, therefore, Eq. 3.51 provides an excellent check on the analysis of the wave motion in the pyramidal shock tube.

It is worth noting here that the total displacement of a fluid particle $\Delta r/r_o$ or $\Delta p_o r_o^2/3\gamma_2 p_1 r_*^2$ is relatively small, and it is also independent of both the specific impedance ratio ε and the parameter ℓ. Consider, for example, the total displacement of the contact surface, for which r_* equals r_o. Even for a relatively large pressure difference across the diaphragm (Δp_o) of one-twentieth of an atmosphere ($p_1/20$), and γ_2 equal to 1.4 for a diatomic driver gas, the total displacement is only $r_o/84$ or 1.2% of the driver length. In general the contact-surface displacement is small and a fluid-particle displacement at a larger radius is even smaller. Consequently the previous assumption for the wave-motion and displacement analyses that the contact-surface displacement was negligible compared to the driver length was very reasonable.

Nondimensional fluid-particle histories for different initial radii r_* of r_o, $2r_o$, $4r_o$ and $8r_o$ in the channel of a pyramidal shock tube have been computed for four different combinations of driver and channel gases, and these four sets of results are given in Figs. 18, 19, 20 and 21. The driver and channel gases, which were taken to have the same temperatures, are shown in each figure. Figures 18 and 19, for driver-to-channel gas combinations of He-Air and Air-Air, respectively, show that the particle displacement increases and then decreases to its final displacement (asymptote indicated). This behaviour is typical of the case of a light driver gas and a heavy channel gas for which the specific impedance ratio ε is less than unity. From the results of Figs. 20 and 21 for driver-to-channel gas combinations of C_4F_8-Air and CO_2-He respectively, the particle displacement increases in a "damped" oscillatory manner to its final displacement. This behaviour is typical of the case of a heavy driver gas coupled to a light channel gas for which the specific impedance ratio ε is greater than unity. In each of the Figs. 18, 19, 20 and 21 the top displacement history for radius r_* equal to r_o is that for the contact surface. The contact-surface displacement is the largest, and particle displacements at increasing radii continually decrease and become, eventually, inconspicuous, because the wave motion being strongest at the diaphragm station becomes weaker with increasing distance and eventually vanishes.

The particle-displacement histories for the previous driver-to-channel gas combinations of He-Air and Air-Air given in Figs. 18 and 19 are also shown in Figs. 22 and 23. In these latter figures, however, the displacement histories are superposed on a time-distance diagram which also depicts the wave motion. Additionally, displacement histories for another driver-to-channel gas combination of SF_6-Air are similarly shown for interest in Fig. 24.

In order to check the validity of the acoustic analysis of the wave motion in the pyramidal shock tube, the UTIAS Travelling-Wave Horn was used to obtain experimental data which could be compared with predicted results. The pyramidal shock tube had a total divergence angle of 7.2 degrees, an overall length of 25m and a driver that was 1.58m long (Refs. 3 and 5). The driver gases used for the experiments were helium (He), air, argon (A), carbon dioxide (CO_2), sulfur dioxide (SO_2), dichlorodifluoromethane (CCl_2F_2) and octafluorocyclobutane (C_4F_8), which covered a large range of both molecular weights and sound speeds (see Table 2). For all experiments the channel gas was air, and the driver and channel gases had the same initial temperature. Overpressure measurements made in the channel of the shock tube for the different driver gases are shown in the top part of Figs. 25 to 31. Note that the driver and channel gases, pressure difference across the diaphragm, driver length and measurement location are given above each oscillogram. Each experimental overpressure signature has been reproduced below its oscillogram, where it is compared directly to the predicted signature. For each one of the seven comparisons the predicted and measured profiles are in good agreement, substantiating the analysis for the wave motion in the pyramidal shock tube. From experimental data such as those shown in Figs. 25 to 31 it was found that the acoustic analysis was still valid when the pressure difference across the diaphragm (Δp_o) was as high as 15 kN/m^2.

3.2 Special Solution

It is of academic interest to investigate the solution of the wave motion in a pyramidal shock tube for the special case of different driver and channel gases which have the same density. For this special case of equivalent densities the ratio of the driver and channel gas sound speeds a_2/a_1, and the specific impedance ratio ε $(a_2\rho_2/a_1\rho_1)$, are both fixed, being equal to the square root of the specific heats ratio $(\gamma_2/\gamma_1)^{1/2}$. Furthermore, the temperature of the driver and channel gases cannot be arbitrary, as the temperature ratio T_2/T_1 must be equal to the ratio of the molecular weights M_2/M_1.

For this special case of equivalent driver and channel gas densities the solution of the wave motion takes a relatively simple form. Certain terms vanish from the differential equations for the velocity potentials $g_i(\xi)$, $f_i(\eta)$ and $h_i(\beta)$ (see Eqs. 3.24, 3.25 and 3.26). The resulting simpler differential equations are given below.

$$g_i''(\xi) = \begin{cases} \dfrac{\Delta p_o r_o^2}{a_1\rho_1(z+1)} \dfrac{a_1}{a_2} (\xi-1) & i = 1 \\ \dfrac{2\varepsilon}{\varepsilon+1} \dfrac{a_1}{a_2} h_{i-1}''(\beta) & i = 2, 3, \ldots, \infty \end{cases} \tag{3.52}$$

$$f_i''(\eta) = \begin{cases} \dfrac{\Delta p_o r_o^2}{a_2 \rho_2 (\varepsilon+1)} (\eta - 1 + \varepsilon) & i = 1 \\ -\dfrac{\varepsilon-1}{\varepsilon+1} h_{i-1}''(\beta) & i = 2, 3, \ldots, \infty \end{cases} \tag{3.53}$$

$$h_i''(\beta) = -f_i''(\eta) \qquad i = 1, 2, \ldots, \infty \tag{3.54}$$

From these results the following recurrence relationships for $g_i''(\xi)$, $f_i''(\eta)$ and $h_i''(\beta)$ can be obtained.

$$f_i''(\eta) = \frac{\Delta p_o r_o^2}{a_2 \rho_2 (\varepsilon+1)} \left(\frac{\varepsilon-1}{\varepsilon+1} \right)^{i-1} (\eta - 2i + 1 + \varepsilon) \qquad i = 1, 2, \ldots, \infty \tag{3.55}$$

$$h_i''(\beta) = \frac{-\Delta p_o r_o^2}{a_2 \rho_2 (\varepsilon+1)} \left(\frac{\varepsilon-1}{\varepsilon+1} \right)^{i-1} (\beta - 2i + 1 + \varepsilon) \qquad i = 1, 2, \ldots, \infty \tag{3.56}$$

$$g_i''(\xi) = \begin{cases} \dfrac{\Delta p_o r_o^2}{a_2 \rho_1 (\varepsilon+1)} (\xi - 1) & i = 1 \\ \dfrac{-\Delta p_o r_o^2}{a_2 \rho_1 (\varepsilon+1)} \dfrac{2}{\varepsilon+1} \left(\dfrac{\varepsilon-1}{\varepsilon+1} \right)^{i-2} (\xi - 2i + 2 + \varepsilon) & i = 2, 3, \ldots, \infty \end{cases} \tag{3.57}$$

These expressions can be integrated to obtain recurrence relationships for $g_i'(\xi)$, $f_i'(\eta)$ and $h_i'(\beta)$, and also for $g_i(\xi)$, $f_i(\eta)$ and $h_i(\beta)$. The results for $g_i'(\xi)$, $f_i'(\eta)$ and $h_i'(\beta)$ can be substituted into the expressions for the total velocity potentials ϕ_1 and ϕ_2 (Eqs. 3.7 and 3.10). Then the two respective expressions for the overpressure and particle velocity of the channel gas follow from Eqs. 3.8 and 3.9, whereas those for the driver gas follow from Eqs. 3.11 and 3.12.

The mathematical expression for the overpressure signature of the wave moving in the channel of a pyramidal shock tube is given below.

$$\Delta p_1 = \frac{\Delta p_o r_o}{(\varepsilon+1) r} \left[(1-\xi) H\{\xi\} + \frac{2}{\varepsilon+1} \sum_{i=2}^{\infty} \left(\frac{\varepsilon-1}{\varepsilon+1} \right)^{i-2} (\xi - 2i + 2 + \varepsilon) H\{\xi - 2i + 2\} \right] \tag{3.58}$$

From this expression it can be shown that the overpressure signature consists of a sequence of diminishing amplitude N-shaped segments, some of which may be inverted, but each having the same duration of $2r_o/a_2$. Five overpressure signatures corresponding to values of ε, a_2/a_1 or $(\gamma_2/\gamma_1)^{1/2}$ of 0.89, 0.81,

1.00, 1.13 and 1.23 are shown in Fig. 13, illustrating the preceding remarks. Although these signatures could have been generated by using Eq. 3.58, they were originally computed from equivalent expressions of Eqs. 3.37, 3.38 and 3.39 of Section 3.1. Note that the signatures have been discussed previously in Section 3.1.

The linear variation in overpressure of the i^{th} N-shaped segment of an overpressure signature can be expressed quite simply as shown below.

$$\Delta p_1 = \frac{\Delta p_o r_o}{(g+1)r}\left(\frac{g-1}{g+1}\right)^{i-1}(2i-1-\xi) \qquad \begin{matrix} 2i-2 < \xi < 2i \\ i = 1, 2, \ldots, \infty \end{matrix} \tag{3.59}$$

This result, which can be derived from Eq. 3.58, is much easier to use than Eq. 3.58 when constructing an overpressure signature. From Eq. 3.59 (or Eq. 3.58) one can show that the slope of the i^{th} linearly varying overpressure segment, or the first derivative of the overpressure with respect to nondimensional time ξ, is given as follows.

$$-\frac{\Delta p_o r_o}{(g+1)r}\left(\frac{g-1}{g+1}\right)^{i-1} \qquad i = 1, 2, \ldots, \infty \tag{3.60}$$

Note that the absolute magnitude of the slope diminishes in the form of a geometric progression having the common ratio $(g-1)/(g+1)$.

The particle-velocity signature of the wave propagating in the channel gas of a pyramidal shock tube can be determined directly from Eqs. 3.9 and 3.57. However, it can also be obtained from the overpressure signature (Eq. 3.58 or 3.59) by using Eq. 3.41. The easiest procedure is to use Eqs. 3.41 and 3.59. Then the particle velocity associated with the i^{th} segment of the signature is given by the following expression.

$$\Delta u_1 = \frac{\Delta p_o r_o}{a_1\rho_1(g+1)r}\left(\frac{g-1}{g+1}\right)^{i-1}\left[(2i-1-\xi) + \frac{1}{2}\frac{a_1}{a_2}\frac{r_o}{r}\{1-(2i-1-\xi)^2\}\right]$$

$$\begin{matrix} 2i-2 < \xi < 2i \\ i = 1, 2, \ldots, \infty \end{matrix} \tag{3.61}$$

Each segment of the signature consists of a near-field and a far-field term. The particle-velocity signature therefore tends with increasing radial distance to take on the same shape as the overpressure. Generally the near-field term is unimportant when the parameter $a_1 r_o/a_2 r$ is less than $1/4$, or when the radial distance r is greater than $4r_o a_2/a_1$ or 2λ, where λ is the wave length of each segment.

The motion of the channel gas and contact surface, owing to the wave motion in the pyramidal shock tube, can be determined from Eq. 3.61 for the particle velocity. As Δu_1 is equal to dr/dt exactly or $a_2 d(r/r_o)/d\xi$ to first order, the particle displacement can be obtained by integration. The first-order particle displacement $r-r_*$ or simply Δr associated with only the i^{th} segment of the signature is given below.

$$\frac{\Delta r}{r_o} = \frac{\Delta p_o r_o}{2\gamma_2 p_1 r_*} \frac{a_2/a_1}{\varepsilon+1} \left(\frac{\varepsilon-1}{\varepsilon+1} \right)^{i-1} \left[1 - (2i-1-\xi)^2 + \frac{2}{3} \frac{a_1}{a_2} \frac{r_o}{r_*} \{1 - \frac{3}{2} (2i-1-\xi) + \frac{1}{2} (2i-1-\xi)^3\} \right] \tag{3.62}$$

$$2i-2 < \xi < 2i$$
$$i = 1, 2, \ldots, \infty$$

From this result the particle displacement $\Delta r/r_o$ at the beginning of only the i^{th} segment ($\xi=2i-2$) is zero, of course, and that at the end of the i^{th} segment ($\xi=2i$) is given by the following expression.

$$\frac{\Delta p_o r_o^2}{3\gamma_2 p_1 r_*^2} \left(\frac{2}{\varepsilon+1} \right) \left(\frac{\varepsilon-1}{\varepsilon+1} \right)^{i-1} \tag{3.63}$$

Hence, the total particle displacement $\Delta r/r_o$ of the i^{th} segment, which now includes the displacements of all previous segments, is given below.

$$\frac{\Delta r}{r_o} = \frac{\Delta p_o r_o^2}{3\gamma_2 p_1 r_*^2} \left[1 - \left(\frac{\varepsilon-1}{\varepsilon+1} \right)^{i-1} + \frac{3/2}{\varepsilon+1} \frac{r_*}{r_o} \frac{a_2}{a_1} \left(\frac{\varepsilon-1}{\varepsilon+1} \right)^{i-1} \left\{ 1 - (2i-1-\xi)^2 + \frac{2}{3} \frac{a_1}{a_2} \frac{r_o}{r_*} \left(1 - \frac{3}{2} (2i-1-\xi) + \frac{1}{2} (2i-1-\xi)^3 \right) \right\} \right] \tag{3.64}$$

$$2i-2 < \xi < 2i$$
$$i = 1, 2, \ldots, \infty$$

At large times ($i \to \infty$, $\xi \to \infty$) the motion of the fluid particle ceases and the final particle displacement $\Delta r/r_o$ is simply $\Delta p_o r_o^2/3\gamma_2 p_1 r_*^2$. For the contact surface the final displacement is $\Delta p_o/3\gamma_2 p_1$. Note that these results are in agreement with those in Section 3.1 (Eqs. 3.50 and 3.51), which were derived by a different analysis.

4. DISCUSSIONS AND CONCLUSIONS

Acoustic analyses have been given for determining the weak wave motion in both low-pressure-ratio rectangular and pyramidal shock tubes. Each analysis, which was sufficiently general to deal with different driver and channel gases having different temperatures, yielded a closed-form solution for the wave motion. Each solution was illustrated graphically with selected overpressure and particle-velocity signatures for the wave moving in the channel gas. Additionally, solutions for the fluid-particle displacement of the channel gas and thus the contact-surface displacement were obtained for both the rectangular and pyramidal shock tubes, and they were also shown graphically with selected results. Although the solutions of the wave motion and fluid-particle displacement for the pyramidal shock tube were quite lengthy, graphical results for the overpressure, particle-velocity and particle displacement were obtained rather easily by utilizing

a relatively small digital computer (IBM II30). Experimental data in the form of overpressure measurements, obtained in conjunction with suitable rectangular and pyramidal shock tubes, verified the analyses and solutions for the wave motion in both shock tubes.

For the special case of identical driver and channel gases having the same temperature, it has been well known that the rectangular and pyramidal shock tubes both produce a single finite-duration wave or pulse in the channel. For example, for the rectangular shock tube see Ref. 18 (similar wave motion of strings), and for the pyramidal shock tube see Refs. 15, 18, 19 and 20. In the case of the rectangular shock tube the pulse is flat-topped (see Fig. 7c), having an amplitude of one-half the pressure difference across the diaphragm ($\Delta p_o/2$) and a wave length of twice the driver length ($2r_o$). For the pyramidal shock tube the pulse is N shaped (see Fig. 11f), having the same wave length of twice the driver length ($2r_o$) and an amplitude which is initially one-half the pressure difference across the diaphragm but diminishes inversely with increasing radial distance ($\Delta p_o r_o/2r$). The general solutions of the wave motion given in Chapter 2 for the rectangular shock tube and in Chapter 3 for the pyramidal shock tube are, of course, in perfect agreement with these well-known results. However, in the past it has not been fully recognized that in the more general case of driver and channel gases having different densities, owing to different molecular weights or temperatures, the amplitude and shape of the waves in the rectangular and pyramidal shock tubes can differ markedly from those of a single flat-topped pulse (see Fig. 7) and N-shaped wave (see Fig. 11) respectively. In fact, this was one of the main reasons why the solutions of the wave motion in the rectangular and pyramidal shock tubes were obtained.

As explained in detail in the Introduction, a pyramidal shock tube utilizing identical driver and channel gases having the same temperature has to be very large (about 200m long) if the N-wave produced in the channel is to simulate a full-scale sonic boom from an SST aircraft. Although a shorter pyramidal shock tube could produce a similar duration simulated sonic boom, provided the sound speed of the driver gas was relatively low, this simulated sonic boom would not have the desired N shape and it would also have undesirable trailing disturbances. Consider, for example, the specific case of sulfur hexafluoride (SF_6) as the driver gas and air in the channel. Owing to such a low sound speed driver gas the pyramidal shock tube needs to be only 50% as long as one which uses air in both the driver and channel. However, the distorted N-wave which is produced in the channel (see Fig. 11k) is quite unsatisfactory for standard sonic-boom-research purposes. Consequently, it can be concluded that the concept of using a low sound speed driver gas to make possible the construction of a relatively short and inexpensive pyramidal shock tube for sonic-boom-research purposes is not very feasible.

At noted in the Introduction, a relatively short pyramidal-pyramidal shock tube utilizing air in both the driver and channel could be used to produce a simulated full-scale sonic boom (see Fig. 5). This simulated sonic boom would also not be N shaped and it would also have undesirable trailing disturbances (see Fig. 3d). Consequently the concept of using such a short and inexpensive pyramidal-pyramidal shock tube for sonic-boom research purposes is also not very feasible. However, if a short and inexpensive sonic-boom simulator is to be built, the pyramidal-pyramidal shock tube is more practical than a pyramidal shock tube which uses different driver and

channel gases. Firstly, although it can be shown that the undesirable distortion in the N-wave produced by either shock tube is about the same, the trailing compression waves or disturbances for the case of the pyramidal-pyramidal shock tube (Fig. 3d) are much less severe than the trailing steep-fronted disturbances for the pyramidal shock tube (Fig. 11f). Secondly, the problems associated with the mixing of the different driver and channel gases in the pyramidal shock tube after the diaphragm is broken is nonexistent for the case of the pyramidal-pyramidal shock tube.

The analysis and solution for the wave motion in a pyramidal-pyramidal shock tube for which the driver and channel gases can not only be different but also have different temperatures is very similar to that given in Chapter 3 for the case of the pyramidal shock tube. For such an analysis, if the radial distance for the driver region is denoted by r, a new radial distance, say R, is needed for the channel. Therefore the length of the driver is r_o and the length of the truncated portion of the channel is R_o. Then, for example, the recurrence relationship of $f_i'(\eta)$ (see Eqs. 3.27 to 3.32) for the pyramidal shock tube can be used for the case of the pyramidal-pyramidal shock tube, provided the parameter ℓ is modified slightly from $(1+\varepsilon)/(\rho_2/\rho_1-1)$ to $(1+\varepsilon)/(\rho_2 r_o/\rho_1 R_o-1)$. Consequently, the analysis and solution for the pyramidal-pyramidal shock tube can be obtained quite easily with this and other slight modifications to the pyramidal-shock-tube results given in Chapter 3. From such a solution it can be shown that the overpressure signature of the wave in the channel is generally not N shaped and also has trailing disturbances, very much like those shown in Fig. 11.

It is worthwhile to discuss one particular solution of the wave motion in a pyramidal-pyramidal shock tube. Then one can answer the interesting question as to whether a pyramidal-pyramidal shock tube using different driver and channel gases can produce a single undistorted N-wave. From the solution of the wave motion, it can be shown that the linear variation in overpressure for an N-wave can occur only if the parameter ℓ becomes infinitely large. (Note that this condition is precisely that used to obtain the special solution given in Section 3.1.) This condition on ℓ is possible only if the ratio of the driver and channel gas densities ρ_2/ρ_1 is exactly equal to the geometrical ratio R_o/r_o. Consequently, one finds the interesting result that the two distortions of the N-wave, one produced by the different driver and channel densities and the other introduced by the different driver and channel divergence angles, cancel exactly if ρ_2/ρ_1 equals R_o/r_o. Even though the N-wave is undistorted, however, it is followed by a series of rapidly diminishing amplitude N-waves having the same duration $(2r_o/a_2)$, exactly like the results shown in Fig. 13. One can conclude, therefore, that a pyramidal-pyramidal shock tube using different driver and channel gases cannot produce a single N-wave.

There would be no significant advantage for building a pyramidal-pyramidal shock tube instead of a pyramidal shock tube to produce an N-wave for the simulation of a full-scale sonic boom. Firstly, of course, the simulated sonic boom, although it would be N shaped, would have undesirable N-shaped disturbances. Secondly, the overall length of the pyramidal-pyramidal shock tube would not be shorter but actually longer than that for a corresponding pyramidal shock tube. It can be shown that, for fixed diaphragm and test section sizes, the reduction in channel length (factor of a_2/a_1) is over-compensated by the increase in channel length, because R_o/r_o must equal ρ_2/ρ_1.

A technique first considered in England (Ref. 9) was discussed in the Introduction. This technique consists of using a low sound speed driver gas in an existing short pyramidal shock tube, thereby producing a simulated sonic boom with a longer-than-normal duration. Because the simulated sonic boom would be an undesirable distorted N-wave having trailing disturbances, according to the results of Chapter 3, it can be concluded that this technique of improving the capability of an existing short pyramidal shock tube to produce a long N-wave is not very practical.

The only type of shock tube which produces a good N-wave is, of course, the pyramidal shock tube, provided the driver and channel gases are identical and have the same temperature. If a full-scale sonic boom is to be simulated then one must recognize the fact that a large pyramidal shock tube is required. It is worth mentioning, however, that smaller sonic-boom simulators such as a loudspeaker-driven booth and a pyramidal horn with a mass-flow valve can also be used for simulation of a full-scale sonic boom (Refs. 3 and 5).

The analyses and solutions of the wave motion for both the rectangular and pyramidal shock tubes is directly applicable, of course, to finite-sized planar and spherical weak explosions. This fundamental work is relevant to the understanding of the wave motion produced by such weak explosions, for which the explosion gas is different than the ambient gas.

5. REFERENCES

1. Kryter, K. D. — The Effects of Noise on Man. Academic Press (1970).

2. Glass, I. I.; Ribner, H. S.; Gottlieb, J. J. — Canadian Sonic Boom Simulation Facilities. Canadian Aeronautics and Space Journal, Vol. 18, No. 8, pp. 235-246 (October 1972).

3. Gottlieb, J. J. — Sonic Boom Research at UTIAS. CASI Journal, Vol. 20, No. 5, pp. 199-222 (May 1974).

4. Carothers, R. — Initial Calibration and Physiological Response Data for the Travelling-Wave Sonic-Boom Simulator. UTIAS Technical Note No. 180 (1972).

5. Gottlieb, J. J. — Simulation of a Travelling Wave in a Pyramidal Horn. UTIAS Report No. 196 (July 1974).

6. Gottlieb, J. J.; Glass, I. I. — Recent Developments in Sonic-Boom Simulation Using Shock Tubes. Canadian Journal of Physics, Vol. 52, No. 3, pp. 207-218 (February 1974).

7. Ellis, N. D.; Rushwald, I. B.; Ribner, H. S. — Development of a Portable Sonic Boom Simulator for Field Use. UTIAS Technical Note No. 190 (July 1974).

8. Franke, R.; Lursat, C.; Evrard, G.; Devriere, F. — Perte Auditive et Récupération chez le Cobaye après Exposition à des Ondes des Choc à Profile Rectangulaire. Institut Franco-Allemand de Recherches de Saint-Louis, Rapport 3/72 (1972).

9. Webb, D.R.B.; Pallant, R. J. — A Device for Simulating the Sonic Bang. Symposium d'Acoustique Aéronautique, sponsored jointly by the Association Française des Ingénieurs et Technicians de l'Aéronautique et de l'Espace and Groupment des Acousticiens de Langue Francaise and the British Acoustical Society, Toulouse, France (1968).

10. Peter, A.; Pfister, M. — Génération d'Ondes en N à l'aide d'un Tube à Choc en Forme de Pyramide. Institut Franco-Allemand de Recherches de Saint-Louis, Notice N1/69 (1969).

11. Ribner, H. S.; Morris, P. J.; Chu, W. H. — Laboratory Simulation of Development of Superbooms by Atmospheric Turbulence. J. Acoust. Soc. Amer., Vol. 53, No. 3, pp. 926-928 (1973).

12. Peter, A.; Brunner, J. J. — Etude d'un Tube à Choc de forme Pyramidale pour la Gènèration d'une Onde en N. Institut Franco-Allemand de Recherches de Saint-Louis, Note Technique T11/70 (1970).

13. Slutsky, H. E.
Arnold, L.
Experimental-Analytical Dynamic Techniques for Application to Sonic Boom Structural and Acoustic Response Determination. FAA Report NO-70-15 (1970).

14. Thery, C.
Peter, A.
Schlosser, F.
Le Générateur de Bang de l'ISL. Institut Franco-Allemand de Recherches des Saint-Louis, Rapport 15/71 (1971).

15. Warren, C.H.E.
Proposal for a Shock-Tube Facility to Simulate Sonic Bangs. Royal Aircraft Establishment Technical Report No. 66344 (November 1966).

16. Tamboulian, R.
Peschke, W.
Description and Capabilities of a Travelling Wave Sonic Boom Simulator. NASA CR-1696 (1970).

17. Glass, I. I.
Martin, W.
Patterson, G. N.
A Theoretical and Experimental Study of the Shock Tube. UTIAS Technical Note No. 2 (1953).

18. Jeffreys, H. J.
Jeffreys, B. S.
Methods of Mathematical Physics. Cambridge, Second Edition, Chapter 19 (1950).

19. Lamb, H. M.
Hydrodynamics. Dover, Sixth Edition, pp. 491-492 (1932).

20. Landau, L. D.
Lifshitz, E. M.
Mechanics of Continuous Media, Gostekhizdat, Section 78 (1944). Translation, Fluid Mechanics, Pergamon, Section 95 (1959).

TABLE 1

RECTANGULAR SHOCK TUBE

Franke, Lursat, Evrard and Devriere (1972)

Gottlieb (July 1974)

PYRAMIDAL SHOCK TUBE

Webb and Pallant (1968)

Peter and Pfister (1969)

Peter and Brunner (1970)

Slutsky and Arnold (1970)

Thery, Peter and Schlosser (1971)

Carothers (1972)

Ribner, Morris and Chu (1973)

Gottlieb and Glass (1974)

Gottlieb (July 1974)

PYRAMIDAL-RECTANGULAR SHOCK TUBE

Warren (1966)

Peter and Pfister (1969)

Peter and Brunner (1970)

Gottlieb and Glass (1974)

Gottlieb (July 1974)

PYRAMIDAL-PYRAMIDAL SHOCK TUBE

Peter and Brunner (1970)

Gottlieb and Glass (1974)

Gottlieb (July 1974)

RECTANGULAR-PYRAMIDAL SHOCK TUBE

Tamboulian and Peschke (1970)

Carothers (1972)

Gottlieb (July 1974)

TABLE 2

SPECIFIC IMPEDANCE RATIO z ($a_2\rho_2/a_1\rho_1 = \sqrt{\gamma_2 M_2/\gamma_1 M_1}$ if $T_1 = T_2$) FOR DIFFERENT DRIVER AND CHANNEL GASES

	DRIVER GAS			CHANNEL GAS								
	M	γ	a/a_{Air}	H_2	He	Air	A	CO_2	SO_2	CCl_2F_2	SF_6	C_4F_8
H_2	2.0	1.40	3.80	1.00	0.65	0.26	0.21	0.22	0.19	0.14	0.13	0.12
He	4.0	1.67	2.93	1.54	1.00	0.41	0.32	0.34	0.29	0.22	0.21	0.18
Air	29	1.40	1.00	3.80	2.46	1.00	0.78	0.84	0.71	0.54	0.51	0.44
A	40	1.67	0.93	4.87	3.16	1.28	1.00	1.08	0.91	0.70	0.65	0.56
CO_2	44	1.30	0.78	4.52	2.93	1.19	0.93	1.00	0.84	0.65	0.60	0.52
SO_2	64	1.26	0.64	5.37	3.48	1.41	1.10	1.19	1.00	0.77	0.72	0.62
CCl_2F_2	121	1.13	0.44	6.99	4.53	1.84	1.43	1.55	1.30	1.00	0.93	0.81
SF_6	144	1.096	0.40	7.51	4.87	1.98	1.54	1.66	1.40	1.07	1.00	0.86
C_4F_8	200	1.055	0.33	8.68	5.63	2.28	1.78	1.92	1.62	1.24	1.16	1.00

TABLE 3

PARAMETER ℓ $[(1 + z)/(\gamma_1 z^2/\gamma_2 - 1)$ with $T_1 = T_2]$ FOR DIFFERENT DRIVER AND CHANNEL GASES

DRIVER GAS				CHANNEL GAS								
	M	γ	a/a_{Air}	H_2	He	Air	A	CO_2	SO_2	CCl_2F_2	SF_6	C_4F_8
H_2	2.0	1.40	3.80	$\mp\infty$	-3.30	-1.36	-1.27	-1.28	-1.22	-1.16	-1.15	-1.13
He	4.0	1.67	2.93	2.58	$\mp\infty$	-1.63	-1.46	-1.48	-1.37	-1.26	-1.24	-1.20
Air	29	1.40	1.00	0.36	0.55	$\mp\infty$	-6.47	-5.40	-3.13	-2.03	-1.89	-1.68
A	40	1.67	0.93	0.31	0.46	6.01	$\mp\infty$	-22.9	-5.09	-2.54	-2.28	-1.95
CO_2	44	1.30	0.78	0.26	0.39	4.22	19.2	$\mp\infty$	-5.90	-2.59	-2.30	-1.95
SO_2	64	1.26	0.64	0.21	0.30	2.00	3.50	4.81	$\mp\infty$	-3.75	-3.01	-2.38
CCl_2F_2	121	1.13	0.44	0.13	0.19	0.89	1.20	1.45	2.58	$\mp\infty$	-12.1	-4.57
SF_6	144	1.096	0.40	0.12	0.17	0.75	0.98	1.17	1.92	10.9	$\mp\infty$	-6.66
C_4F_8	200	1.055	0.33	0.10	0.14	0.56	0.69	0.82	1.23	3.43	5.54	$\mp\infty$

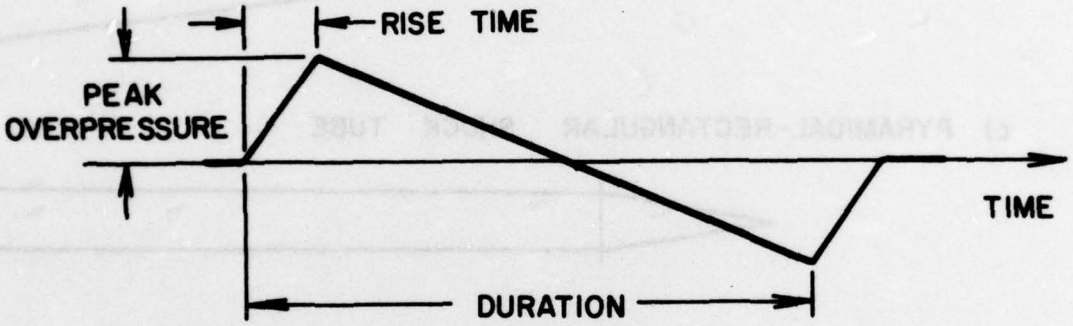

FIG. 1 IDEALIZED OVERPRESSURE SIGNATURE OF A SONIC BOOM

a) RECTANGULAR SHOCK TUBE

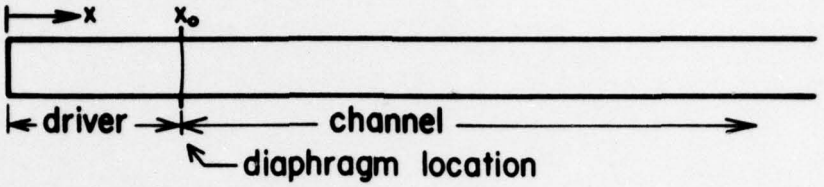

b) PYRAMIDAL SHOCK TUBE

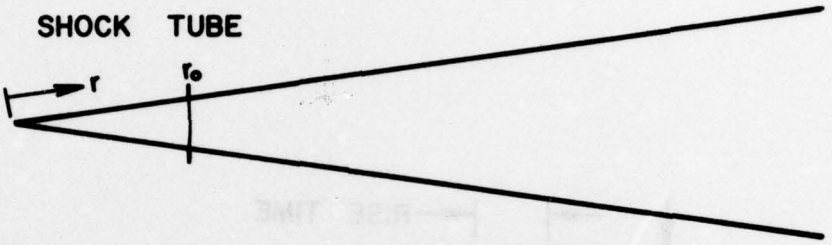

c) PYRAMIDAL-RECTANGULAR SHOCK TUBE

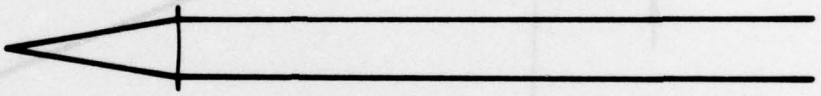

d) PYRAMIDAL-PYRAMIDAL SHOCK TUBE

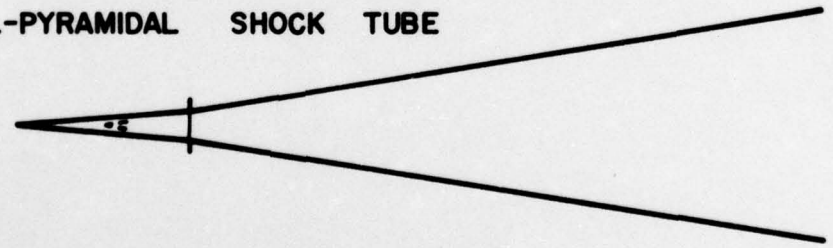

e) RECTANGULAR-PYRAMIDAL SHOCK TUBE

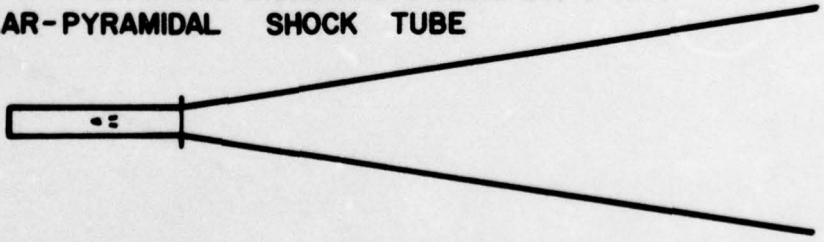

FIG. 2 SHOCK TUBES WHICH HAVE BEEN ASSESSED FOR SONIC-BOOM SIMULATION PURPOSES

a) RECTANGULAR SHOCK TUBE

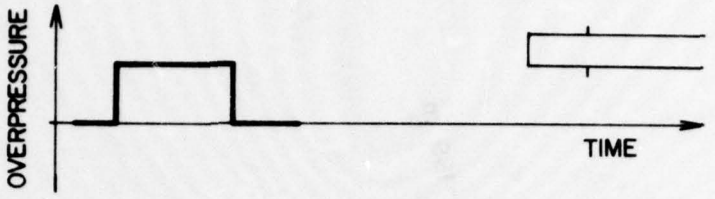

b) PYRAMIDAL SHOCK TUBE

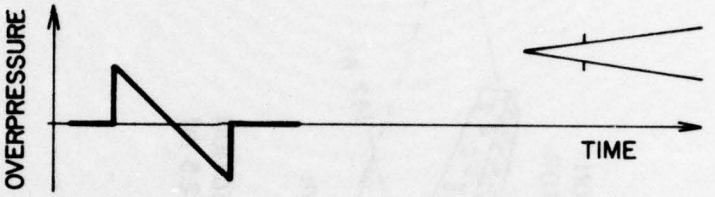

c) PYRAMIDAL-RECTANGULAR SHOCK TUBE

d) PYRAMIDAL-PYRAMIDAL SHOCK TUBE

e) RECTANGULAR-PYRAMIDAL SHOCK TUBE

FIG. 3 OVERPRESSURE SIGNATURES IN THE CHANNEL OF VARIOUS LOW-PRESSURE-RATIO SHOCK TUBES

DIAPHRAGM LOCATION	N-WAVE DURATION
a	100 ms
b	135 ms
c	270 ms
d	300 ms
e	330 ms

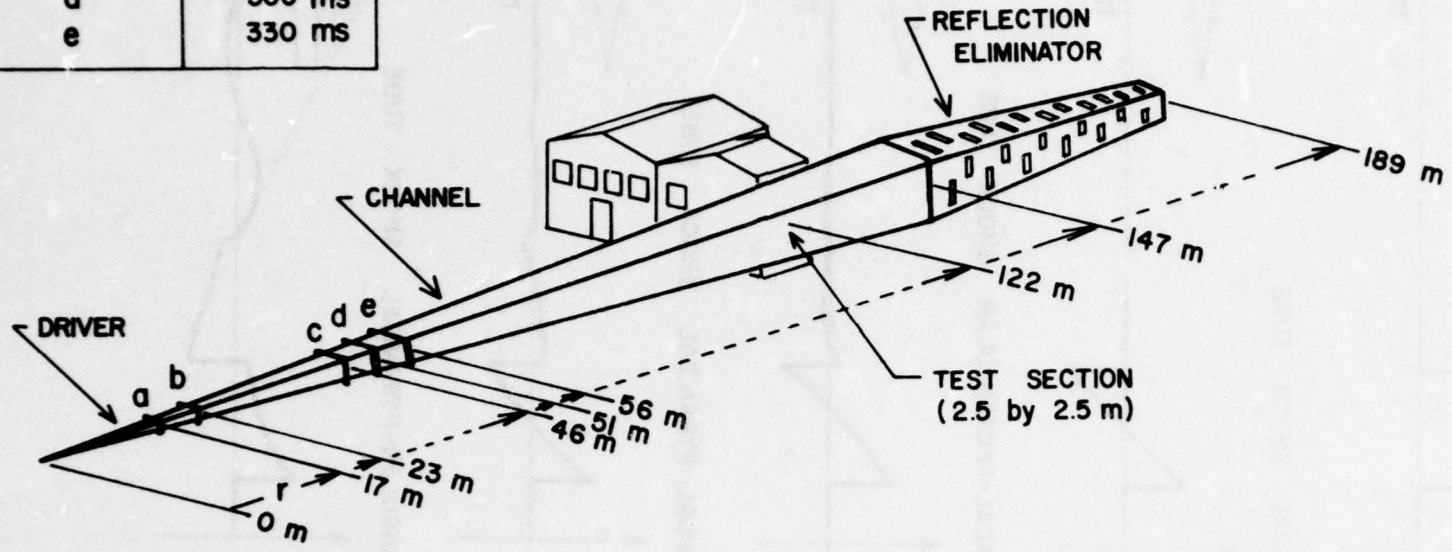

FIG. 4 THE FRANCO-GERMAN SONIC BOOM SIMULATOR

a) PYRAMIDAL SHOCK TUBE (long channel)

b) PYRAMIDAL-PYRAMIDAL SHOCK TUBE (short channel)

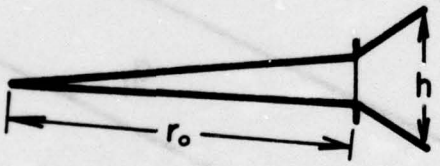

FIG. 5 COMPARISON OF PYRAMIDAL AND PYRAMIDAL-PYRAMIDAL SHOCK TUBES WHICH PRODUCE EQUIVALENT-DURATION SIMULATED SONIC BOOMS

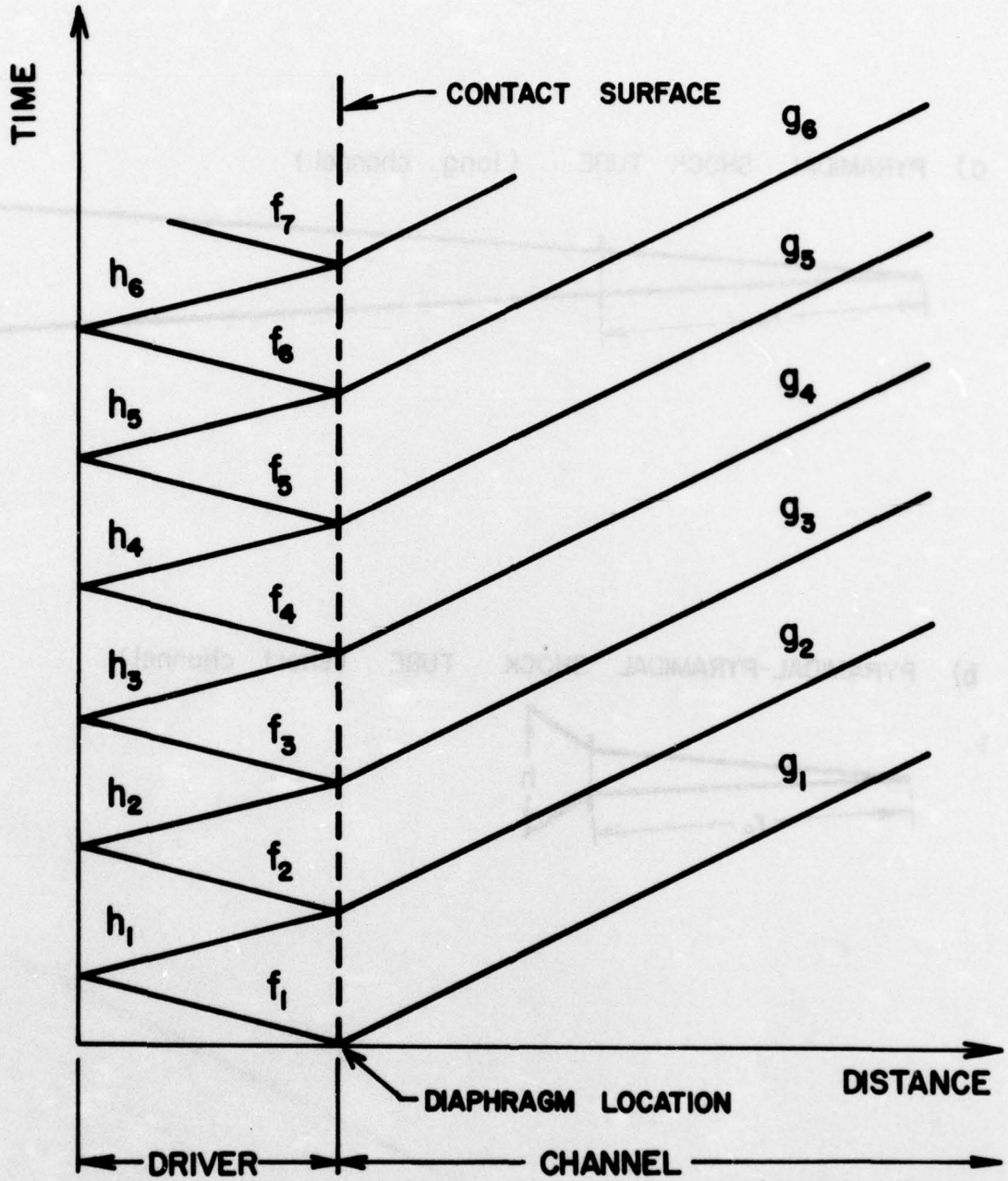

FIG. 6 TIME-DISTANCE DIAGRAM ILLUSTRATING THE WAVE MOTION IN A LOW-PRESSURE-RATIO RECTANGULAR AND PYRAMIDAL SHOCK TUBE

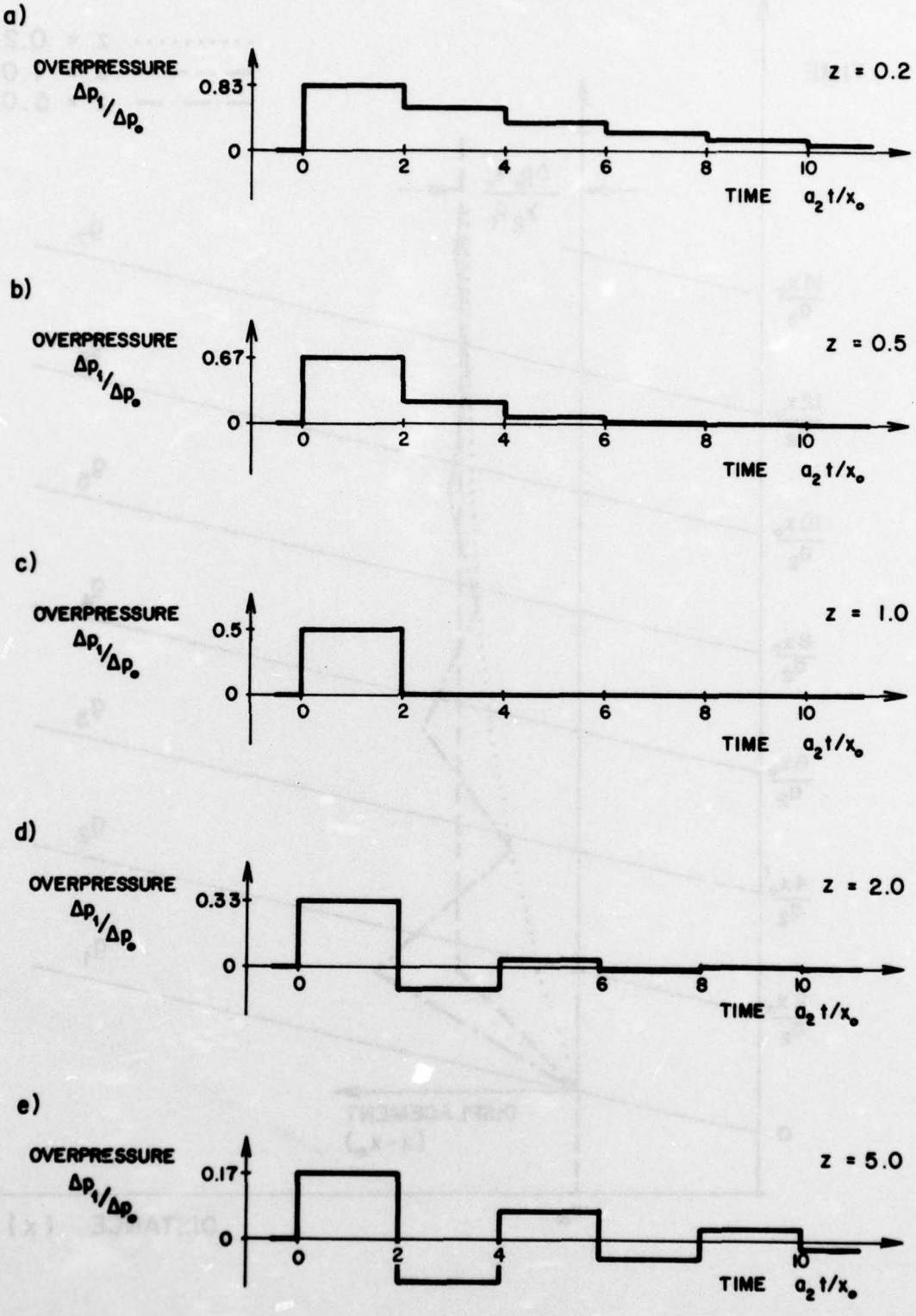

FIG. 7 OVERPRESSURE SIGNATURES IN THE CHANNEL OF A RECTANGULAR SHOCK TUBE FOR DIFFERENT DRIVER AND CHANNEL GASES

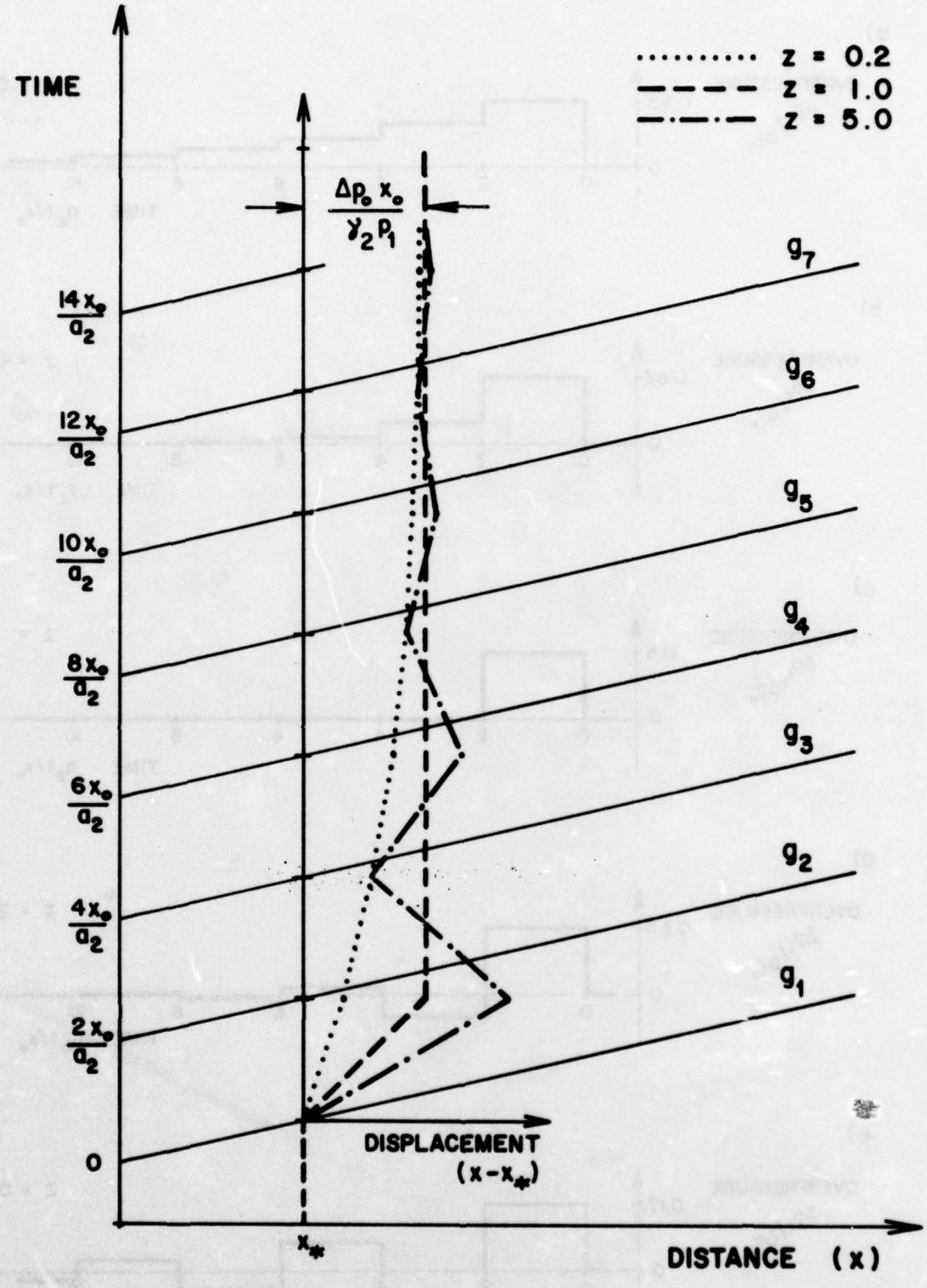

FIG. 8 MOTION OF A FLUID PARTICLE IN THE CHANNEL OF A RECTANGULAR SHOCK TUBE

a) DRIVER GAS: AIR
CHANNEL GAS: AIR
MEASUREMENT LOCATION: x = 1 m

Δp_o = 10 kN/m^2
x_o = 46 cm

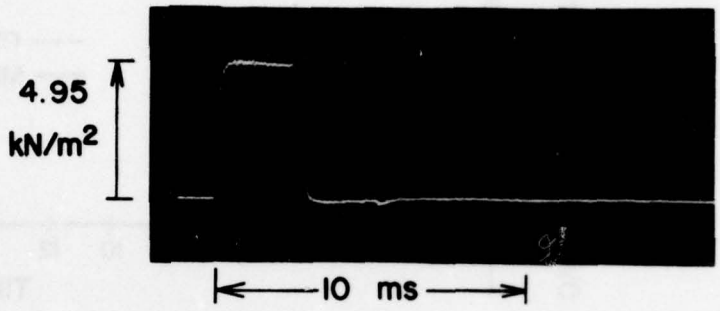

b) DRIVER GAS: HELIUM
CHANNEL GAS: AIR
MEASUREMENT LOCATION: x = 2.1 m

Δp_o = 10 kN/m^2
x_o = 1.5 m

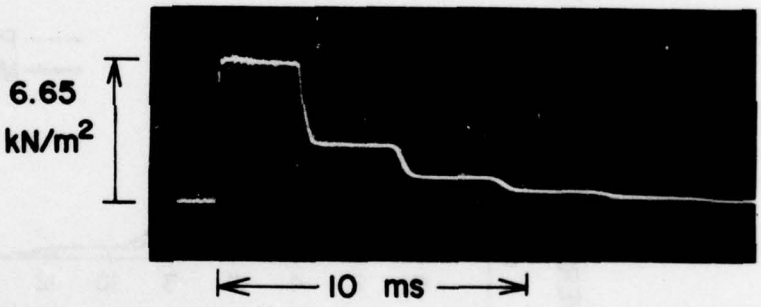

c) DRIVER GAS: AIR
CHANNEL GAS: HELIUM
MEASUREMENT LOCATION: x = 1 m

Δp_o = 10 kN/m^2
x_o = 46 cm

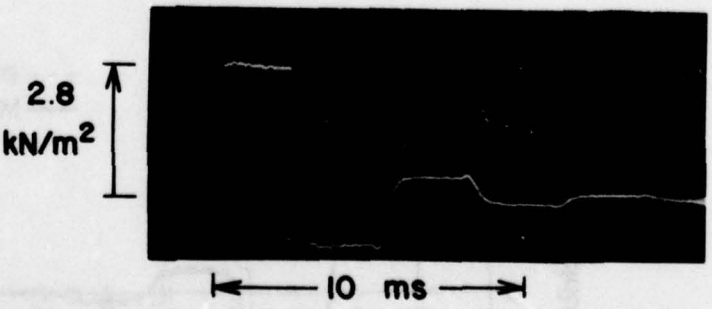

FIG. 9 OVERPRESSURE MEASUREMENTS MADE IN THE CHANNEL OF A RECTANGULAR SHOCK TUBE.

a) DRIVER GAS: AIR
CHANNEL GAS: AIR
MEASUREMENT LOCATION: x = 1 m

Δp_o = 10 kN/m^2

x_o = 46 cm

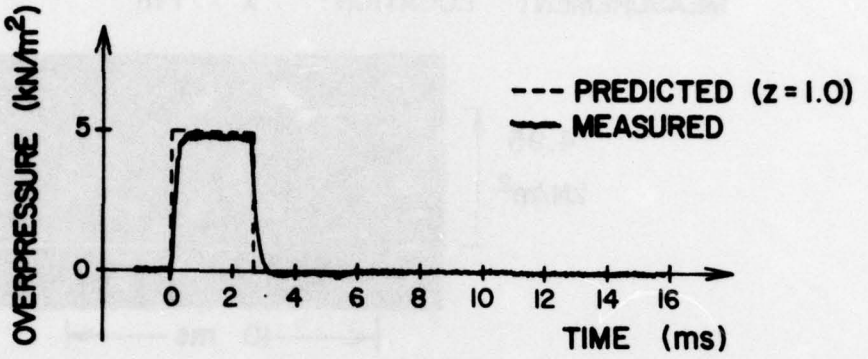

b) DRIVER GAS: HELIUM
CHANNEL GAS: AIR
MEASUREMENT LOCATION: x = 2.1 m

Δp_o = 10 kN/m^2

x_o = 1.5 m

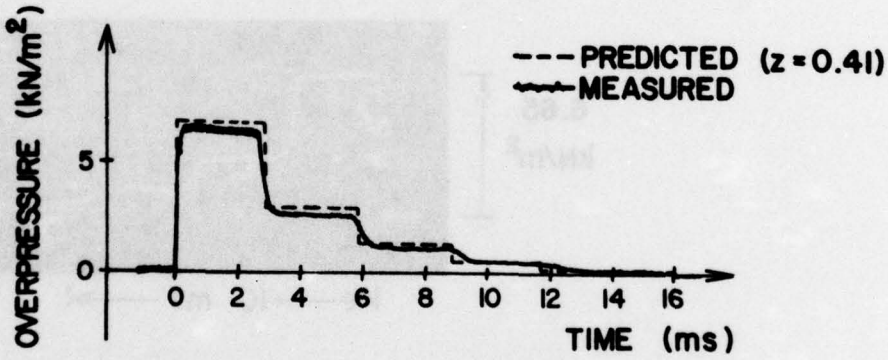

c) DRIVER GAS: AIR
CHANNEL GAS: HELIUM
MEASUREMENT LOCATION: x = 1 m

Δp_o = 10 kN/m^2

x_o = 46 cm

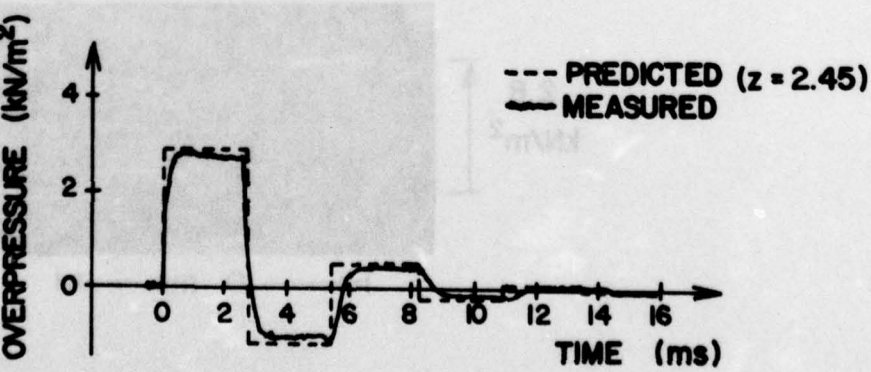

FIG. 10 COMPARISON OF PREDICTED AND MEASURED OVERPRESSURE SIGNATURES FOR A RECTANGULAR SHOCK TUBE.

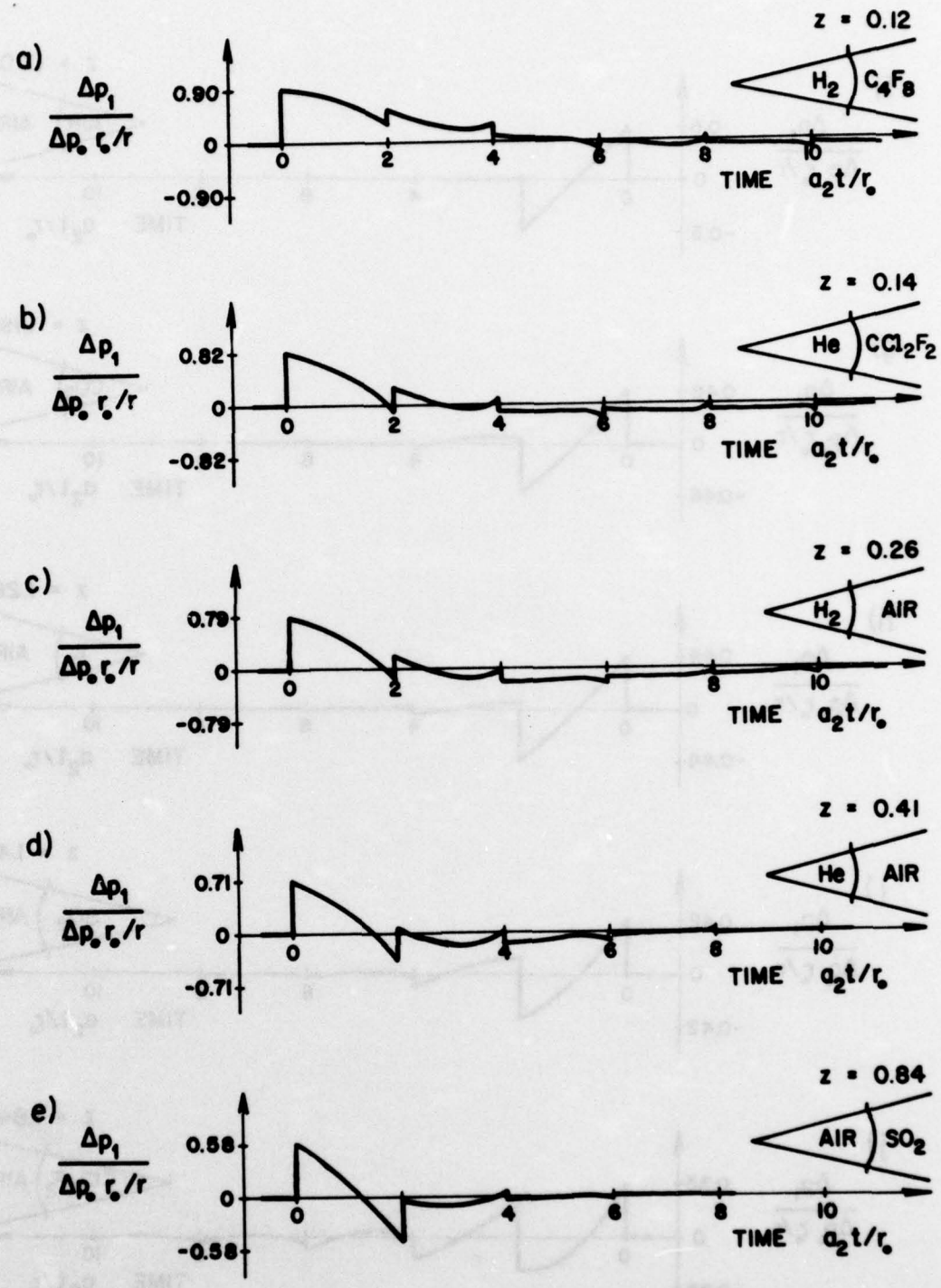

FIG. 11a to 11e OVERPRESSURE SIGNATURES FOR THE CHANNEL OF A PYRAMIDAL SHOCK TUBE FOR WHICH THE DRIVER AND CHANNEL GASES ARE DIFFERENT BUT HAVE IDENTICAL TEMPERATURES

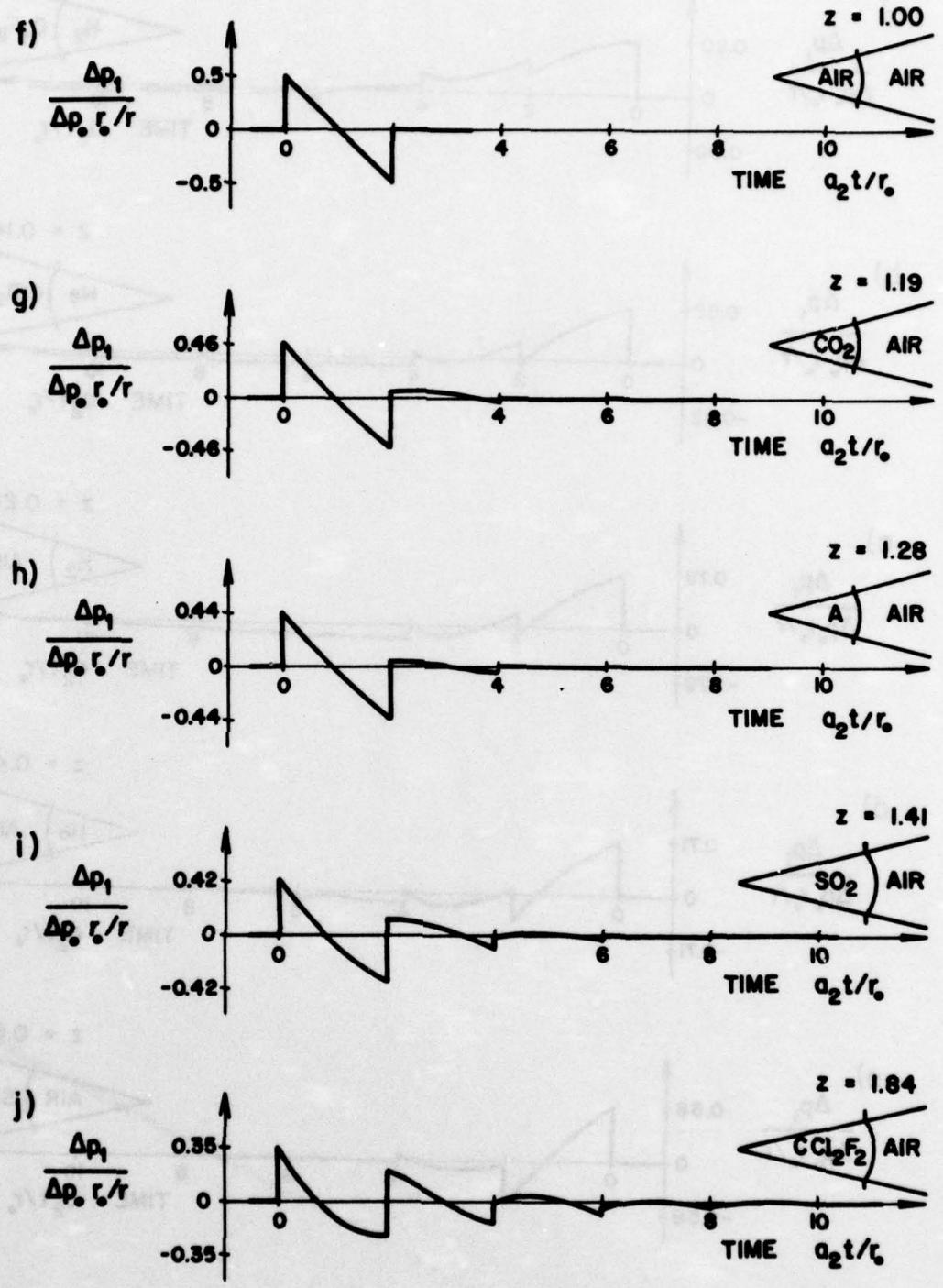

FIG. 11f to 11j OVERPRESSURE SIGNATURES FOR THE CHANNEL OF A PYRAMIDAL SHOCK TUBE FOR WHICH THE DRIVER AND CHANNEL GASES ARE DIFFERENT BUT HAVE IDENTICAL TEMPERATURES

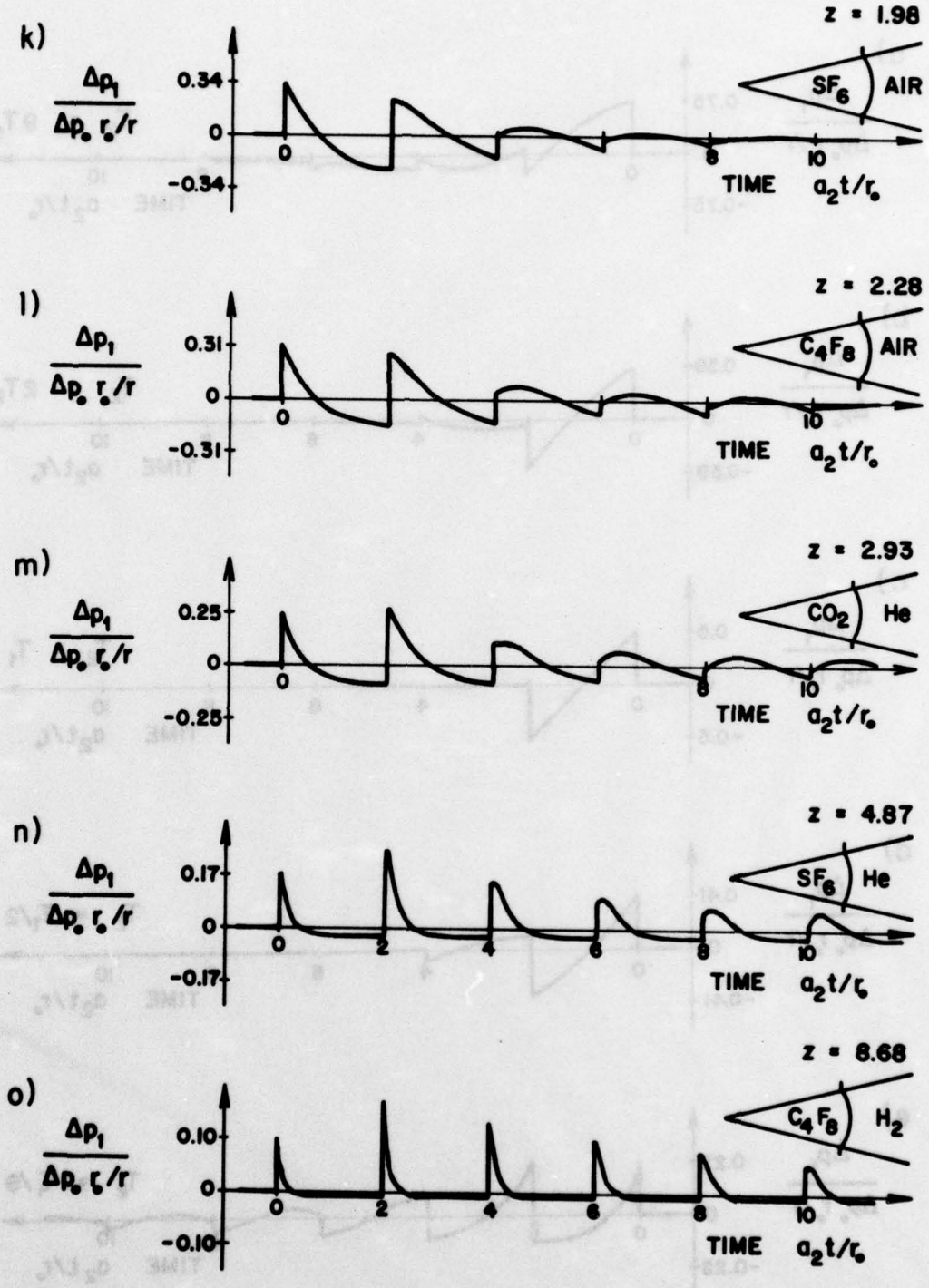

FIG. 11k to 11o OVERPRESSURE SIGNATURES FOR THE CHANNEL OF A PYRAMIDAL SHOCK TUBE FOR WHICH THE DRIVER AND CHANNEL GASES ARE DIFFERENT BUT HAVE IDENTICAL TEMPERATURES

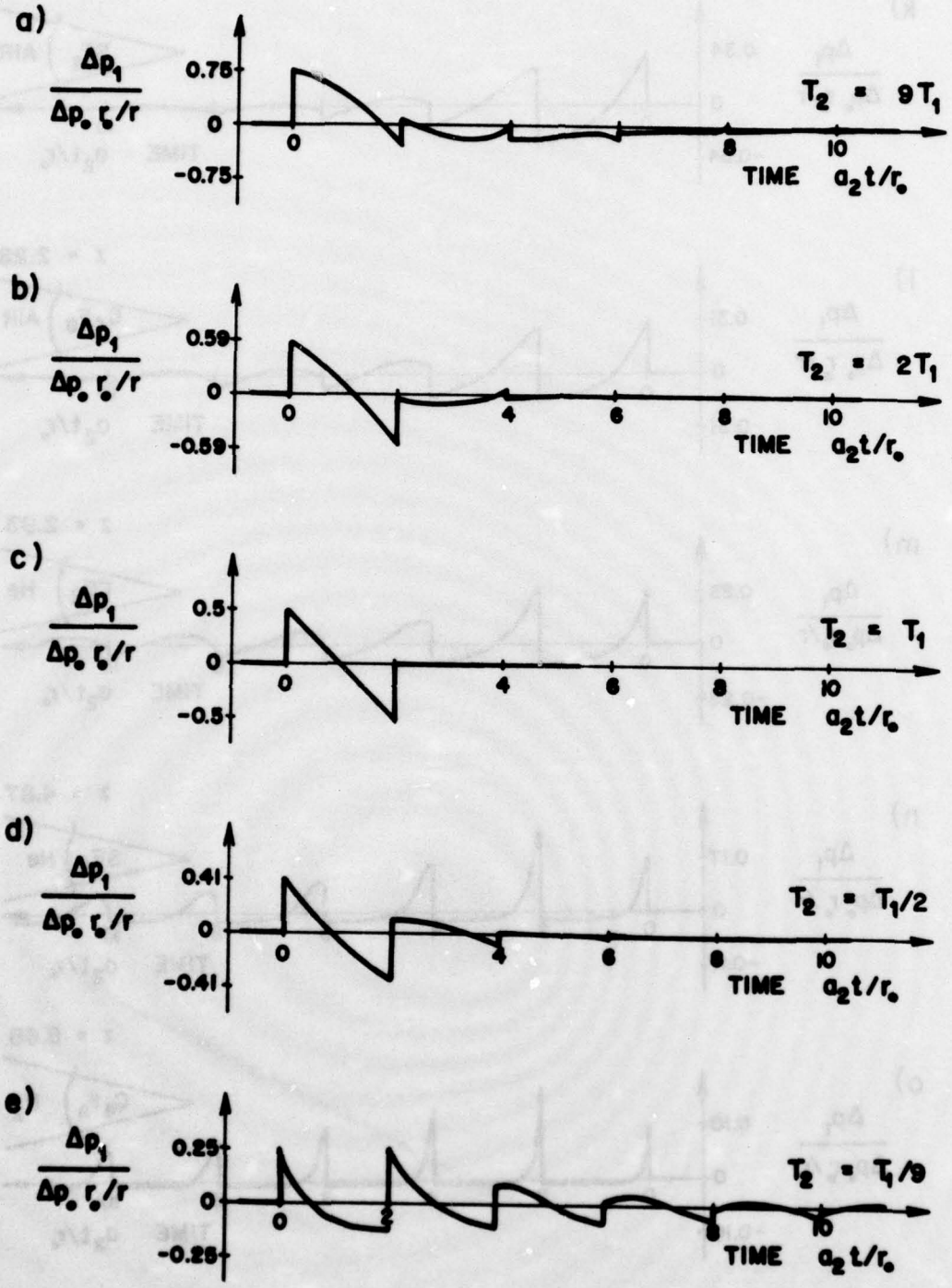

FIG. 12 OVERPRESSURE SIGNATURES FOR THE CHANNEL OF A PYRAMIDAL SHOCK TUBE FOR WHICH THE DRIVER AND CHANNEL GASES ARE IDENTICAL BUT HAVE DIFFERENT TEMPERATURES

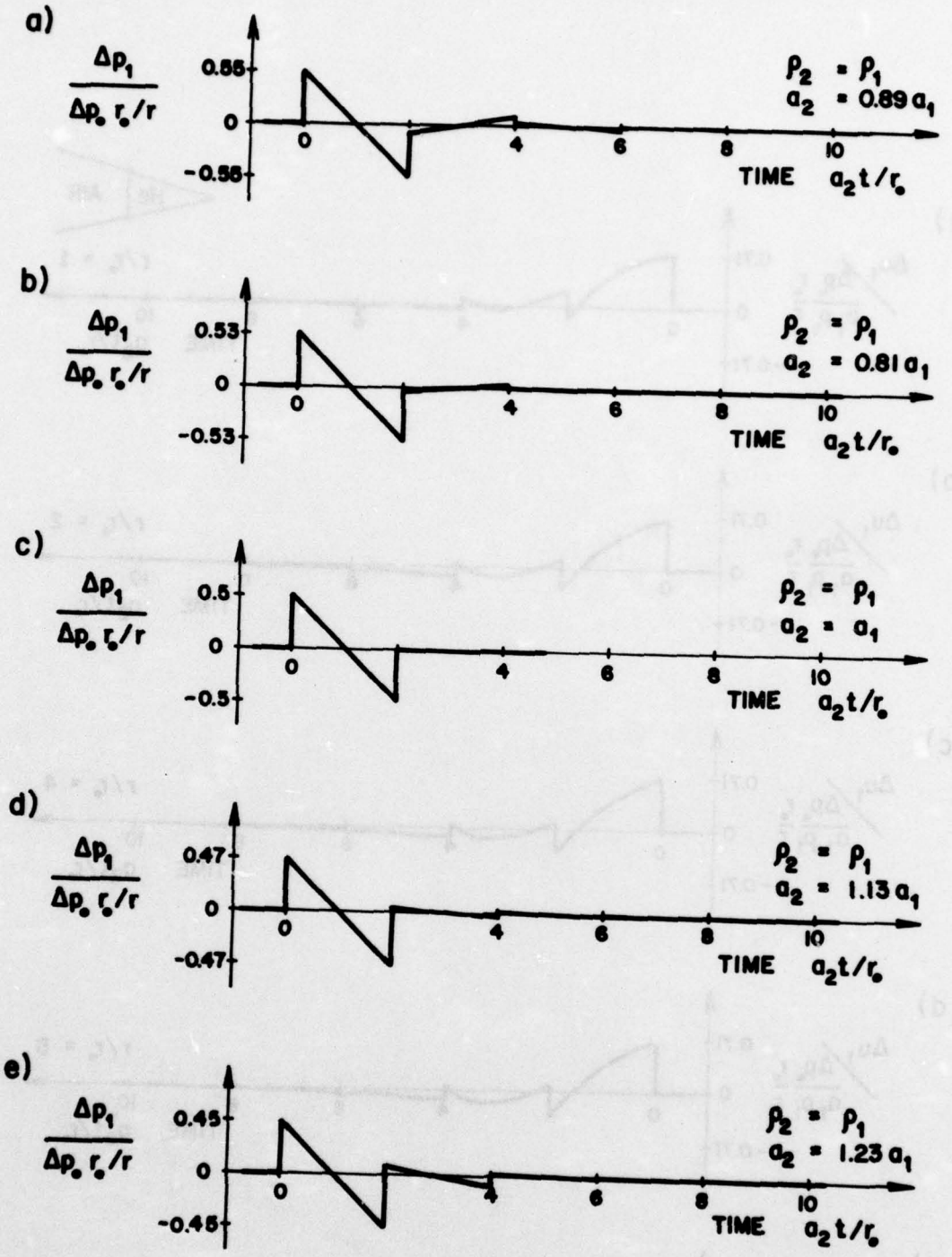

FIG. 13 OVERPRESSURE SIGNATURES FOR THE CHANNEL OF A PYRAMIDAL SHOCK TUBE FOR WHICH THE DIFFERENT DRIVER AND CHANNEL GASES HAVE EQUIVALENT DENSITIES BUT DIFFERENT SOUND SPEEDS

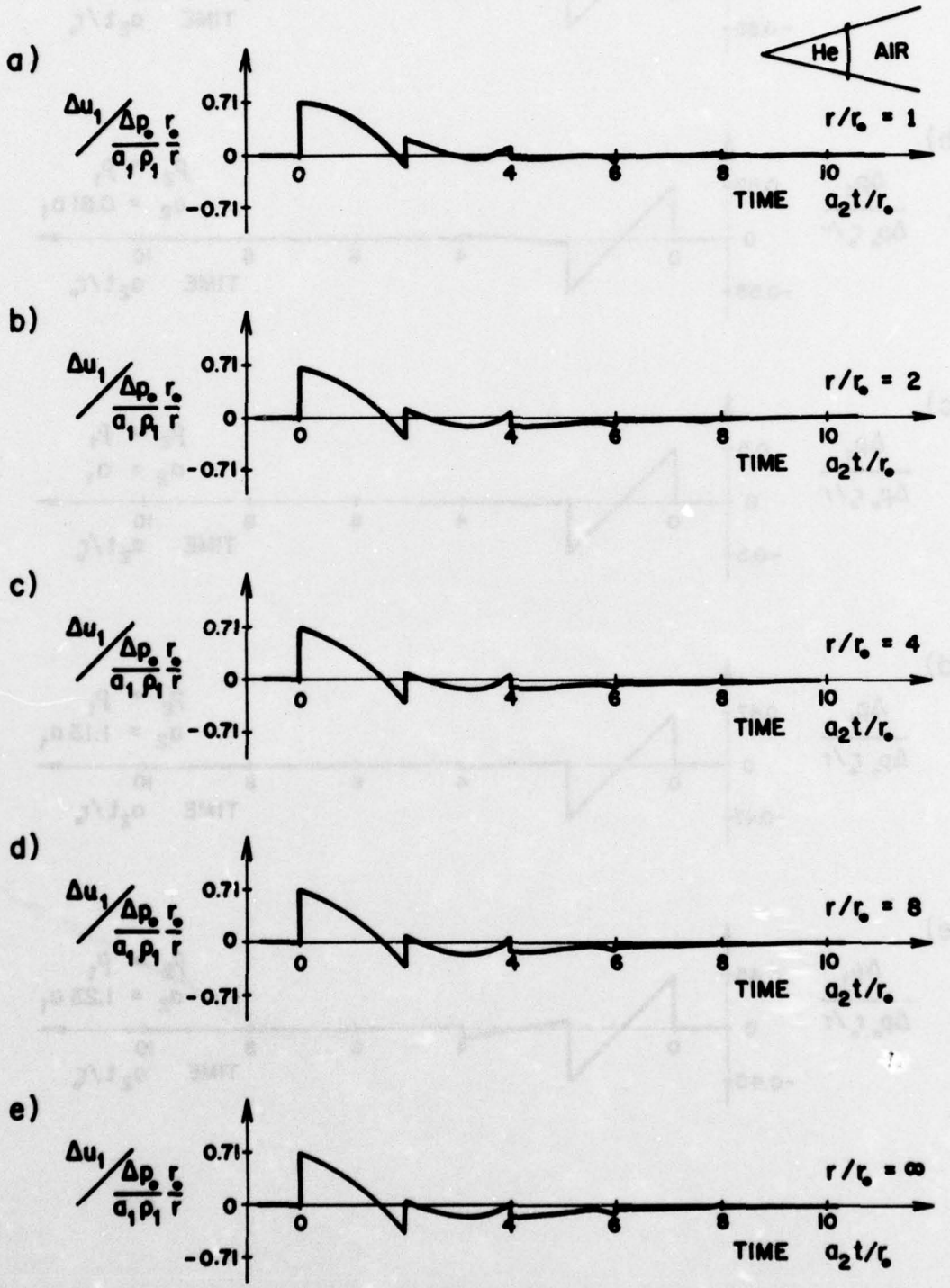

FIG. 14 FIVE NONDIMENSIONAL PARTICLE-VELOCITY SIGNATURES FOR DIFFERENT RADII IN THE CHANNEL OF A PYRAMIDAL SHOCK TUBE

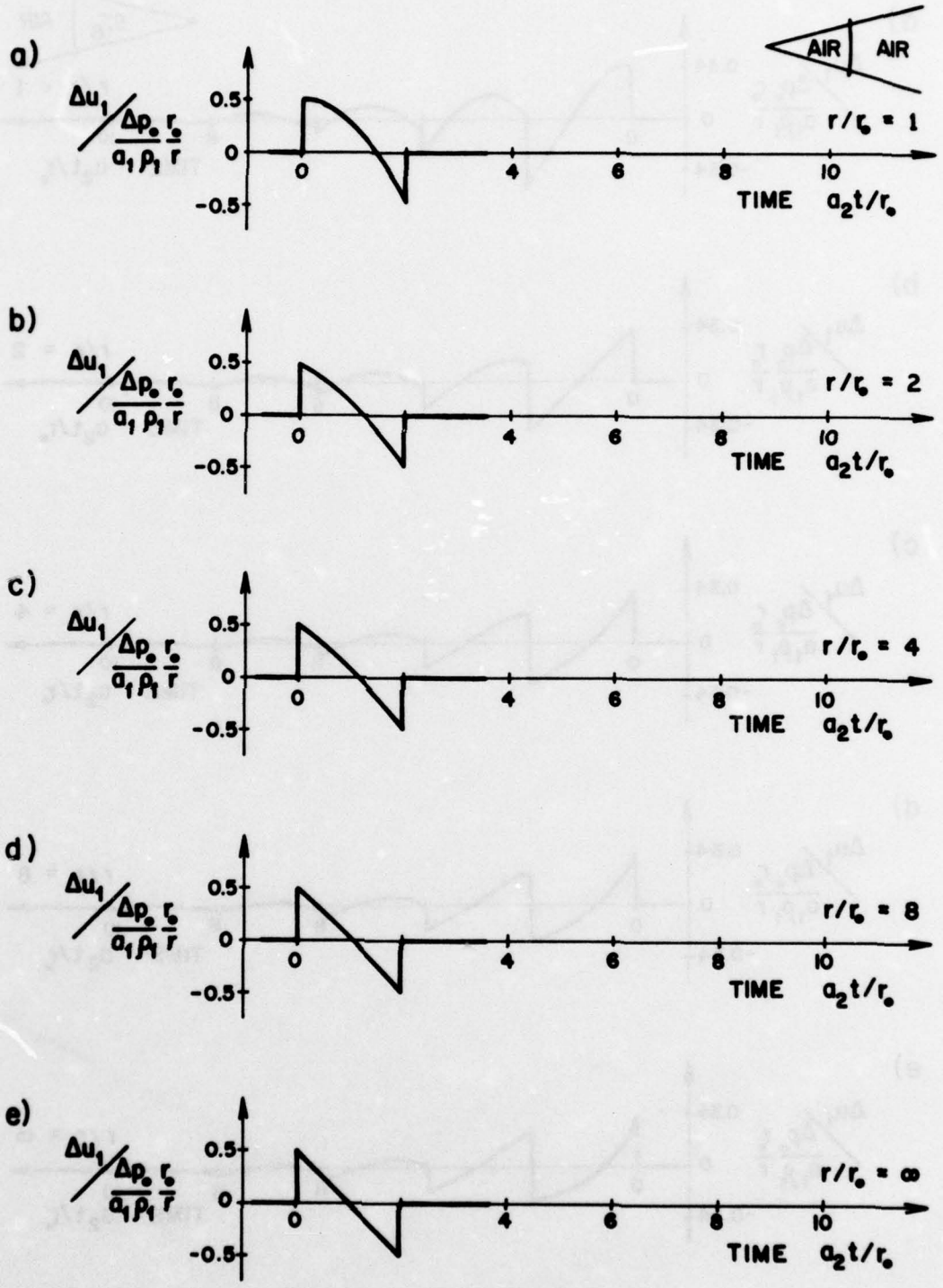

FIG. 15 FIVE NONDIMENSIONAL PARTICLE-VELOCITY SIGNATURES FOR DIFFERENT RADII IN THE CHANNEL OF A PYRAMIDAL SHOCK TUBE

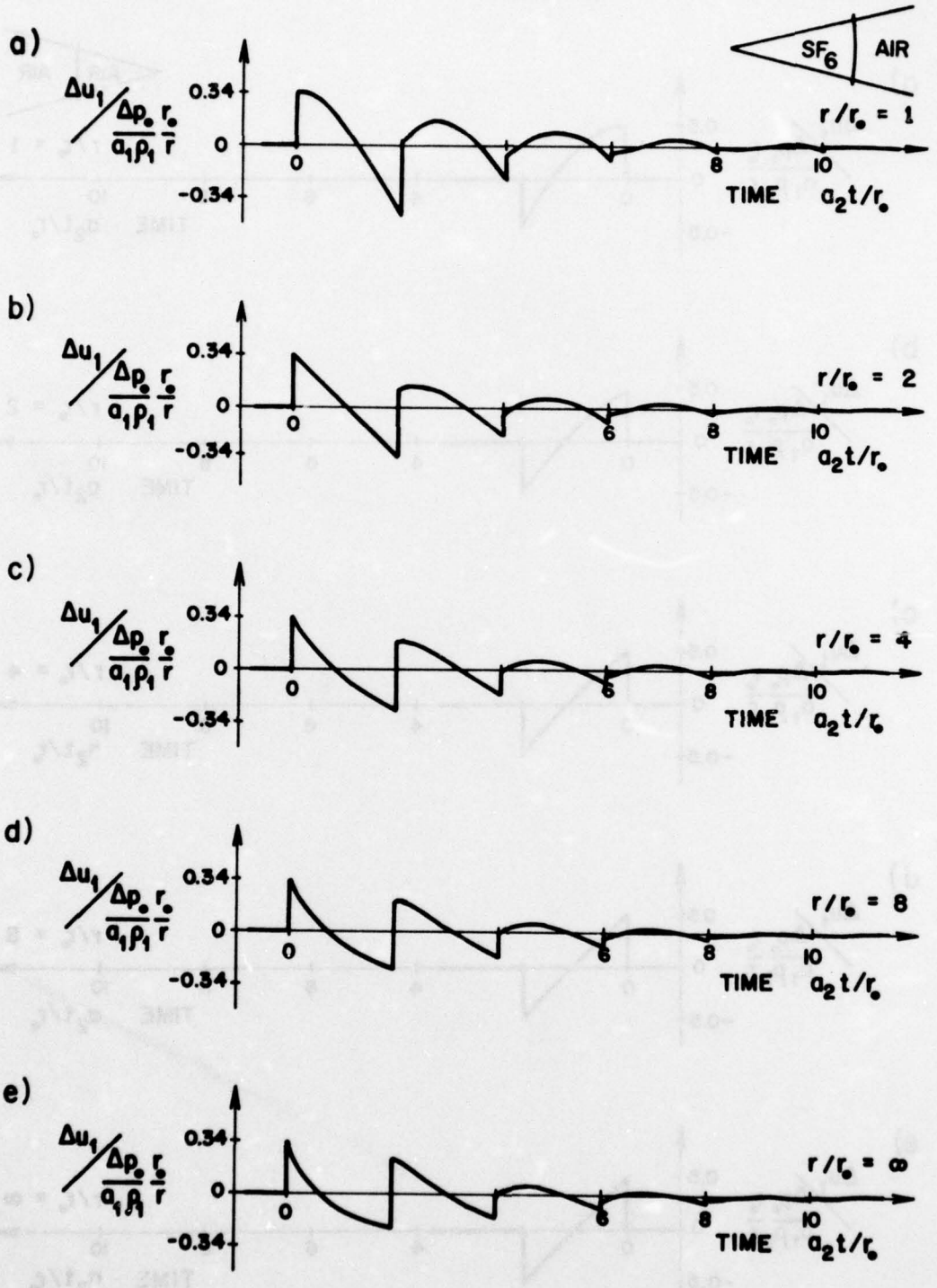

FIG. 16 FIVE NONDIMENSIONAL PARTICLE-VELOCITY SIGNATURES FOR DIFFERENT RADII IN THE CHANNEL OF A PYRAMIDAL SHOCK TUBE

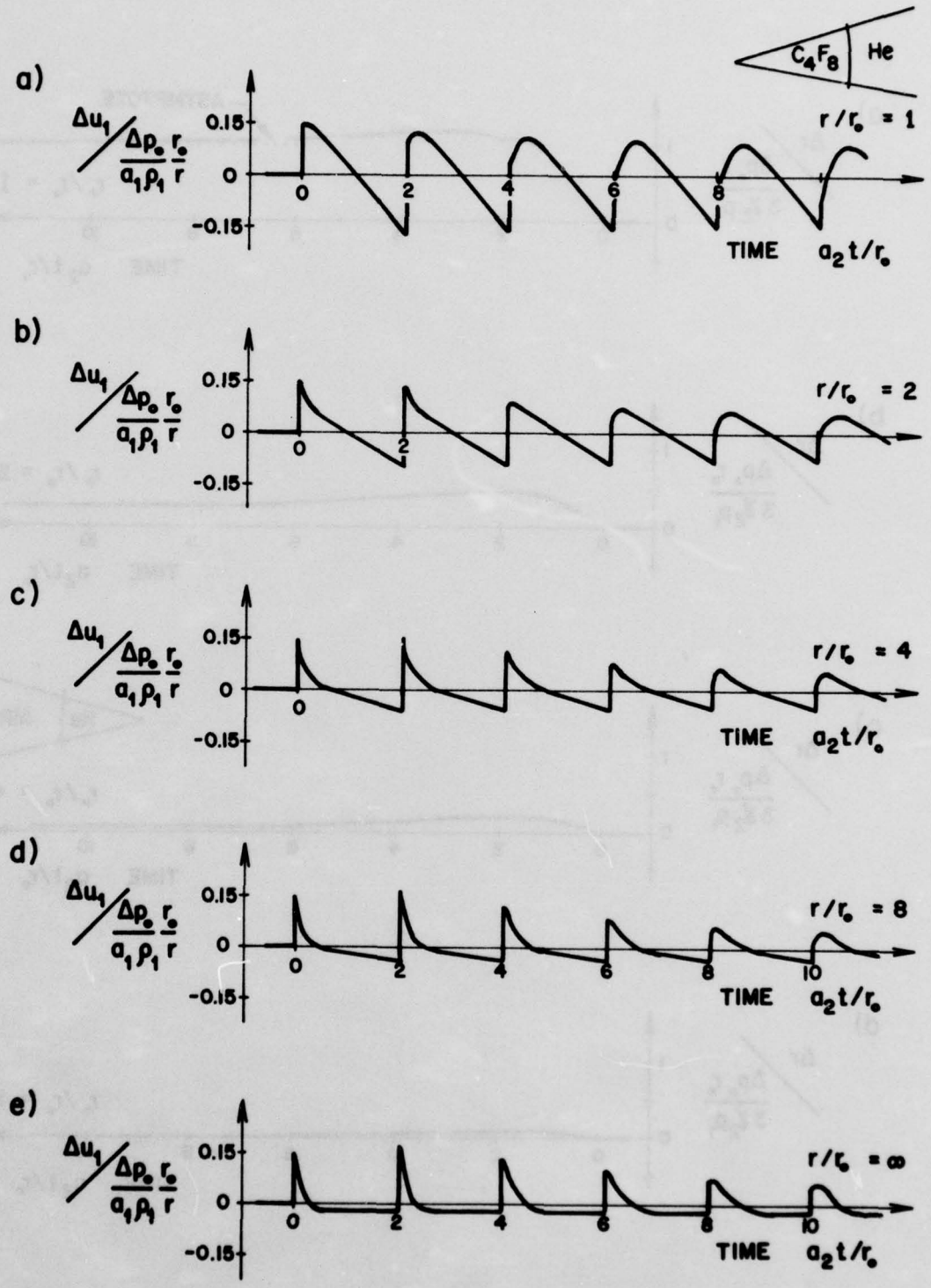

FIG. 17 FIVE NONDIMENSIONAL PARTICLE-VELOCITY SIGNATURES FOR DIFFERENT RADII IN THE CHANNEL OF A PYRAMIDAL SHOCK TUBE

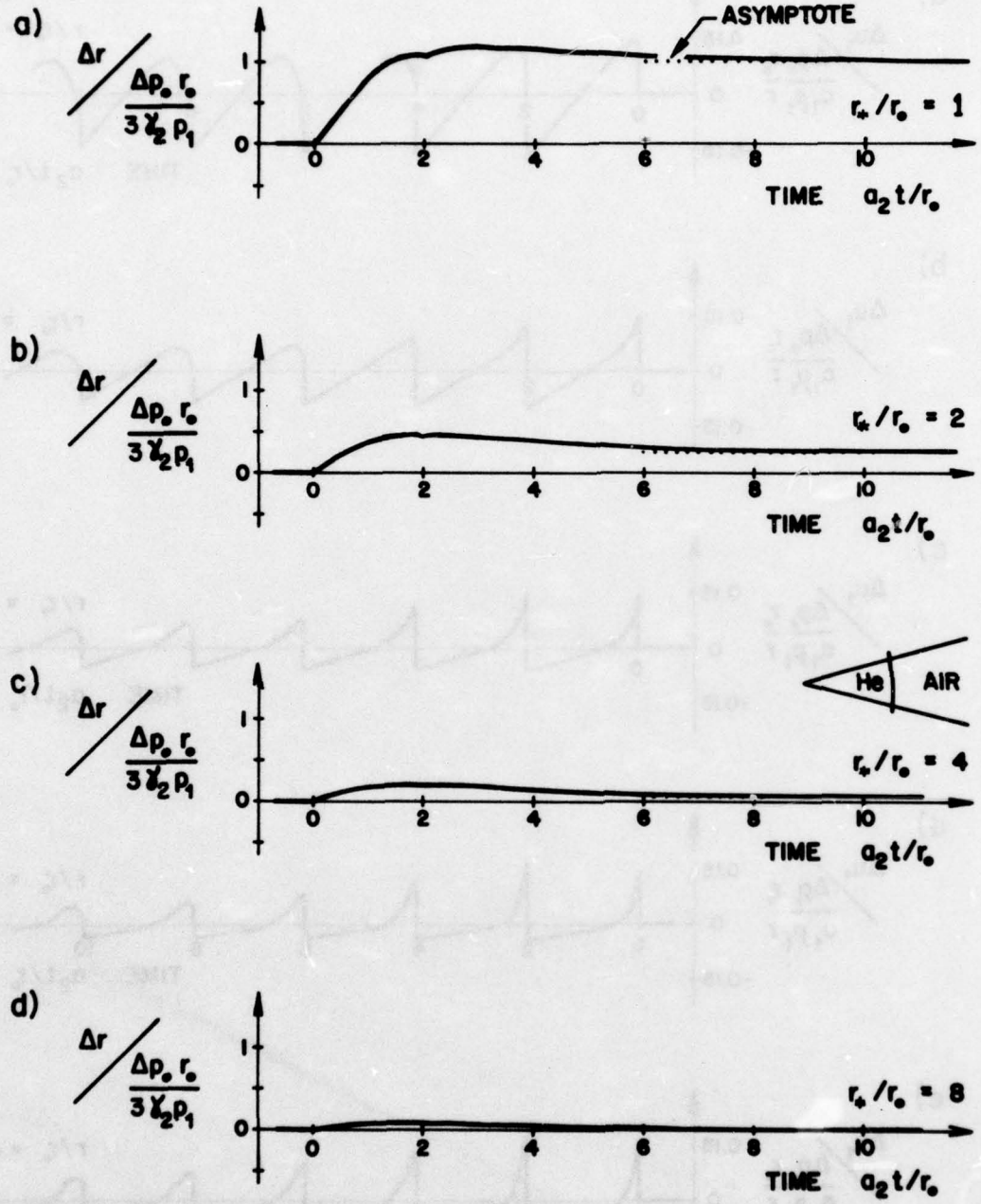

FIG. 18 FOUR NONDIMENSIONAL DISPLACEMENT HISTORIES OF A FLUID PARTICLE AT DIFFERENT RADII IN THE CHANNEL OF A PYRAMIDAL SHOCK TUBE

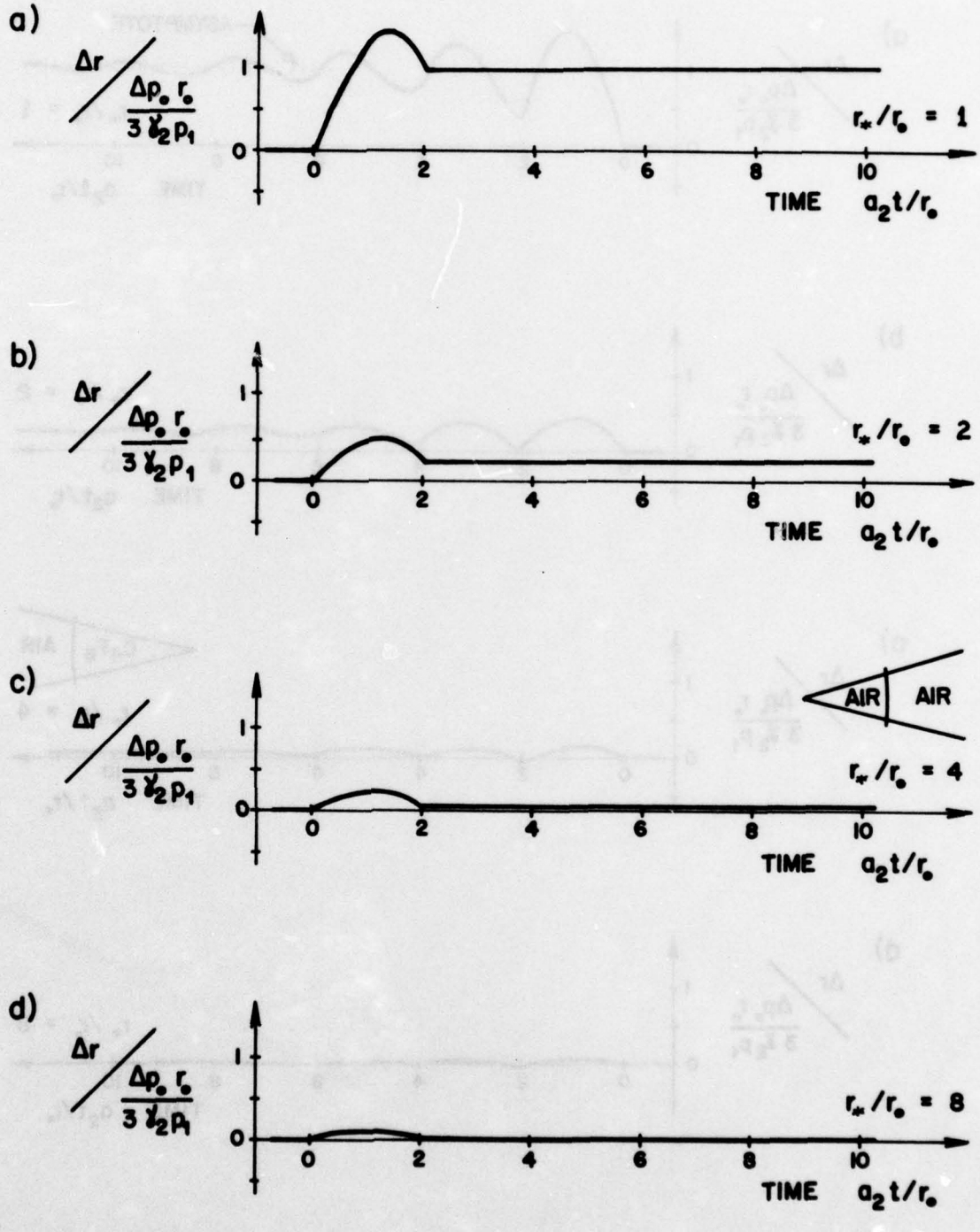

FIG. 19 FOUR NONDIMENSIONAL DISPLACEMENT HISTORIES OF A FLUID PARTICLE AT DIFFERENT RADII IN THE CHANNEL OF A PYRAMIDAL SHOCK TUBE

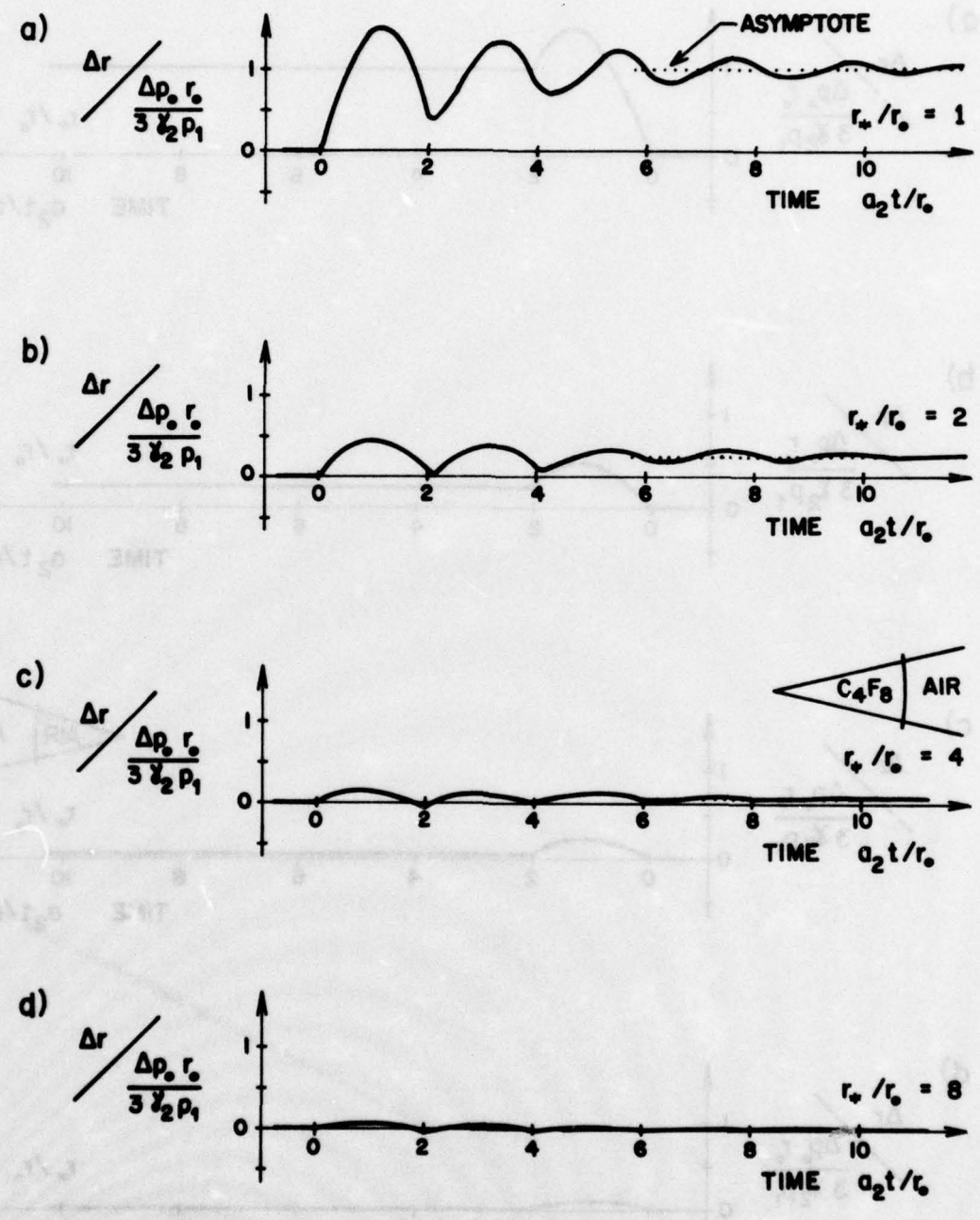

FIG. 20 FOUR NONDIMENSIONAL DISPLACEMENT HISTORIES OF A FLUID PARTICLE AT DIFFERENT RADII IN THE CHANNEL OF A PYRAMIDAL SHOCK TUBE

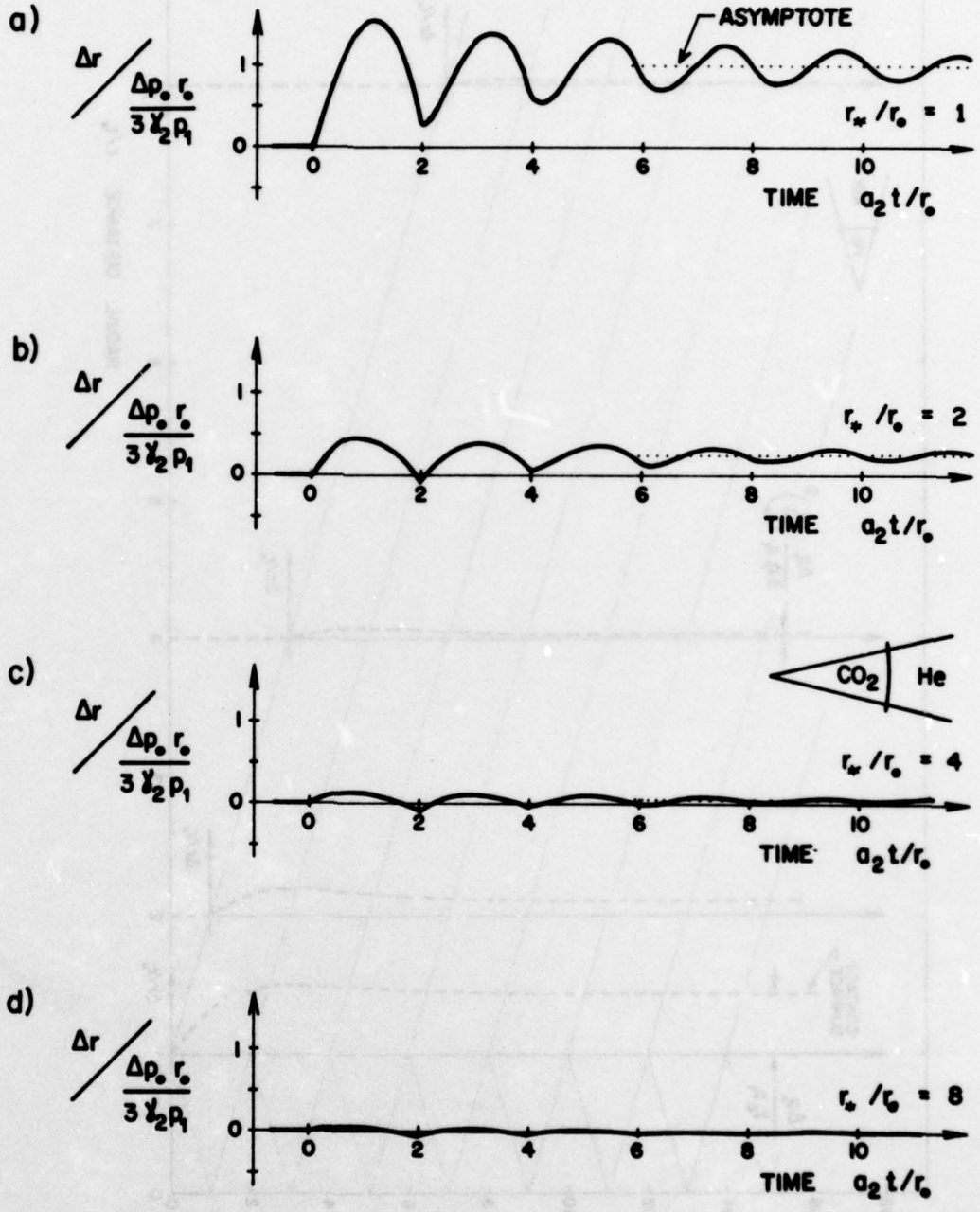

FIG. 21 FIVE NONDIMENSIONAL DISPLACEMENT HISTORIES OF A FLUID PARTICLE AT DIFFERENT RADII IN THE CHANNEL OF A PYRAMIDAL SHOCK TUBE

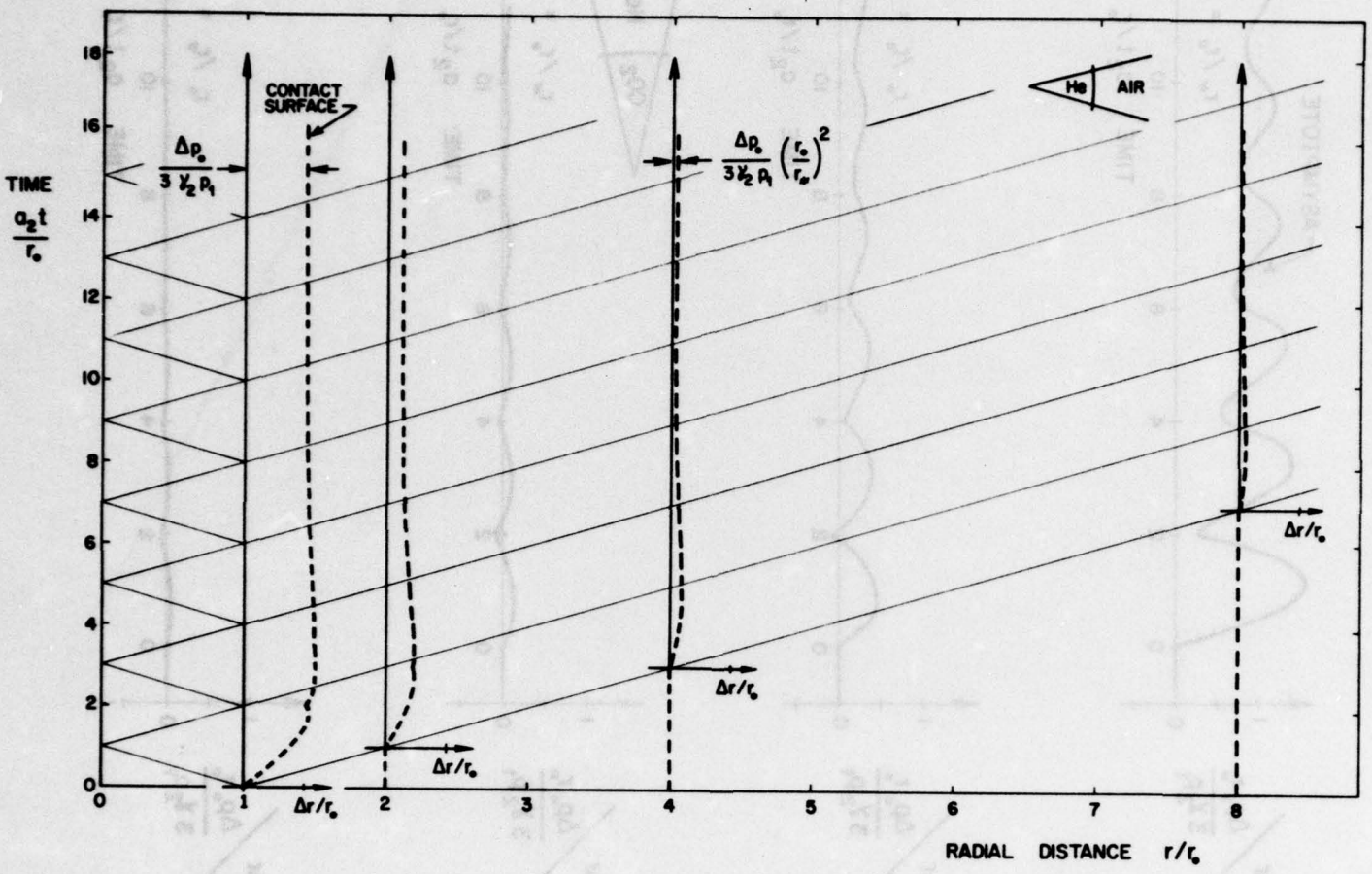

FIG. 22 PARTICLE-DISPLACEMENT HISTORIES AT DIFFERENT RADII IN THE CHANNEL OF A PYRAMIDAL SHOCK TUBE

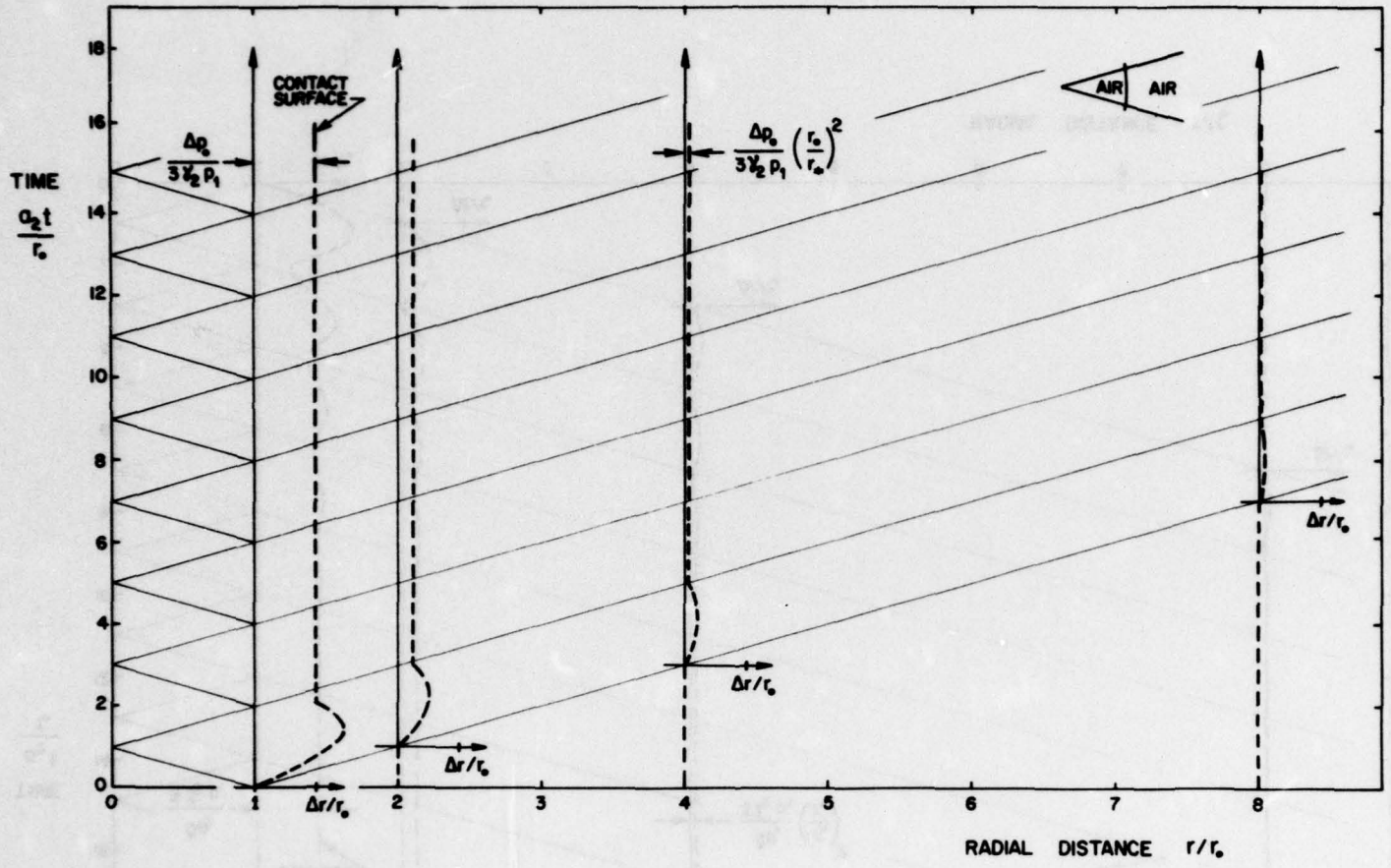

FIG. 23 PARTICLE-DISPLACEMENT HISTORIES AT DIFFERENT RADII IN THE CHANNEL OF A PYRAMIDAL SHOCK TUBE

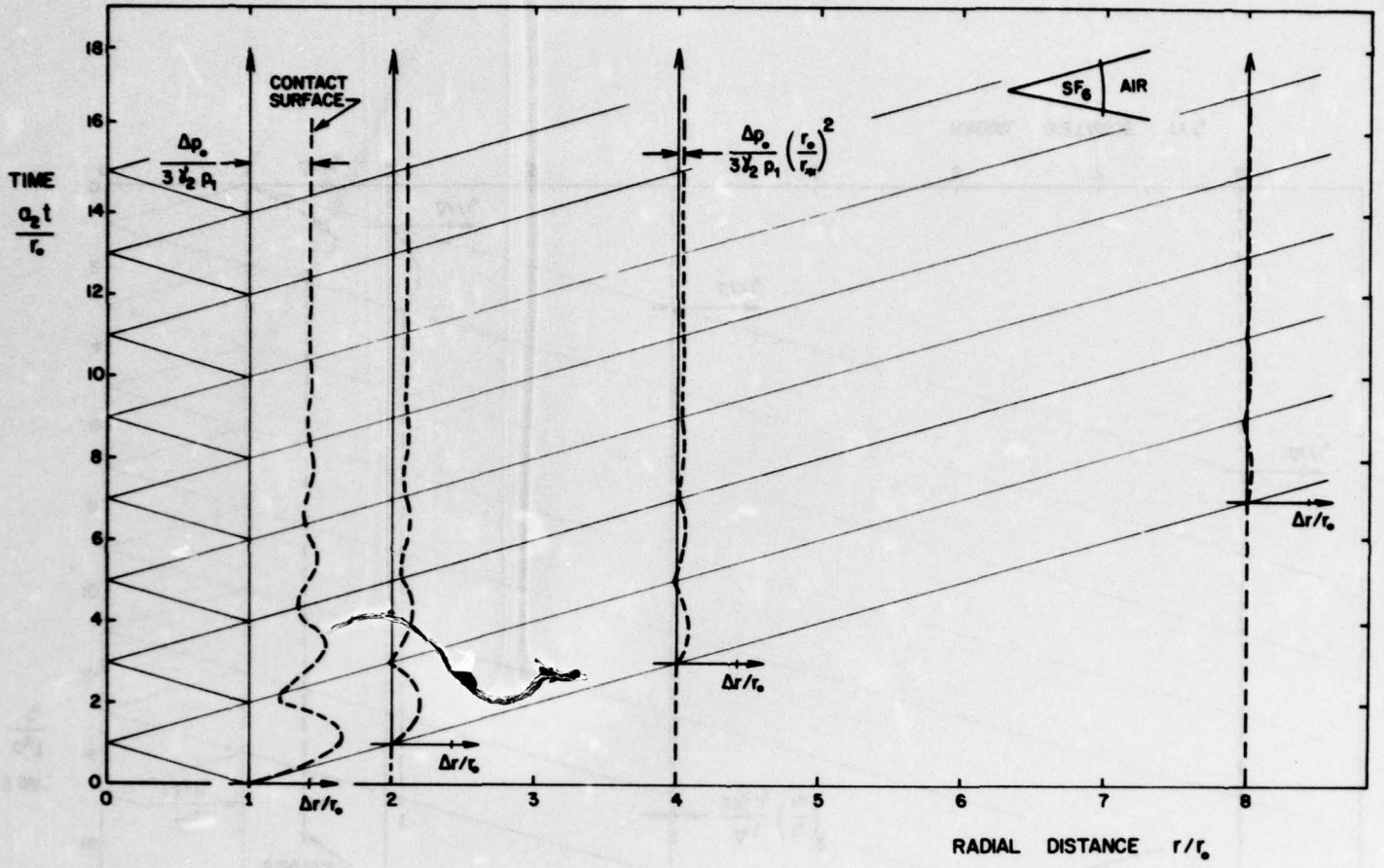

FIG. 24 PARTICLE-DISPLACEMENT HISTORIES AT DIFFERENT RADII IN THE CHANNEL OF A PYRAMIDAL SHOCK TUBE

a)

DRIVER GAS: HELIUM (He)
CHANNEL GAS: AIR
DRIVER OVERPRESSURE (Δp_o): 2400 N/m^2
DRIVER LENGTH (r_o): 1.58 m
MEASUREMENT LOCATION (r): 4.6 m

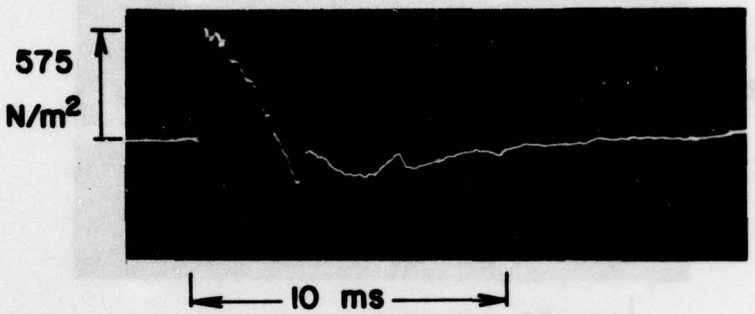

b)

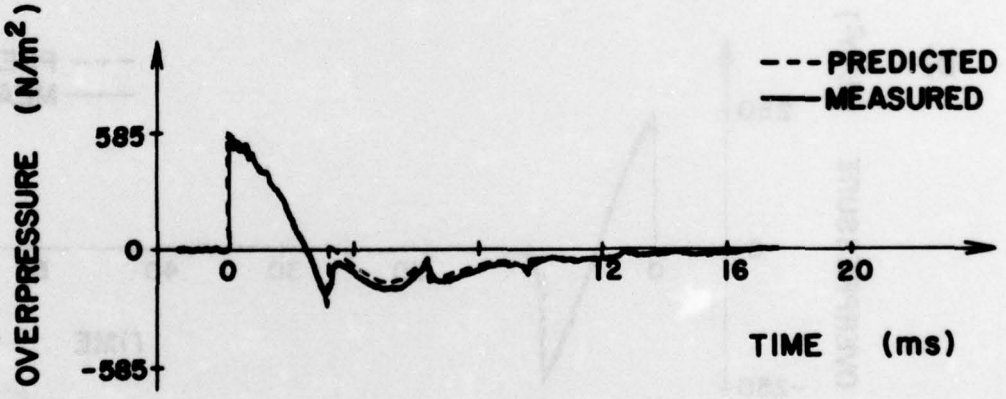

FIG. 25 COMPARISON OF MEASURED AND PREDICTED OVERPRESSURE SIGNATURES OF A PYRAMIDAL SHOCK TUBE

a)

DRIVER GAS : AIR
CHANNEL GAS : AIR
DRIVER OVERPRESSURE (Δp_o) : 2400 N/m^2
DRIVER LENGTH (r_o) : 1.58 m
MEASUREMENT LOCATION (r) : 7.6 m

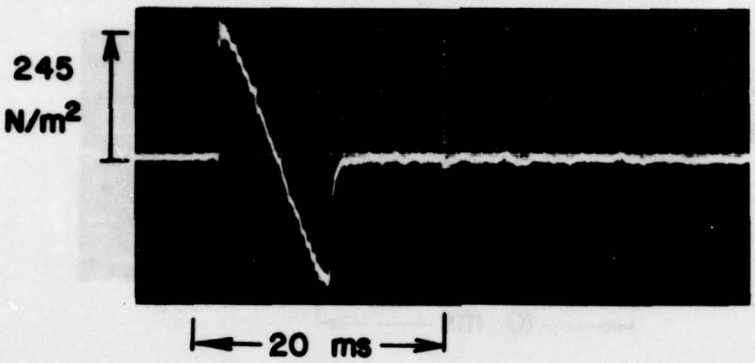

b)

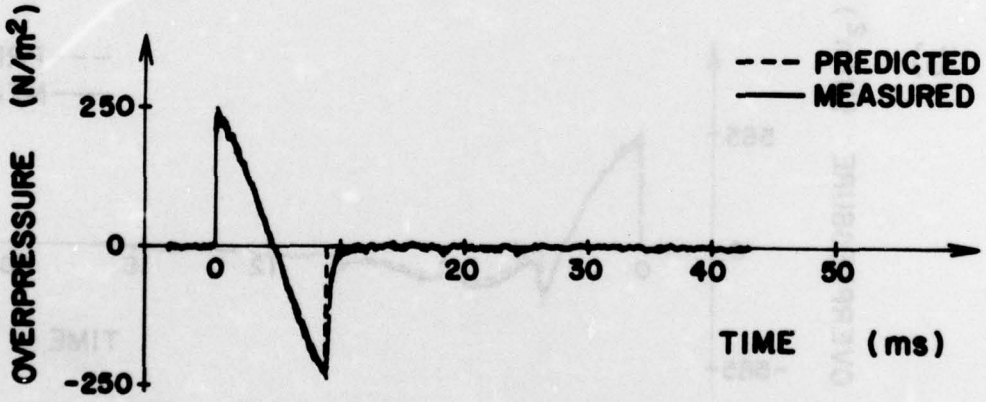

FIG. 26 COMPARISON OF MEASURED AND PREDICTED OVERPRESSURE SIGNATURES OF A PYRAMIDAL SHOCK TUBE

a)

DRIVER GAS: ARGON (A)
CHANNEL GAS: AIR
DRIVER OVERPRESSURE (Δp_o): 2400 N/m^2
DRIVER LENGTH (r_o): 1.58 m
MEASUREMENT LOCATION (r): 7.6 m

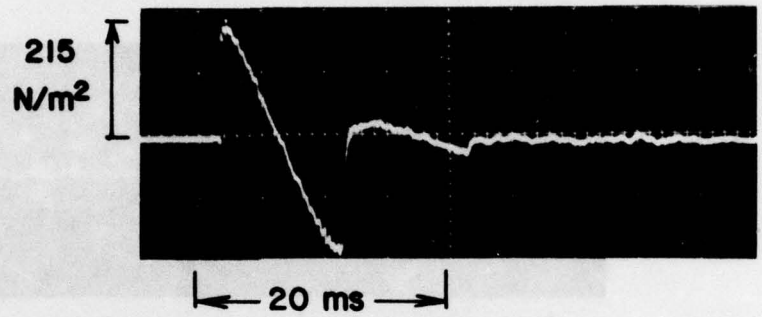

b)

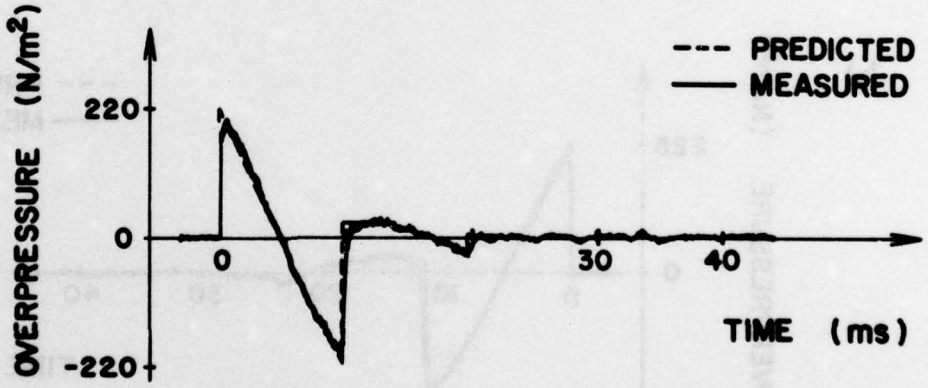

FIG. 27 COMPARISON OF MEASURED AND PREDICTED OVERPRESSURE SIGNATURES OF A PYRAMIDAL SHOCK TUBE

a)

DRIVER GAS: CARBON DIOXIDE (CO_2)
CHANNEL GAS: AIR
DRIVER OVERPRESSURE (Δp_o): 2400 N/m^2
DRIVER LENGTH (r_o): 1.58 m
MEASUREMENT LOCATION (r): 7.6 m

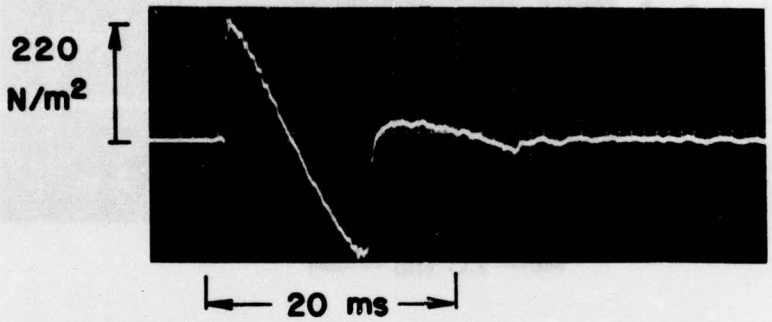

b)

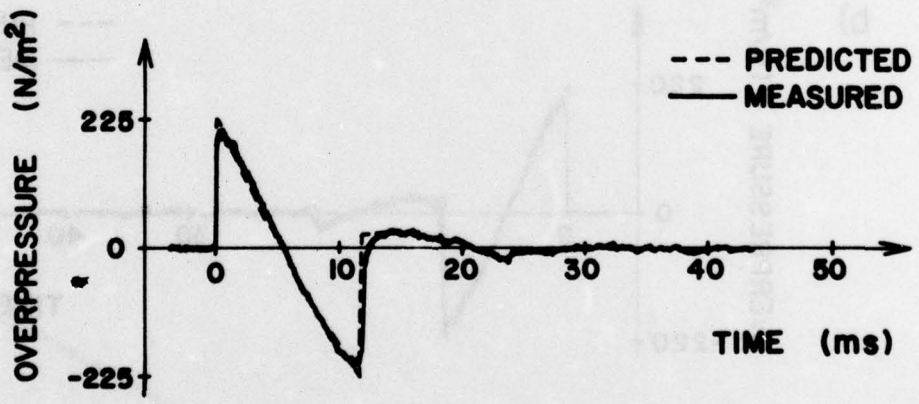

FIG. 28 COMPARISON OF MEASURED AND PREDICTED OVERPRESSURE SIGNATURES OF A PYRAMIDAL SHOCK TUBE

a)

DRIVER GAS: SULFUR DIOXIDE (SO_2)
CHANNEL GAS: AIR
DRIVER OVERPRESSURE (Δp_s): 2400 N/m^2
DRIVER LENGTH (r_s): 1.58 m
MEASUREMENT LOCATION (r): 7.6 m

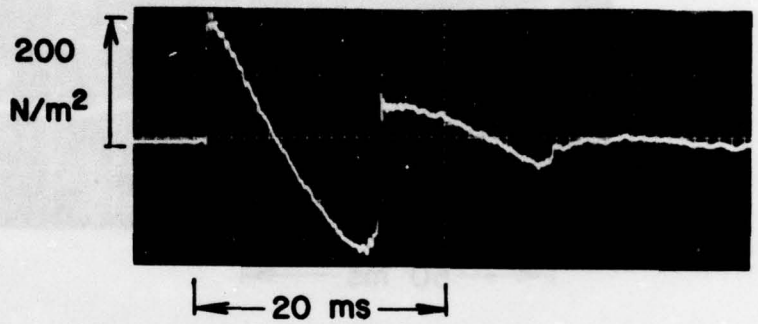

b)

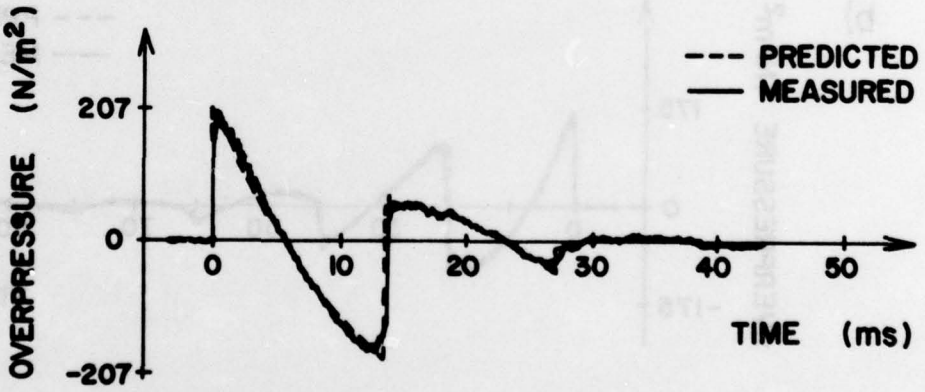

FIG. 29 COMPARISON OF MEASURED AND PREDICTED OVERPRESSURE SIGNATURES OF A PYRAMIDAL SHOCK TUBE

a) DRIVER GAS: DICHLORODIFLUOROMETHANE (CCl_2F_2)
CHANNEL GAS: AIR
DRIVER OVERPRESSURE (Δp_o): 2400 N/m^2
DRIVER LENGTH (r_o): 1.58 m
MEASUREMENT LOCATION (r): 7.6 m

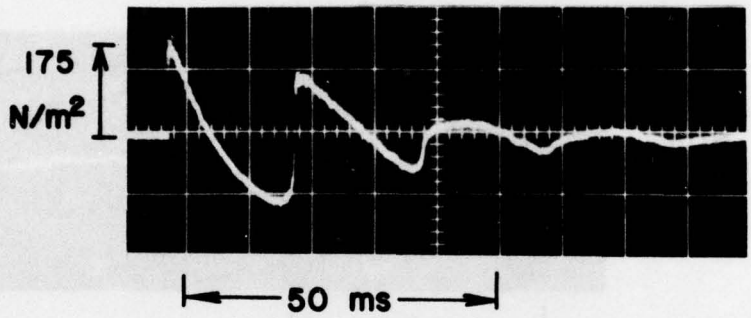

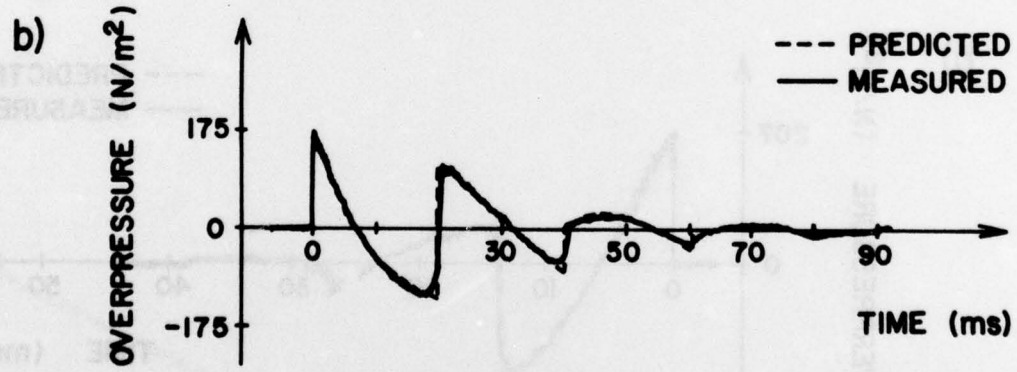

FIG. 30 COMPARISON OF MEASURED AND PREDICTED OVERPRESSURE SIGNATURES OF A PYRAMIDAL SHOCK TUBE

a) DRIVER GAS: OCTAFLUOROCYCLOBUTANE (C_4F_8)
CHANNEL GAS: AIR
DRIVER OVERPRESSURE (Δp_o): 2400 N/m^2
DRIVER LENGTH (r_o): 1.58 m
MEASUREMENT LOCATION (r): 7.6 m

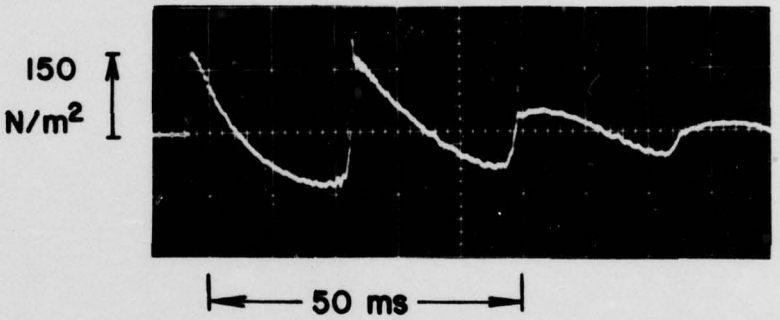

b)

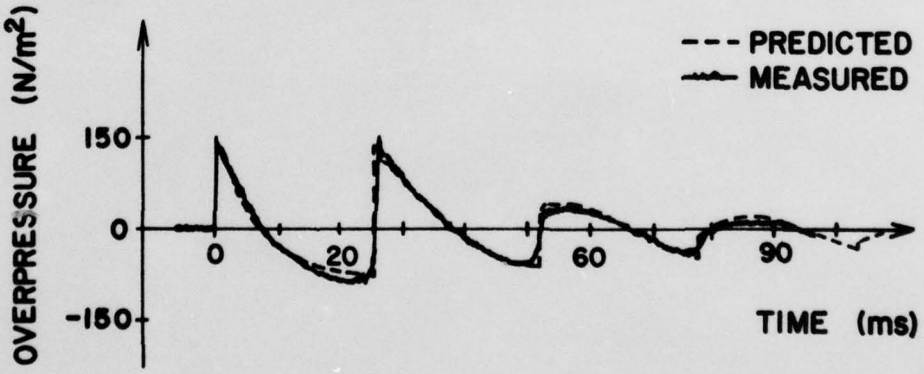

FIG. 31 COMPARISON OF MEASURED AND PREDICTED OVERPRESSURE SIGNATURES OF A PYRAMIDAL SHOCK TUBE

APPENDIX A

The following expression for the i^{th} velocity potential $f_i'(\eta)$ was derived in Chapter 3 (Eq. 3.29).

$$f_i'(\eta) = \frac{\Delta p_o r_o^2 \ell}{a_2 \rho_2 (\varepsilon+1)} \sum_{j=1}^{i} \binom{i-1}{j-1} \left(\frac{\varepsilon-1}{\varepsilon+1}\right)^{i-j} \left(\frac{2}{\varepsilon+1}\right)^{j-1} I_j'(\eta-2i+1)$$

If $\Delta p_o r_o^2 \ell / a_2 \rho_2 (\varepsilon+1)$, $(\varepsilon-1)/(\varepsilon+1)$ and $2/(\varepsilon+1)$ are denoted by A, B and C respectively, the first five velocity potentials can be expressed as follows.

$$f_1'(\eta) = A[I_1'(\eta-1)]$$

$$f_2'(\eta) = A[B\, I_1'(\eta-3) + C\, I_2'(\eta-3)]$$

$$f_3'(\eta) = A[B^2 I_1'(\eta-5) + 2BC\, I_2'(\eta-5) + C^2 I_3'(\eta-5)]$$

$$f_4'(\eta) = A[B^3 I_1'(\eta-7) + 3B^2 C\, I_2'(\eta-7) + 3BC^2 I_3'(\eta-7) + C^2 I_4'(\eta-7)]$$

$$f_5'(\eta) = A[B^4 I_1'(\eta-9) + 4B^3 C\, I_2'(\eta-9) + 6B^2 C^2 I_3(\eta-9) + 4BC^3 I_4'(\eta-9) + C^4 I_5'(\eta-9)]$$

The j^{th} function $I_j'(\eta-2i+1)$ derived in Chapter 3 (Eq. 3.32) can be expressed in the following form.

$$I_j'(\omega) = (1+\varepsilon+\ell)\left(\frac{\omega}{\ell} - j\right) + \varepsilon + \sum_{k=1}^{j} \frac{k(1+\varepsilon+\ell)-\varepsilon}{(j-k)!} \left(\frac{\omega}{\ell}\right)^{j-k} \exp(-\omega/\ell)$$

The first four functions are listed below for convenience and illustration.

$$I_1'(\omega) = (1+\varepsilon+\ell)\left(\frac{\omega}{\ell} - 1\right) + \varepsilon + (1+\ell)\exp(-\omega/\ell)$$

$$I_2'(\omega) = (1+\varepsilon+\ell)\left(\frac{\omega}{\ell} - 2\right) + \varepsilon + \left[\, (1+\ell)\frac{\omega}{\ell} + (2+2\ell+\varepsilon) \,\right] \exp(-\omega/\ell)$$

$$I_3'(\omega) = (1+\varepsilon+\ell)\left(\frac{\omega}{\ell} - 3\right) + \varepsilon + \left[\frac{(1+\ell)}{2!}\left(\frac{\omega}{\ell}\right)^2 + (2+2\ell+\varepsilon)\frac{\omega}{\ell} + (3+3\ell+\varepsilon) \right] \exp(-\omega/\ell)$$

$$I_4'(\omega) = (1+\varepsilon+\ell)\left(\frac{\omega}{\ell} - 4\right) + \varepsilon + \left[\frac{(1+\ell)}{3!}\left(\frac{\omega}{\ell}\right)^3 + \frac{(2+2\ell+\varepsilon)}{2!}\left(\frac{\omega}{\ell}\right)^2 + (3+3\ell+\varepsilon)\frac{\omega}{\ell} + (4+4\ell+\varepsilon) \right] \exp(-\omega/\ell)$$

$$J_2''(\omega) = [(1+\ell)(\omega/\ell)^2/2! + \varepsilon(\omega/\ell)]\exp(-\omega/\ell)$$

$$J_3''(\omega) = [(1+\ell)(\omega/\ell)^3/3! + \varepsilon(\omega/\ell)^2/2!]\exp(-\omega/\ell)$$

$$J_4''(\omega) = [(1+\ell)(\omega/\ell)^4/4! + \varepsilon(\omega/\ell)^3/3!]\exp(-\omega/\ell)$$

APPENDIX B

The following expression for the overpressure in the channel of a pyramidal shock tube utilizing different driver and channel gases was derived in Chapter 3 (Eqs. 3.37, 3.38 and 3.39).

$$\Delta p_1 = \frac{\Delta p_o}{\varepsilon+1}\frac{r_o}{r}\sum_{i=1}^{\infty}[g_i''(\xi)H\{\xi-2i+2\}]$$

$$g_i''(\xi) = \begin{cases} J_o''(\xi) & i = 0 \\ \sum_{j=1}^{i-1}\binom{i-2}{j-1}\left(\frac{\varepsilon-1}{\varepsilon+1}\right)^{i-j-2}\left(\frac{2}{\varepsilon+1}\right)^{j} J_j''(\xi-2i+2) & i = 2, 3, \ldots, \infty \end{cases}$$

$$J_j''(\omega) = \begin{cases} -\ell + (1+\ell)\exp(-\omega/\ell) & j = 0 \\ \left[\frac{1+\ell}{j!}\left(\frac{\omega}{\ell}\right)^{j} + \frac{\varepsilon}{(j-1)!}\left(\frac{\omega}{\ell}\right)^{j-1}\right]\exp(-\omega/\ell) & j = 1, 2, \ldots, \infty \end{cases}$$

If $(\varepsilon-1)/(\varepsilon+1)$ and $2/(\varepsilon+1)$ are denoted by B and C respectively, the first five functions for $g_i''(\xi)$ can be expressed as follows.

$$g_1''(\xi) = J_o''(\xi)$$

$$g_2''(\xi) = C\,J_1''(\xi-2)$$

$$g_3''(\xi) = BC\,J_1''(\xi-4) + C^2J_2''(\xi-4)$$

$$g_4''(\xi) = B^2C\,J_1''(\xi-6) + 2BC^2J_2''(\xi-6) + C^3J_3''(\xi-6)$$

$$g_5''(\xi) = B^3C\,J_1''(\xi-8) + 3B^2C^2J_2''(\xi-8) + 3BC^3J_3''(\xi-8) + C^4J_4''(\xi-8)$$

The first five functions of $J_j''(\xi-2i+2)$ are listed below.

$$J_o''(\omega) = -\ell + (1+\ell)\exp(-\omega/\ell)$$

$$J_1''(\omega) = [(1+\ell)(\omega/\ell) + \varepsilon]\exp(-\omega/\ell)$$

UTIAS REPORT NO. 199

Institute for Aerospace Studies, University of Toronto
4925 Dufferin Street, Downsview, Ontario, Canada, M3H 5T6

WAVE MOTION IN LOW-PRESSURE-RATIO RECTANGULAR AND PYRAMIDAL SHOCK TUBES

Gottlieb, James Joseph 82 pages (app.) 31 figures 3 tables

1. Shock tube 2. Acoustic wave 3. Sonic boom 4. Simulator

I. Gottlieb, James Joseph II. UTIAS Report No. 199

Closed-form solutions based on acoustic theory have recently been obtained to describe the wave motion in both low-pressure-ratio rectangular (constant area) and pyramidal shock tubes which utilize different driver and channel gases. These new solutions are in excellent agreement with experimental data. This work should be of interest to researchers who are using shock tubes or similar devices to produce impulse noise, in particular the simulated sonic boom, in order to facilitate studies of the effects of impulse sound on humans, animals and structures. Furthermore, this work is relevant to the understanding of the wave motion produced by weak planar and spherical explosions of finite size.

Available copies of this report are limited. Return this card to UTIAS, if you require a copy.

UTIAS REPORT NO. 199

Institute for Aerospace Studies, University of Toronto
4925 Dufferin Street, Downsview, Ontario, Canada, M3H 5T6

WAVE MOTION IN LOW-PRESSURE-RATIO RECTANGULAR AND PYRAMIDAL SHOCK TUBES

Gottlieb, James Joseph 82 pages (app.) 31 figures 3 tables

1. Shock tube 2. Acoustic wave 3. Sonic boom 4. Simulator

I. Gottlieb, James Joseph II. UTIAS Report No. 199

Closed-form solutions based on acoustic theory have recently been obtained to describe the wave motion in both low-pressure-ratio rectangular (constant area) and pyramidal shock tubes which utilize different driver and channel gases. These new solutions are in excellent agreement with experimental data. This work should be of interest to researchers who are using shock tubes or similar devices to produce impulse noise, in particular the simulated sonic boom, in order to facilitate studies of the effects of impulse sound on humans, animals and structures. Furthermore, this work is relevant to the understanding of the wave motion produced by weak planar and spherical explosions of finite size.

Available copies of this report are limited. Return this card to UTIAS, if you require a copy.

UTIAS REPORT NO. 199

Institute for Aerospace Studies, University of Toronto
4925 Dufferin Street, Downsview, Ontario, Canada, M3H 5T6

WAVE MOTION IN LOW-PRESSURE-RATIO RECTANGULAR AND PYRAMIDAL SHOCK TUBES

Gottlieb, James Joseph 82 pages (app.) 31 figures 3 tables

1. Shock tube 2. Acoustic wave 3. Sonic boom 4. Simulator

I. Gottlieb, James Joseph II. UTIAS Report No. 199

Closed-form solutions based on acoustic theory have recently been obtained to describe the wave motion in both low-pressure-ratio rectangular (constant area) and pyramidal shock tubes which utilize different driver and channel gases. These new solutions are in excellent agreement with experimental data. This work should be of interest to researchers who are using shock tubes or similar devices to produce impulse noise, in particular the simulated sonic boom, in order to facilitate studies of the effects of impulse sound on humans, animals and structures. Furthermore, this work is relevant to the understanding of the wave motion produced by weak planar and spherical explosions of finite size.

Available copies of this report are limited. Return this card to UTIAS, if you require a copy.

UTIAS REPORT NO. 199

Institute for Aerospace Studies, University of Toronto
4925 Dufferin Street, Downsview, Ontario, Canada, M3H 5T6

WAVE MOTION IN LOW-PRESSURE-RATIO RECTANGULAR AND PYRAMIDAL SHOCK TUBES

Gottlieb, James Joseph 82 pages (app.) 31 figures 3 tables

1. Shock tube 2. Aoostic wave 3. Sonic boom 4. Simulator

I. Gottlieb, James Joseph II. UTIAS Report No. 199

Closed-form solutions based on acoustic theory have recently been obtained to describe the wave motion in both low-pressure-ratio rectangular (constant area) and pyramidal shock tubes which utilize different driver and channel gases. These new solutions are in excellent agreement with experimental data. This work should be of interest to researchers who are using shock tubes or similar devices to produce impulse noise, in particular the simulated sonic boom, in order to facilitate studies of the effects of impulse sound on humans, animals and structures. Furthermore, this work is relevant to the understanding of the wave motion produced by weak planar and spherical explosions of finite size.

Available copies of this report are limited. Return this card to UTIAS, if you require a copy.

UTIAS REPORT NO. 199

Institute for Aerospace Studies, University of Toronto
4925 Dufferin Street, Downsview, Ontario, Canada, M3H 5T6

WAVE MOTION IN LOW-PRESSURE-RATIO RECTANGULAR AND PYRAMIDAL SHOCK TUBES

Gottlieb, James Joseph 82 pages (app.) 31 figures 3 tables

1. Shock tube 2. Acoustic wave 3. Sonic boom 4. Simulator

I. Gottlieb, James Joseph II. UTIAS Report No. 199

Closed-form solutions based on acoustic theory have recently been obtained to describe the wave motion in both low-pressure-ratio rectangular (constant area) and pyramidal shock tubes which utilize different driver and channel gases. These new solutions are in excellent agreement with experimental data. This work should be of interest to researchers who are using shock tubes or similar devices to produce impulse noise, in particular the simulated sonic boom, in order to facilitate studies of the effects of impulse sound on humans, animals and structures. Furthermore, this work is relevant to the understanding of the wave motion produced by weak planar and spherical explosions of finite size.

Available copies of this report are limited. Return this card to UTIAS, if you require a copy.

UTIAS REPORT NO. 199

Institute for Aerospace Studies, University of Toronto
4925 Dufferin Street, Downsview, Ontario, Canada, M3H 5T6

WAVE MOTION IN LOW-PRESSURE-RATIO RECTANGULAR AND PYRAMIDAL SHOCK TUBES

Gottlieb, James Joseph 82 pages (app.) 31 figures 3 tables

1. Shock tube 2. Acoustic wave 3. Sonic boom 4. Simulator

I. Gottlieb, James Joseph II. UTIAS Report No. 199

Closed-form solutions based on acoustic theory have recently been obtained to describe the wave motion in both low-pressure-ratio rectangular (constant area) and pyramidal shock tubes which utilize different driver and channel gases. These new solutions are in excellent agreement with experimental data. This work should be of interest to researchers who are using shock tubes or similar devices to produce impulse noise, in particular the simulated sonic boom, in order to facilitate studies of the effects of impulse sound on humans, animals and structures. Furthermore, this work is relevant to the understanding of the wave motion produced by weak planar and spherical explosions of finite size.

Available copies of this report are limited. Return this card to UTIAS, if you require a copy.

UTIAS REPORT NO. 199

Institute for Aerospace Studies, University of Toronto
4925 Dufferin Street, Downsview, Ontario, Canada, M3H 5T6

WAVE MOTION IN LOW-PRESSURE-RATIO RECTANGULAR AND PYRAMIDAL SHOCK TUBES

Gottlieb, James Joseph 82 pages (app.) 31 figures 3 tables

1. Shock tube 2. Acoustic wave 3. Sonic boom 4. Simulator

I. Gottlieb, James Joseph II. UTIAS Report No. 199

Closed-form solutions based on acoustic theory have recently been obtained to describe the wave motion in both low-pressure-ratio rectangular (constant area) and pyramidal shock tubes which utilize different driver and channel gases. These new solutions are in excellent agreement with experimental data. This work should be of interest to researchers who are using shock tubes or similar devices to produce impulse noise, in particular the simulated sonic boom, in order to facilitate studies of the effects of impulse sound on humans, animals and structures. Furthermore, this work is relevant to the understanding of the wave motion produced by weak planar and spherical explosions of finite size.

Available copies of this report are limited. Return this card to UTIAS, if you require a copy.

UTIAS REPORT NO. 199

Institute for Aerospace Studies, University of Toronto
4925 Dufferin Street, Downsview, Ontario, Canada, M3H 5T6

WAVE MOTION IN LOW-PRESSURE-RATIO RECTANGULAR AND PYRAMIDAL SHOCK TUBES

Gottlieb, James Joseph 82 pages (app.) 31 figures 3 tables

1. Shock tube 2. Acoustic wave 3. Sonic boom 4. Simulator

I. Gottlieb, James Joseph II. UTIAS Report No. 199

Closed-form solutions based on acoustic theory have recently been obtained to describe the wave motion in both low-pressure-ratio rectangular (constant area) and pyramidal shock tubes which utilize different driver and channel gases. These new solutions are in excellent agreement with experimental data. This work should be of interest to researchers who are using shock tubes or similar devices to produce impulse noise, in particular the simulated sonic boom, in order to facilitate studies of the effects of impulse sound on humans, animals and structures. Furthermore, this work is relevant to the understanding of the wave motion produced by weak planar and spherical explosions of finite size.

Available copies of this report are limited. Return this card to UTIAS, if you require a copy.

UNCLASSIFIED

SECURITY CLASSIFICATION OF THIS PAGE *(When Data Entered)*

REPORT DOCUMENTATION PAGE

READ INSTRUCTIONS BEFORE COMPLETING FORM

1. REPORT NUMBER: AFOSR - TR - 77 - 0624
2. GOVT ACCESSION NO.
3. RECIPIENT'S CATALOG NUMBER

4. TITLE *(and Subtitle)*: WAVE MOTION IN LOW-PRESSURE-RATIO RECTANGULAR AND PYRAMIDAL SHOCK TUBES.

5. TYPE OF REPORT & PERIOD COVERED: INTERIM

6. PERFORMING ORG. REPORT NUMBER

7. AUTHOR(s): JAMES JOSEPH GOTTLIEB

8. CONTRACT OR GRANT NUMBER(s): AF-AFOSR-2274-72
AFOSR 72-2274

9. PERFORMING ORGANIZATION NAME AND ADDRESS
UNIVERSITY OF TORONTO
INSTITUTE FOR AEROSPACE STUDIES, 4925 DUFFERIN ST
DOWNSVIEW, ONTARIO, CANADA, M3H 5T6

10. PROGRAM ELEMENT, PROJECT, TASK AREA & WORK UNIT NUMBERS
9781-03
61102F

11. CONTROLLING OFFICE NAME AND ADDRESS
AIR FORCE OFFICE OF SCIENTIFIC RESEARCH/NA
BLDG 410
BOLLING AIR FORCE BASE, DC 20332

12. REPORT DATE: Dec 75

13. NUMBER OF PAGES: 86 P.

14. MONITORING AGENCY NAME & ADDRESS *(if different from Controlling Office)*
UTIAS-199

15. SECURITY CLASS. *(of this report)*: UNCLASSIFIED

15a. DECLASSIFICATION/DOWNGRADING SCHEDULE

16. DISTRIBUTION STATEMENT *(of this Report)*

Approved for public release; distribution unlimited.

17. DISTRIBUTION STATEMENT *(of the abstract entered in Block 20, if different from Report)*

18. SUPPLEMENTARY NOTES

19. KEY WORDS *(Continue on reverse side if necessary and identify by block number)*
SHOCK TUBE
ACOUSTIC WAVE
SONIC BOOM
SIMULATOR

20. ABSTRACT *(Continue on reverse side if necessary and identify by block number)*

Closed-form solutions based on acoustic theory have recently been obtained to describe the wave motion in both low-pressure-ratio rectangular (constant area) and pyramidal shock tubes which utilize different driver and channel gases. These new solutions are in excellent agreement with experimental data. This work should be of interest to researchers who are using shock tubes or similar devices to produce impulse noise, in particular the similated sonic boom, in order to facilitate studies of the effects of impulse sound on humans, animals and structures. Furthermore, this work is relevant to the understanding of the wave motion produced by weak planar and spherical explosions of finite size.

DD FORM 1 JAN 73 1473 EDITION OF 1 NOV 65 IS OBSOLETE

UNCLASSIFIED

SECURITY CLASSIFICATION OF THIS PAGE *(When Data Entered)*

178920 EHH